Gold acting as Lewis base in the formation of hydrogen and halogen bonds

by
Ferdinand George Groenewald

Thesis presented in partial fulfilment of the requirements for the degree Doctor of Philosophy in Chemistry at the University of Stellenbosch

Supervisor: Prof. Catharine Esterhuysen
Co-supervisor: Prof. Jan Dillen
Faculty of Science
Department of Chemistry & Polymer Science

March 2016

Declaration

By submitting this thesis/dissertation electronically, I declare that the entirety of the work contained therein is my own, original work, that I am the sole author thereof (save to the extent explicitly otherwise stated), that reproduction and publication thereof by Stellenbosch University will not infringe any third party rights and that I have not previously in its entirety or in part submitted it for obtaining any qualification.

March 2016

Abstract

A systematic theoretical investigation was performed to determine the hydrogen bond acceptor ability of the Au^I metal centre in anionic and neutral complexes, where it acts as a Lewis base. The study was initiated by revisiting an accepted hydrogen-bond acceptor of gold, i.e. the Au^- ion, which is known to form hydrogen bonds in the gas phase and some solutions. Six hydrogen bonded donors were selected, i.e. HF, H_2O, NH_3, HCN, C_2H_2 and CH_4, with each yielding stable hydrogen bond conformations with the Au^- ion. Trends in the interaction energies and geometrical data were identified and used to benchmark the study by comparison to the work of others. The procedure was then repeated for our model complex, the $[(Me)_2Au]^-$ ion which formed hydrogen bonds to all six hydrogen bond donors, with interaction energies ranging from -2.4kcal/mol to -16.00 kcal/mol. Geometrical data, in conjunction with Atoms in Molecules analysis were consistent with those of the Au^- ion and with hydrogen bonding agreeing with the characteristics listed in the IUPAC definition for hydrogen bonding. $[(Me)_2Cu]^-$ and $[(Me)_2Ag]^-$ do not yield $M^I\cdots H$ interactions, while $Au^I\cdots H$ hydrogen-bond formation is dependent on the electrostatic surface potential.

The effect of electron-withdrawing and electron-donating ligands, i.e. CF_3^- and $C(Me)_3^-$, on gold's hydrogen bond acceptor abilities, and hence its Lewis basicity, was identified by comparison to the results obtained for the $[(Me)_2Au]^-$ model complex. Electron donation does not affect the interaction energies due to intermolecular repulsion between the hydrogen-bond donor and the ligand coordinated to Au(I), but influences the $Au^I\cdots H$ distances and the properties of the BCP separating Au and H. Conversely, electron-withdrawing ligands affect the interaction energies as well as the calculated geometrical and AIM parameters and is consistent with weakening of the hydrogen bond. The $Au^I\cdots H$ interaction energies for both electron-withdrawing and electron-donating ligands were lower than those for the model complex. Nevertheless, they are consistent with the IUPAC definition.

A range of neutral *N*-heterocyclic carbene (NHC) Au(I) complexes, containing different anionic ligands (R, where R = H^-, CH_3^- , Cl^-, OH^-) were found to yield stable adducts with H_2O, HF and NH_3. In addition to the $Au^I\cdots$H-X hydrogen bonds, H-X$\cdots$H-N hydrogen bonds were also identified, with the second hydrogen bond adding the most stability to the total interaction energy; the most stable hydrogen bonded adduct was found to be Au(NHC)Cl.NH_3. Nevertheless, AIM analysis revealed that all $Au^I\cdots HF$ and $Au^I\cdots H_2O$ interactions are hydrogen bonds, while NH_3 forms weak dispersion-type $Au^I\cdots H$ interactions,

with only the Au(NHC)CH_3 complex yielding an $Au^I\cdots H$ interaction to NH_3 that is characteristic for a hydrogen bond.

Halogen bonds between the Au^- ion and six different halogen bond donors, i.e. ICH_3, $BrCH_3$, $ClCH_3$, ICF_3, $BrCF_3$ and $ClCF_3$, were identified, where the auride anion behaves similarly to the I^- and Br^- ions in the formation of the trihalide species, with high interaction energies up to -33.3 kcal/mol and large accumulation of electron density between the Au and X atoms. $[(Me)_2Au]^-$ was found to yield stable adducts with short $Au^I\cdots X$ distances to five of the six halogen-bond donors, along with extremely directional $Au^I\cdots$X-R angles and bond elongation upon X-bond formation. It was found that increasing the X-R bond polarisability influences the bond strength and yielded more stable adducts. All the geometrical and AIM data were consistent with the IUPAC definition of halogen bonding.

Uittreksel

‘n Sistematiese teoretiese ondersoek om te bepaal of die Au^{I} metaal as ‘n waterstofbinding akseptor kan optree is onderneem. Ons begin die ondersoek deur na ’n voorbeeld van goud te kyk wat alreeds ‘n aanvaarde waterstofbindingakseptor is: die Au^{-} ioon. Die auried anioon is bekend as waterstofbinding akseptor in die gas fase asook in sekere oplosmiddels. Ons ondersoek is gedoen in die gas fase waar ons gevind het dat die auried anioon aan ses verskillende tipes waterstofbindingdonor molekules bind. Die resultate het tendense in die geometriese waardes asook die interaksie energieë gelewer en het ons toegelaat om die akkuraatheid van ons metodes te bepaal en as ‘n maatstaf te gebruik. Hierdie tendense kon toe gebruik word om met ons model kompleks, die $[(Me)_2Au]^{-}$ ioon te vergelyk. Dié model kompleks het, net soos die Au^{-} ioon, waterstofbindings met al ses waterstofbinding donors gevorm met interaksie energiëe wat tussen -2.4 kcal/mol en -16.00 kcal/mol wissel. Sowel die geometriese data asook “Atome in Molekules” (AIM) analises dui aan dat die $Au^{I}\cdots H$ interaksie ’n waterstofbinding is wat met die IUPAC definisie korrieleer. Die $[(Me)_2Cu]^{-}$ en $[(Me)_2Ag]^{-}$ ione vorm geen $M^{I}\cdots H$ waterstofbondings met die elektrostatiese potensiële oppervlaktes nie wat aandui dat die vorming van die $Au^{I}\cdots H$ interaksie as gevolg van dié oppervlakte is.

Effekte van die elektron-donerende- en elektron-ontrekkendegroepe wat aan die goud koördineer was ook ondersoek om te bepaal of dit die Lewis basisiteit van Au(I) beïnvloed. Die resultate stel vas dat die elektron-donerendegroepe geen effek op die interaksie energie het nie; inteendeel dit word verswak indien dit met ons model kompleks vergelyk word, as gevolg van afstotende interaksies tussen die goud kompleks en die waterstofbindingdonor. Die invloed word wel in die $Au\cdots H$ afstande en AIM resultate gesien. Die effekte van die elektron-ontrekkendegroepe is wel meer opvallend met ’n noemenswaardige destabilisering in die $Au^{I}\cdots H$ interaksie energie. Alhoewel daar duidelike veranderinge in die interaksie energiëe, geometriese data asook die AIM analise is, stem die eienskappe van die interaksie ooreen met waterstofbindings soos deur IUPAC gedefinieer.

Vervolgens is die ondersoek vergroot na die *N*-heterosikliesekarbene (NHC) Au(I) komplekse met ‘n anioniese ligand (R, waar R = H^{-}, CH_3^{-} , Cl^{-}, OH^{-}) wat aan die teenoorgestelde kant koördineer uitgebrei. Stabiele waterstofgebinde produkte het met die H_2O, HF en NH_3 donor molekules gevorm, alhoewel twee waterstofbindings gevorm het: die $Au^{I}\cdots$H-X en ’n H-X$\cdots$H-N. Die AIM analise het geblyk dat die $Au^{I}\cdots H$ interaksies van H_2O

en HF waterstofbindings is, terwyl die $Au^{I}\cdots H$ interaksie van NH_3 is ’n swak van der Waals-tiepe interaksie is.

Die mees stabiele waterstofbindingsproduk is $Au(NHC)Cl.NH_3$, omdat daar gevind is dat die H-X⋯H-N interaksie die grootste bydrae tot die algehele stabiliteit van die sisteem maak.

Om verder te bewys dat Au(I) as ’n Lewis basis kan optree, is die studie verryk deur na die vermoë van Au(I) om as ‘n halogeenbinding akseptor op te tree te kyk. Om sistematies te bly het ons weereens met die auried anioon begin en gevind dat dit vorm ‘n halogeen binding met elk van die ses donor molekules verder tree Au^- soos die I^- and Br^- haliede in die trihaliede spesies op. Die stabilisering betrokke by die produkte is -33.3 kcal/mol, wat gepaard gaan met ’n hoë elektrondigtheid tussen die twee atome wat bind. $[(Me)_2Au]^-$ het getoon dat dit die vermoë het om met vyf van die ses halogeenbindingsdonor molekules te bind met kort $Au^{I}\cdots X$ afstande, duidelike rigtinggewend interaksies en X-R bindingsrekking op lewering van die produk. ’n Verhoging in die X-R binding se polariseerbaarheid het tot ‘n meer stabiele interaksie energie gelei. Al die geometriese en AIM data het saamgestem met die IUPAC definisie van halogeenbindings.

Acknowledgements

First and foremost, I would like to thank my supervisors, Prof. Catharine Esterhuysen and Prof. Jan Dillen for their sound advice and support during the past three years. Thank you for always being available when called upon and for the countless discussions on topics related to my project. Thank you for providing the necessary tools and computational resources enabling me to perform the research shown here in this study, which would not have been possible otherwise. Secondly, I would like to thank Prof Raubenheimer for his research input, many ideas and the time we spent discussing my results.

I would like to extend my thanks to my family and friends for the continuous support and countless philosophical discussions about science in general. Furthermore, I would like to show my gratitude towards the Supramolecular Materials Chemistry group at the University of Stellenbosch for welcoming me to their group and the support they showed me during my PhD.

Finally, I would like to thank the University of Stellenbosch for providing the necessary facilities. The financial assistance (reference number SFH13072222708) of the National Research Foundation (NRF) towards this research is hereby acknowledged. Opinions expressed and conclusions arrived at, are those of the author and are not necessarily to be attributed to the NRF. Also, I would like to thank Charl Möller, the administrator of University of Stellenbosch's Rhasatsha HPC (http://www.sun.ac.za/hpc), for his help managing Gaussian's insatiable appetite for resources and maintaining a stable cluster. This is where the majority of the computations were performed to obtain the results shown here.

This body work is dedicated to the loving memory of my grandfather and grandmother whom I both lost to cancer, and is also dedicated to my dear friend who passed away in 2007 after a tragic car accident. Last, but not least, I would like to dedicate this work to Carla Pretorius. We have been through so much together during 2015.

“I'm reaching for the random or whatever will bewilder me.
Whatever will bewilder me.
And following our will and wind we may just go where no one's been.
We'll ride the spiral to the end and may just go where no one's been.

Spiral out. Keep going...”

TOOL – Lateralus

Publications and Posters

Publications

This study

Groenewald F, Esterhuysen C, Dillen J, Raubenheimer H, Angew. Chem., *Insight into the elusive Au···HO hydrogen bond,* DOI: 10.1002/anie.201508358R1 and 10.1002/ange.201508358R1

Other work

Groenewald F, Dillen J, Struct Chem, *Conformational analysis of caprolactam, cycloheptene and caprolactone,* DOI 10.1007/s11224-011-9921-x

Groenewald F, Dillen J, Mateura M, Struct Chem, *A computational investigation of the effect of the double bond on the conformations of seven membered rings*, DOI 10.1007/s11224-012-0073-4

Groenewald F, Esterhuysen C, Dillen J, Theo Chem Acc, *Extensive theoretical investigation: Influence of the electrostatic environment on the* $I_3^-\cdots I_3^-$ *anion-anion interaction*, In press, DOI: 10.1007/s00214-012-1281-0

Conferences

My MSc work was presented as a poster at Indaba 7 held in the Kruger National Park in 2012 entitled: *Computational investigation of* $I_3^-\cdots I_3^-$ *interactions*

This work was presented as a flash presentation and as a poster at the IUCr Year of Crystallography meeting held at University Free State in 2014 entitled: *Proposal of a new supramolecular synthon: Gold(I) acting as a Lewis base; an extensive theoretical investigation*

This work was presented as a flash presentation and as a poster at Indaba 8 held in the Kruger National Park in 2015 entitled: *Proposal of a new supramolecular synthon: Gold(I) acting as a Lewis base; an extensive theoretical investigation*

Glossary

aug	augmented
AIM	Atoms in Molecules
BCP	Bond Critical Point
BSSE	Basis set superposition error
cc	Correlation consistent
CC	Coupled Cluster
CP	Critical Points
CSD	Cambridge Structural Database
CT	Charge Transfer
CT-TBP	Charge transfer trigonal bipyramidal adducts
DF	Density Functional
DFT	Density Functional Theory
DMA	Dimethylaurate Au(I) anion
E_C	Correlation energy
ECP	Electrostatic Core Potential
E_{INT}	Interaction Energy
ESP	Electrostatic Surface Potential
E_{XC}	Exchange-correlation energy
E_X	Exchange energy
GGA	Generalised Gradient Approximation
H-bond	Hydrogen bond
HF	Hartree-Fock
IUPAC	International Union of Applied and Applied Chemistry
IR	Infrared
MP2	Møller-Plesset 2nd order perturbation theory with aug-cc-pVTZ-pp basis set
MP2*	MP2 with cc-pVTZ-pp basis set
NBO	Natural Bond Orbital
NCI	Noncovalent Interactions
NHC	*N*-Heterocyclic Carbene
pp	pseudo potentials
QM	Quantum Mechanics
RDG	Reduced Density Gradient

vdW	van der Waals
WFT	Wave Function Theory
X-bond	Halogen bond

Table of Contents

1. Introduction 1
1.1 The hydrogen bond 1
1.2 Hydrogen bonding involving transition metals 3
1.3 Gold in the context of hydrogen bonding 5
1.4 Halogen bonding 8
1.5 Theoretical methods and capabilities 11
1.6 Characterisation of noncovalent interactions 13
1.7 Aims and objectives 16
2. Gold setting the gold standard among transition metals as a H-bond acceptor – a theoretical investigation 20
2.1. Abstract 20
2.2. Introduction 20
2.3. Methodology 24
2.4. Results and Discussion 25
2.5. DMA anionic complex $[(Me)_2Au]^-$ 33
2.6. Comparison of the H-bonded adducts of Au^- to $[(Me)_2Au]^-$ 43
2.7 Comparison of Cu(I), Ag(I) and Au(I) analogues 45
2.8 Conclusions 51
3. Theoretical investigation on the inductive effects of ligands on the Lewis basicity of the Au(I) centre within anionic complexes 56
3.1. Abstract 56
3.2. Introduction 56
3.3. Methodology 59
3.4. Results and Discussion 60
3.5. Conclusions 71
4. Theoretical investigation of neutral Au(NHC)R (R = H^-,CH_3^-, Cl^-, OH^-) complexes that are hydrogen-bonded to H_2O, NH_3 and HF 75
4.1. Abstract 75
4.2. Introduction 75
4.3. Methodology 78
4.4. Results and Discussion 80
4.5. Conclusions 94

5. Gold acting as a Lewis base in the formation of halogen bonds;
A theoretical investigation 99
5.1. Abstract 99
5.2. Introduction 99
5.3. Methodology 101
5.4. Results and Discussion 104
5.5. Conclusions 130
6. Conclusions…. 135
Appendix A – Supplementary information

1. Introduction

1.1. Hydrogen bonding

The hydrogen bond (H-bond) has been the subject of countless theoretical and experimental studies for over one hundred years (see ref [1] and references therein), mostly due to its complex nature and the vast number of examples of different types of H-bonds observed to this day. This is testament to the importance of H-bonding in various fields and chemical processes. We would like to provide the reader with a brief overview of hydrogen bonding and will start off with the definition of H-bonding and how it applies to transition metal complexes, followed by known facts regarding the role of gold in H-bonding. This will be followed by a description of halogen bonding (X-bonding) and its similarities to H-bonding, with particular focus on halogen bonding in the context of transition metal complexes, progressing to Au(I) complexes.

Let us start this overview by considering the 2011 IUPAC definition of the hydrogen bond [2], which reads as follows: "The hydrogen bond is an attractive interaction between a hydrogen atom from a molecule or a molecular fragment X-H in which X is more electronegative than H, and an atom or a group of atoms in the same or a different molecule, in which there is evidence of bond formation." An H-bond can be depicted as X-H···Y-Z, where the dots represent the H-bond, with X-H being the H-bond donor and the Y atom or anion as the H-bond acceptor. Evidence for the occurrence of H-bonding can be experimentally or theoretically determined; ideally, a combination of both. The authors of the IUPAC definition list a number of criteria that need to be satisfied for an interaction to be deemed an H-bond and point out that the more criteria that are met, the more trustworthy the characterisation is. We will briefly highlight most of the criteria for H-bonding from the IUPAC definition:

- Forces involved in H-bonding are electrostatic, charge-transfer and dispersion type interactions.
- The H···Y bond strength increases as the electronegativity of X increases.
- The closer the X-H···Y angle is to linearity (180º) the stronger the H-bond, and the shorter the H···Y distance becomes.
- Upon H-bond formation, elongation of the X-H bond occurs along with a red shift in the infrared (IR) frequency of the X-H bond stretch. The more elongated the X-H

bond becomes, the shorter the H···Y distance becomes. However, blue shifted H-bonds also exist and arise due to a decrease of the X-H bond length.

The IUPAC definition also contains a few characteristics of hydrogen bonds, such as that when the electron density topology of an H-bonded system is analysed, a bond path connecting H and Y is observed along with a (3,-1) bond critical point (BCP, *vide infra*) between the H and Y atoms. Also, H-bonds are involved in proton-transfer reactions and may be considered "the partially activated precursors to such reactions."

In order to extend our understanding of H-bonds, we would also like to highlight a few facts and comments made by Steiner [1] in his review entitled "The Hydrogen Bond in the Solid State". The classical view of H-bonding is where it is represented as $X^{\delta-}$-$H^{\delta+}\cdots A^{\delta-}$, where X = O and N; A = O, N, S, halide *etc*. The problem with the classical view is that it is limited with respect to describing other H-bonds that are less frequently seen, hence the much broader IUPAC definition given above. Steiner states that the classical H-bond is just one of many known today and that H-bonding is a much broader phenomenon. However, he also states that the classical H-bond is a very abundant one and also very important. Steiner proposes a definition of the H-bond that could be applied to most H-bond examples, that reads as follows;

An X-H···A interaction is called a "hydrogen bond", if 1. It constitutes a local bond, and 2. X-H acts as proton donor to A.

Steiner also states that "The second requirement is related to the acid/base properties of X-H and A, and has the chemical implementation that a hydrogen bond can at least in principle be understood as an incipient proton-transfer reaction from X-H to A. It excludes, for example, pure van der Waals (vdW) contacts, agostic interactions…" As will be seen later, we distinguish between H-bonds and van der Waals (vdW) type interactions with the help of Atoms in Molecules (AIM). Steiner further points out that apart from the general definitions for H-bonds, there are various specialised definitions that are based on different sets of properties. As we can see judging from the IUPAC definition and the one provided by Steiner, it is extremely challenging to write a definition that encompasses all the known examples of H-bonding, including all the examples that have yet to be observed. However, the definitions listed here do provide sufficient information for us to characterise classical and nonconventional H-bonds. The parameters utilised in determining if an intermolecular interaction is a H-bond will be discussed later in this dissertation. We will follow Steiner's terminology that pertains to the donor-acceptor definition, which agrees with the IUPAC

definition, but differs from other authors who refer to electron acceptors and donors. Furthermore, we also use Steiner's terminology in referring to interaction energies, where a negative interaction energy is referred to as stabilising while a positive value refers to a destabilising interaction energy. Steiner also provides the reader with a list of H-bonds with stabilisation energies from -0.2 kcal/mol to -39 kcal/mol, along with a table that defines the properties of "strong", "moderate" and "weak" H-bonds. For instance, H-X bond elongation upon H-bond formation can range from 0.02 Å, for weak H-bonds, to 0.25 Å for strong H-bonds. Bond angles can vary from 90º (weak H-bonds) to 180º (strong and directional). Furthermore, H-bond interaction energies between 15-40 kcal/mol are considered as strong, 4-15 kcal/mol as moderate and when the interaction energy is below 4 kcal/mol it can be considered a weak H-bond.

1.2. H-bonding involving transition metals

Since the discovery of H-bonding, observations of nonconventional examples of H-bonding have continually been made. One example is H-bonding to metal centres, which seems counterintuitive when compared to classical examples of H-bonding such as that in the H_2O dimer. Conventional knowledge of transition metals (TMs) is that they are positively charged, inert atoms unable to form noncovalent interactions with neighbouring molecules, other than the expected coordination bonds.

TMs can act as both Lewis acids, i.e. agostic interactions, and Lewis bases, i.e. H-bond acceptors (see ref [3] and references therein). Martín [3] points out that metal centres (Pt, Co, Rh, Ir,Ni) that act as Lewis bases are in the d^8 and d^{10} electron configurations, while the differences between agostic interactions and hydrogen bonds yield "different structural and spectroscopic features."

In a recent study performed in 2010 by Rizzato and co-workers [4] on platinum, they published a structure obtained with neutron diffraction where H_2O is H-bonded to the Pt^{II} centre. The authors mention that water-to-metal hydrogen bonding has been previously suggested to exist by Braga and co-workers [5]. This is a rare case where this $Pt^{II}\cdots H$ interaction was suggested to exist before an experimental structure were obtained. To illustrate how significant their results were we quote Rizzato and co-workers [4] "…the first unambiguous structural evidence for nonconventional hydrogen bonding between a water molecule and a metal center." The interaction energy calculated with the MP2 method for H_2O bonding to the Pt(II) complex is -3.9 kcal/mol, and when two H_2O molecules bond to the Pt(II) complex the interaction energy becomes -7.3 kcal/mol. They also concluded that these

stabilising interaction energies were solely a product of dispersion-type interactions due to the repulsive nature of the interaction energy calculated at the Hartree-Fock (HF) level of theory, since HF does not account for electron correlation.

In 2003, in an article entitled "Metals and hydrogen bonds" Brammer [6] stated that metals can play a considerable and varied role in the formation of hydrogen bonds, be it directly or indirectly. He highlights an example where platinum acts as an H-bond acceptor such that D-H···M interactions can be viewed as Lewis acid-Lewis base interactions, where the metal acts as a Lewis base. He also mentions that Co, Rh and Ir can act as H-bond acceptors.

Zhao *et al.*[7] studying the N-H···Co hydrogen bond showed that if the basicity of the Co centre is increased the strength of the H-bond increases. They utilised IR as method of detection, noting that the change in ν(CO) is consistent with the metal centre acting as a Lewis base when the N-H···Co H-bond forms. ^{1}H NMR investigations also supported the crystallographic data in this regard suggesting that this interaction can be detected in solution. Furthermore, solution IR studies [8-10] have shown that alcohols act as H-bond donors to d^8 Co, Rh and Ir centres and also to d^6 Fe, Ru and Os metal centres.

Other metal centres that also form these unconventional H-bonds [C-H···M] are the Cu and Ni complexes studied by Siddiqui and Tiekink (see ref [11] and references therein). They provide us with geometrical parameters for C-H···M hydrogen bonds, i.e. 2.55 < C-H···M < 3.00 Å and 122º < θ < 178º. Although, these geometrical parameters are limited to Cu and Ni complexes containing the $(\cdots HCNM)_2$ synthon, they provide experimental insight as to what can be expected when investigating X-H···M hydrogen bonds. Siddiqui and Tiekink [11] conclude "$(\cdots HCNM)_2$ synthons can and do form in Ni and Cu complexes and lead to well-defined supramolecular architectures ranging from 0-D to 2-D." This shows what a significant influence these M···H interactions could have on their packing arrangement in the solid state. They showed that C-H···M hydrogen bonds play an important role when other conventional H-bonding motifs are absent. Interestingly, the authors mention that their Cambridge Structural Database (CSD) searches revealed that square planar complexes outnumber the tetrahedral complexes, consistent with steric hindrance.

Brammer [6], provided seven characteristic features of X-H···M hydrogen bonds, three of which are that "the metal atom is electron rich (typically a late transition metal) with filled d-orbitals suitably orientated to facilitate the hydrogen bond", the proton is acidic in nature, and the intermolecular interaction has a geometry that is close to 180º. Two applications of X-H···M intermolecular interactions are the protonation and deprotonation of metal centres,

and oxidative addition of D-H groups (D = N, O). Most importantly, "In crystal structures containing heavy elements, both transition and main group metals, new intermolecular interactions are increasingly being recognised as being important in directing supramolecular assembly…" [11] It seems that even though the nature of these weak C-H···M intra-/intermolecular interactions (which may be agostic, anagostic or hydrogen bond-type interactions) is well understood, the role that they play in supramolecular aggregation patterns is relatively unexplored.

1.3. Gold in the context of H-bonding

The best known and understood examples of gold acting as an H-bond acceptor are with the auride anion, which is known to exist in alkali salts such as $Cs^{+}Au^{-}$ and in solutions such as liquid ammonia and amines (see ref [12] and references therein). The effect of hydrogen bonding to the auride anion can, for instance, to be observed in Mössbauer spectra. Also, it is known that the auride anion behaves similarly to halogens when acting as an H-bond acceptor. In 2008, Kryachko [13] performed a short study on the ability of the auride anion to act as H-bond acceptor. The main aim of the research was to compare experimental to theoretical results, where H-bonded adducts of the Au^{-} ion hydrogen bonding to one or two molecules of H_2O, NH_3 and HF were investigated. Geometries of these adducts were included, and in summary, gold was unquestionably found to enter the manifold of novel H-bond acceptors.

However, since Au(I) complexes are more stable than Au^{-}, and thus appear more frequently in solution and crystal structures than the auride anion we are interested in the Au(I) centre's ability to act as a H-bond acceptor.

In order to provide the reader with a complete picture of the behaviour of Au(I) we should mention that gold can act as a Lewis acid and is currently, in the literature, a well-known example of where Au(I) interacts with a close lying C-H bond, forming an agostic interaction which has a bonding mechanism that is the exact opposite of H-bonding. Agostic interactions are where there is a charge transfer from the σ_{C-H} orbital to the metal centre, whereas H-bonding involves charge transfer from the metal centre to the σ^* orbital of the H-bond donor. Thakur and Desiraju [14] have shown that agostic or H-bond adducts of metal complexes can be distinguished by Natural Bond Orbital (NBO) analysis using the E2 delocalisation energy. The authors explicitly state that the metal centre has to be electron deficient and this criterion is essential for agostic interactions to occur. Furthermore, they conclude that NBO can distinguish between agostic and H-bonding when difficulty arises

with classification utilising geometrical parameters. Essentially, the authors state that when a borderline case emerges where it is difficult to determine whether a M···H-C contact is an agostic or weak H-bond type interaction, NBO can be employed to differentiate between the two types. We will not be discussing agostic interactions further, since we do not consider examples in this study where the Au(I) centre is electron deficient, but it is important for the reader to be aware of this fundamental difference between the two bonding mechanisms. This is what makes this study so challenging, since agostic interactions are known to exist and are relatively well understood, where Au acts as a Lewis acid, whereas there is very little evidence currently for Au acting as a Lewis base.

Schmidbaur *et al.* [12] performed a structural search of the CSD and found that although there are contacts between H atoms and Au(I) atoms, some of which are intramolecular contacts, this does not necessarily imply that an H-bond has been formed. Nevertheless they hypothesise about why the $Au^{I}\cdots HX$ interaction would be possible to observe and why it needs investigating. Their arguments are: i) gold is one of the most electronegative metals, due to relativistic effects, and could be negatively polarised similarly to when an atom bonds to a halogen; ii) the radius of gold is subject to relativistic contractions and has a significant influence on its intermolecular interactions; iii) Au^{+} has the lowest coordination number (CN 2) possible for transition metals and bonds to ligands in a linear array making the metal centre readily accessible to approaching H-bond donors and; iv) the affinity of bulk gold can change by application of electrical charge to accommodate H-bonding to water.

At this stage, however, very few experimental results are available for Au(I) acting as H-bond acceptor: to our knowledge, there are only two crystal structures (published in 2014) where an Au···H hydrogen bond has been identified as such [15]. These were obtained by Koskinen and co-workers, with both Au(I) complexes containing a *N*-methylbenzothiazole-2-thione (mbtt) ligand and a halogen consisting of either chlorine or bromine as the second ligand, thus yielding a neutral Au(I) complex. The structures were investigated using AIM analysis, which showed an atomic interaction line connecting the Au and H atoms, along with a BCP, which are two of the criteria for H-bond formation as defined by IUPAC (*vide supra*). The interaction energy of the $Au^{I}\cdots H$ hydrogen bond was calculated at -1.67 kcal/mol, which is relatively low. The authors comment that even though this interaction is relatively weak, it is the only directing intermolecular interaction along one of the crystallographic axes.

As mentioned earlier, Steiner also proposes that H-bonding should be viewed as an “incipient proton-transfer reaction”. We believe that this is a good way to look at and understand the results shown here, where gold(I) acts as a proton acceptor and we are essentially seeing the

proton transfer intermediate. When one considers H-bonding adducts to be proton-transfer reactions, the stable observed H-bonded adduct can be viewed as a "frozen" stage of the reaction.

Nevertheless we believe that the $Au^{I}\cdots H$ interaction could be experimentally more frequently observed and possibly utilised as a directing interaction in the rational design of supramolecular materials or even as a drug that could bind to proteins via the H-bonding mechanism. By showing that Au^{I} can act as Lewis base, it might better the understanding of the role of gold in medicinal chemistry in that drugs could be designed with this $Au^{I}\cdots H$ interaction in mind. Schmidbaur *et al.* [12] mentions an increasing interest displayed by a number of research groups in studying gold's H-bonding capabilities since it is used in diagnostics and therapy and could play a role in the medicinal properties of gold, influenced by its ability to form noncovalent bonds such as H-bonds. In addition, gold clusters and nanoparticles are becoming increasingly important in the medical field with regards to diagnostics and therapy, while several research groups are interested in gold's ability to form H-bonds to peptides, pteridines, uracils and other DNA bases (see ref [12] and references therein). Within these substrates there are classical H-bond donors and acceptors that "may thus exhibit specific docking properties." [12]

The medicinal properties of gold were discovered as long ago as 1890 when Koch [16] established that the dicyano Au(I) anionic complex could be used as a treatment for tuberculosis. These dicyano complexes were made popular by Danish physicians in the mid 1920s, but eventually "toxicity was considered to outweigh the alleged therapeutic benefit of all gold compounds" [17]. If we consider that the dicyano gold complex is anionic, it might be able to form H-bonds and its success could be attributed to this fact. Gold is also known, in some cases, to enhance the efficacy of cancer treatments [18], while Au(I) and Au(III) lipophilic complexes have therapeutic applications as anti-cancer treatments [19]. Recently, in a review [20] Tiekink states that systematic studies on the anti-cancer abilities of gold only started to appear in the 1980s and that various gold compounds, neutral and charged, are being investigated, although "…a clear understanding of the mechanism of action of these compounds has yet to be delineated." We hope that our study would add to this body of work needed to improve our understanding of gold's ability to form noncovalent interactions.

Typically gold compounds with anti-tumour properties contain a P-Au-S moiety in a linear arrangement although the phosphine groups may be replaced by *N*-heterocyclic carbenes, which could induce H-bonding to Au, as we will see later in this dissertation. An important advantage to Au compounds with NHC ligands is that they can be monitored by exploiting

their luminescent properties. The compound 1,2-bis(diphenylphosphino)ethane digold-dichloro [Dppe$(AuCl)_2$] has yielded promising indications of anti-tumour activity, where there is "substantial evidence to support a direct role for the gold in the anticancer activity of this complex." [21] We postulate, however, that this "direct role" of gold could possibly be due to its unknown H-bonding capabilities.

Gold complexes are being developed for HIV treatment (see ref [20] and references therein), while gold drugs are used to treat a variety of rheumatic diseases, including rheumatoid arthritis and have yielded promising results when gold therapy was employed to treat inflammatory skin disorders [21]. It is interesting to note that the active metabolite might be aurocyanide that forms due to the release of cyanide during phagocytosis, which gold then binds to. Aurocyanide is known to be able to readily enter cells and inhibit what is referred to as "oxidation bursts". If we are allowed to postulate, this mobility of the aurocyanide might be a result of weak H-bonds to gold.

Our primary aim is to broaden the understanding of gold's ability to form other noncovalent interactions to what is known in the literature, with one example being H-bond formation capabilities as a function of the coordinating ligands, where evidence is particularly lacking. Since Ag(I) and Cu(I) are also group 11 metals with a CN of 2 and therefore readily accessible to approaching molecules, we will also briefly investigate their ability to act as H-bond acceptors.

1.4. Halogen bonding

Halogen bonding (X-bonding) has been described as "a world parallel to hydrogen bonding" [22], where one of the similarities is that a Lewis base acts as the hydrogen-bond or halogen-bond acceptor. We therefore deemed it a logical expansion, due to these striking parallels [22] along with the directional tendencies [23], to determine if gold exhibits the characteristics of a Lewis base that can interact with halogens or if it is selective towards protons. To quote Brammer *et al.* [24] "Preferences for interaction geometries at the acceptor (Lewis base) are also generally consistent with those observed for hydrogen bonds…" This serves as motivation that if the Au(I) atom can act as a hydrogen-bond acceptor, it should also be able to act as halogen-bond acceptor with similar geometrical parameters. As a result, a brief overview of halogen bonding will follow.

Gonnade *et al.* [25] state that the earliest observation of a halogen atom forming an adduct with an electron donor, i.e. a Lewis base, goes back as far as 1863 with the $NH_3\cdots I_2$ adduct. The authors further point out that "These noncovalent interactions can be strong enough to

control aggregation of organic molecules in solids, solutions, liquid crystals and gas phase" (see ref [25] and references therein).

Halogen bonding was not fully understood until recently when the existence of a "σ-hole" on halogen atoms was proposed by Clark and co-workers [26] in 2007. The σ-hole is formed by a partially occupied *p*-orbital that results in a positive electrostatic potential at the tip of the halogen atom. Shortly afterwards the concept was proven and well described in an overview paper written by Politzer and co-workers [27]. The σ-hole is also referred to as "polar-flattening" since its existence is brought upon by a depletion of electron density at the tip of the halogen atom.

Since the σ-hole is usually the relatively most positive (or least negative) electrostatic region of the molecule, it also explains how halogens can interact favourably with negative sites on neighbouring molecules, thus forming halogen bonds. The directionality of halogen bonding further confirms that the origin of the σ-hole is electrostatic in nature [28]. For instance, electrophiles approach halogens at angles between 100º and 165º, while nucleophiles form almost linear adducts with X-bond donors due to the electrostatic surface potentials of the halogens [25].

Shields *et al.* [23] concluded that the linearity of hydrogen and halogen bonds can be linked to the electrostatic surface potential plots of the H-bond and X-bond donors. Furthermore, X-bonding's linearity is a result of the lone pairs on the X-bond donor atoms. The authors also state that "While hydrogen bonding does show a greater propensity for nonlinearity, the nature of the interaction fundamentally parallels halogen bonding…" They concluded that H-bonding and X-Bonding are subsets of σ-hole bonding.

To contextualise X-bonding in biological systems, we refer the reader to a review by Gonnade *et al.* [25] where they describe a survey performed on halogen bonds in proteins and nucleic acids in the protein database (PDB) that led them to conclude that the large number of halogen bonds observed "clearly demonstrate the potential significance of these interactions in ligand binding and recognition." The authors concluded by stressing the importance and applications of halogen bonding in various fields.

The most well understood and frequently studied examples of metal complexes involved in halogen bonds are the M-X···X-M type halogen bonds. Most of these studies focus on how the metal centre influences the properties of the M-X···X-M halogen bond. A comprehensive overview of these was published in 2008 by Brammer and co-workers [24] entitled "Combining metals with halogen bonds". Here they looked at C-X···X'-M halogen bonds that form networks in crystal structures. They established that the strength of these interactions

could be manipulated by changing the organic halogen-bond donor or inorganic halogen-bond acceptor.

Libri *et al.* [29] showed that metal fluorides can form strong hydrogen and halogen bonds, while Lu and co-workers [30] reported halogen bonds ranging in strength from -1.52 to -15.53 kcal/mol. This gives us a good idea of what to expect for X-bonds in the extreme case: Au···X distances should be up to 10 % shorter than the sum of the vdW radii, linear orientations close to 180º and strong interaction energies around -15 kcal/mol. Another study of strong halogen bonds, performed by Smith *et al.* [31] involves metal hydrides forming X-bonds. This occurs via the hydride that acts as halogen bond acceptor/Lewis base and halogen bonds to, for example, C_6F_5I. The calculated interaction energy of Cp_2TaH_3 binding to C_6F_5I was found to be -3.20 kcal/mol.

To our knowledge, very few stabilising M···X interactions have been reported where the metal acts as the Lewis base such that M···X-R angles are ~180º. Chemical intuition tells us that since transition metals are typically positive, they would interact as a Lewis acid and interact with the negative regions of the halogen atom, so that the M···X-R angles would deviate substantially from linearity. Au···X-R angles of approximately 180º could thus be indicative of the Lewis basicity of the gold.

Interestingly, Liau *et al.*[32] published a structure for $[Ph_3PPNPPh_3]^+ \bullet [Au(CN)]^- \bullet 0.5\ CH_2Cl_2$ containing a Cl···Au contact between the anionic aurate complex and the solvent molecule. They state that this contact is preferred over the anion-anion interactions, but do not comment on whether this could be a stabilising interaction, or a halogen bond. This Cl···Au contact the authors refer to could be a halogen bond to gold, since the gold complex is anionic, a possible candidate for Au(I) to act as a Lewis base. Another investigation worth mentioning was performed in 2004 by Schneider *et al*. [33] where it was found that oxidative addition of iodine to metals could be tuned by selecting different ligands, so that the bulkier phosphine ligands are not as readily oxidised as was the case with small trialkylphosphine ligands. More importantly, they obtained a crystal structure where an Au···I contact was observed. This suggests that an intermediate could exist where the halogenated compound forms a halogen bond to gold before the oxidative addition occurs. The fact that the bulkier ligand did not undergo oxidation could be since its electron-donating effects could be less than the trialkylphosphine ligands.

1.5. Theoretical methods and capabilities

Quantum chemistry is extremely powerful as it can be used to calculate a variety of molecular properties. For instance, using the Gaussian09 software package one can calculate high accuracy energies, optimised geometries, IR and Raman spectra, electron density, atomic charges, ionisation potentials, NMR shielding and chemical shifts, NMR spin-spin coupling constants, optical rotation values, UV/Visible spectra, vibration-rotation coupling and perform thermochemical analysis. Some of these properties may be calculated more accurately than others; the point, however, is that there is a wide range of observable quantities that can be theoretically determined. Most quantum chemical studies determining potential energies of conformers and noncovalent interaction energies calculated at the atomic/molecular level are performed in the gas phase. The reason for this is to minimise external influences on the calculated parameters and to be able to conclude that the obtained results are solely dependent on the chemistry of the individual molecules.

We will now provide the reader with an extremely brief and simple background on the fundamental differences between the two main groups of theory, i.e. the Wave Function Theory (WFT) methods, e.g. Hartree-Fock, and the Density Functional Theory (DFT) methods, also known as Kohn-Sham density functional theory. For more information, please see ref [34]. The main aim of these methods is to calculate the most accurate energy of the system possible by solving the Schrödinger equation. However, this is not possible for any system other than H and H_2^+ and as a result, assumptions had to be made in order to obtain the most accurate ground state energy value. These approximations separate DFTs from WFT methods with regards to accuracy and computational cost. WFT methods calculate the energy as a function of the orbitals and DFT methods calculate the energy as a function of the electron density. Thus, the number of assumptions made by DFT methods is more than that made by WFT methods, which therefore introduces a bias in the DFT methods. The Kohn-Sham theory utilises the exchange-correlation energy (E_{XC}), which consists of the sum of the exchange energy (E_X) and the correlation energy (E_C). The first term accounts for electrostatic contributions and the second for the weaker interactions such as vdW-type interactions. This sum of E_X and E_C is commonly utilised for all Generalised Gradient Approximation (GGA) functionals. The hybrid-GGAs (e.g. B3LYP) have a scaled E_X energy along with the exact HF exchange energy that contribute to the total E_{XC} energy. The WFT methods are known to be computationally expensive, since molecular properties are calculated *ab initio*, which means that only fundamental constants are utilised in calculating

atomic properties. In particular, the computational cost of MP2 can also be attributed to the treatment of the correlation energy.

Density Functionals (DFs) are utilised in quantum mechanical calculations because they are computationally less expensive than the Coupled-Cluster and other *ab initio* methods (e.g. HF and MP2) but yield satisfactory results when the computational cost is considered. This is also why DFs are preferred when systems with a large number of atoms are modelled, e.g. crystal structures, proteins *etc*. In the context of this dissertation, we utilise quantum mechanical methods to model noncovalent interactions, which consist of various components such as electrostatic and charge-transfer *etc*. along with those from weaker interactions such as dispersion. The latter, also referred to as dispersion, is the most difficult noncovalent interaction to account for. The biggest drawback of DFs is that they do not accurately account for this dispersion-type interaction. This is also true for the better known *ab initio* Hartree-Fock method; however, MP2 is an improvement on HF with regards to electron correlation, but is known to overestimate dispersion-type interactions when large basis sets are utilised [35].

For a comprehensive review on Density Functionals (DFs) in coordination chemistry and how they are utilised, we direct the reader towards the recent paper by Tsipis [36]. Jacob's ladder of density functional approximations for exchange correlation energy, which was summarised by Perdew and Schmidt [37] in 2001, gives the order of increasing chemical accuracy of DFs as follows: Local Density Approximation (LDA), Generalised Gradient Approximation (GGA), meta-GGA, a combination of an exact exchange and correlation method, followed by a combination of exact exchange and exact partial correlation method. Density Functionals thus fall within six major groups (in increasing order): LDA, GGA, meta-GGA, Hybrid DFs, double hybrid DFs, and range-separated DFs. The TPSS and B3LYP DFs have been selected since the first is a meta-GGA and the second a hybrid-GGA, as described by Tsipis [36]. These two methods supersede the LDA and GGA type DFs. B3LYP is the most widely used hybrid functional in quantum chemistry and shows excellent results for geometries, energies and also properties of molecules [36] with TPSS selected as the meta-GGA for comparison since the author describes it as the only nonempirical meta-GGA functional. These two DFs were selected due to their ranking on Jacob's ladder. Furthermore, no dispersion corrections were added to B3LYP or TPSS due to the fact that Gaussian09 rev B.01 only includes the D2 correction [38], which has not been scaled for the gold atom. Also, it has been previously shown [39] that B3LYP performs quite well for H-bonds, which suggest that if this DF yields comparable interaction energies to MP2, it

shows that dispersion interactions aren't that prominent. Higher levels of theory such as Coupled-Cluster (CCSD, CCSD(T) and CCSDT) were not utilised due to time constraints and high computational cost.

Along with these DFT and WFT methods, basis sets are utilised to describe the orbitals of the molecule. Ideally, one would have an infinitely large basis set to describe each atom, however, this is not computationally viable and one has to select a finite basis set. The larger the basis set, the more accurate the representation of the orbitals within a molecule, resulting in a more accurate energy. We selected the correlation-consistent (cc) type basis sets initially designed by Dunning [40], but developed for the group 11 metals by Friggen *et al.* [41]. The basis sets we have chosen also contain a pseudo potential (pp) that is aimed at recovering the correlation energy of the core electrons. Additional diffuse functions could be added to these basis sets and are denoted as the augmented ("aug" prefix) basis set; these are important for large atoms with loosely bound electrons, such as would be found in anions.

Another factor that needs to be taken into consideration is the computational time of calculations with DFs versus MP2, where DFs are known to yield better results for the time sacrificed, while MP2 may be extremely time consuming at times; this is another reason why we prefer to use a smaller basis set rather than with the augmented equivalent.

The two DFs were selected as we were interested to see if computationally less expensive methods could model these interactions and if so, how accurate they are. If we find that the DFs are capable of modelling these interactions, yielding comparable results to the more expensive MP2 methods, it would allow other researchers to apply those methods to study larger systems, such that gold forming H-bonds to amino acids, peptides or other biological systems.

1.6. Characterising noncovalent interactions

In addition to obtaining interaction energies and geometrical parameters for the hydrogen- and halogen-bonded adducts from optimised geometries, Atoms in Molecules (AIM) and Noncovalent Interaction (NCI) analyses were performed to further characterise the intermolecular interactions of interest. The analyses were performed at the highest level of theory, i.e. MP2/aug-cc-pVTZ-pp to ensure a high-quality wave function. AIM was selected as a tool due to the fact that the theory is built around electron density and its derivatives, yielding the most tangible values from an experimental point of view, since electron density can be measured by X-ray diffraction methods. Since the conception and introduction of AIM

by Bader [42] it has become well established and a much-employed quantum mechanical tool.

To quote Popelier[43] "One of the great advantages of using electron density (ρ) as a source of information, as AIM does, is that an experimental electron density can be analysed just as well as a calculated one." He also states that a theoretical wave function contains all the information there is to know about a quantum system and the electron density can be obtained by mathematical manipulation of the wave function. Furthermore, a wave function can be calculated using an *ab initio* method, which implies that it is constructed with no experimental data by only using fundamental constants. In short, AIM uses the electron density as its information source to calculate different properties.

Extremely high electron density values correspond to the positions of the nuclei and have to be normalised by means of an unbiased approach in order to obtain a three-dimensional (3D) picture of the density without normalising to an external reference of electron density. Thus, a gradient vector was defined that enables molecular density to be normalised as its own reference. The gradient vector, $\nabla\rho$, points towards the greatest increase in the electron density. A collection of gradient vectors makes up a gradient vector field. All the gradient vectors terminate at the nucleus and the gradient field makes the vectors appear as if they are "attracted" towards the nucleus, thus a nucleus is defined as a Nuclear Attractor (NA). For all intents and purposes, all gradient vectors terminating at the NA have a gradient equal to zero at the position corresponding to the NA and also never intersect. In other words, the gradient field "naturally" illustrates what portion of the total density belongs to a particular atom. The points where the gradient vectors have a zero gradient are referred to as Critical Points (CPs). One also finds that CPs referred to as non-nuclear attractors (NNAs) exist: they are 3D maxima in the electron density (ρ), but with no nuclei present.

Within the AIM theory atoms are defined by their atomic basins, this is a "region in space dominated by a nucleus" [43]. A region exists between atoms called the interatomic surface (IAS), which also has a robust mathematical definition. The IAS is defined as a surface that is not crossed by gradient paths and is often noted as being an independent object. The IASs are represented by zero-flux surfaces, also illustrated as lines, and are what separates atoms. When a bond is formed a CP is observed between the atoms at the IAS, which is defined as a Bond Critical Point, and, in short, is where the IAS reaches its maximum value of electron density. A BCP is a three-dimensional saddle point where the electron density is at a minimum value between the two atoms involved in the bond and a maximum in the other two directions, which "acts as a gateway between two bonded atoms." Popelier states that

"numerous properties can be evaluated at the BCP and used to characterise a bond." [43] A BCP occurs along a line of maximum electron density connecting two nuclei that is referred to as an Atomic Interaction Line (AIL). Popelier warns that AILs should be interpreted with care since they suggest that the atoms are in a state of "attractive stability". A representation of a molecule with a number of AILs is referred to as a molecular graph. The properties at the BCP give a "fingerprint" of the interaction [44], be it covalent or noncovalent. For instance, Nakanishi *et al*.[44] have reported ranges for three AIM parameters that are characteristic of van der Waals and H-bond type interactions by studying the behaviour of the electron density, Laplacian of the electron density and the total electronic energy density at the BCP for a range of weak to strong noncovalent and covalent interactions.

Another method to be employed in gaining qualitative insight into interactions is the NCI method, since it provides a region in three dimensions showing where noncovalent interactions occur, even in the absence of an AIL. The reason for performing the NCI plot analysis parallel to the AIM study is to probe for additional interactions, which could either induce a "false positive" result yielding interaction energies not representative of only the Au···H or Au···X interaction, or aid in the hydrogen- and halogen-bond formation. Since the introduction of this method in 2010 by Johnson *et al.* [45] the paper has been cited over 430 times, which illustrates the valuable insight it provides the chemist. The NCI plotting method relies on two quantum mechanical quantities, i.e. the electron density and the Laplacian of the electron density. The electron density is converted to the reduced electron density gradient (*s*) defined by the density and its first derivative, to give the regions where intermolecular interactions are present, by the following equation obtained from [45]:

$$s = 1/(2(3\pi^2)^{\frac{1}{3}})|\nabla\rho|/\rho^{4/3})$$

Here *s* is a "fundamental dimensionless quantity in DFT and used to describe the deviation from a homogenous electron distribution." The Laplacian of the electron density ($\nabla^2\rho$) consists of three eigenvalues, arranged in increasing order, i.e. λ_1, λ_2 and λ_3, obtained by reducing the Hessian matrix. The sign of the second eigenvalue of the Laplacian of the density is utilised to determine whether the interaction is bonding or non-bonding ($\lambda_2 < 0$, bonding; $\lambda_2 > 0$, non-bonding). The sign of λ_2 is multiplied by the density in order to colour the reduced gradient plot and is denoted as sign(λ_2)*ρ, which is plotted over the regions defined by *s*. Furthermore, it has been shown that if λ_2 is close to 0 but still negative it is a dispersion-type interaction, and as the stabilisation of the interaction increases λ_2 becomes more negative. The most significant and revolutionary fact about this method is that one does

not need to use a level of theory that fully accounts for dispersion-type interactions to determine if the interaction is dispersive in nature, since it performs an analysis of the density (reduced density) and the second eigenvalue of the Laplacian of the electron density. This enables the NCI analysis of large systems such as crystal structures or proteins utilising computationally less expensive methods such as DFT. Another immense advantage is that the NCI plot method is independent of the atomic interaction line and bond critical points that are needed by AIM to gain insight into the intermolecular interaction. This is exactly how Johannson and Swart [46] employed the NCI plot method, by analysing intramolecular halogen-halogen interactions where no atomic interaction line is present, enabling them to conclude qualitatively that the interaction is a dispersion-type interaction. To quote Johannson and Swart "The beauty of the approach lies in its ability to pinpoint the interactions in real-space, thus enabling a graphical visualisation of the regions where non-covalent interactions occur." However, one possible drawback to NCI plots could be how they perform with long range interactions that are far beyond the sum of vdW radii for any two interacting atoms where the reduced density is zero. Nevertheless, we have to conclude that this method is extremely useful even though it is somewhat limited to short range interactions in cases where atomic interaction lines are present or, most importantly, where no atomic interaction lines are found.

1.7. Aims and objectives

The main aim of this study is to prove that Au(I) can act as a hydrogen and halogen bond acceptor, i.e. as a Lewis base. Our investigation starts with the Au^- ion and its ability to act as H-bond and X-bond acceptor, since it is already known to exist and also to act as an H-bond acceptor. Calculating these Au^--containing systems enables us to obtain geometrical, energetic and AIM parameters, as well as generate NCI plots, that will serve as reference points. Furthermore, we assume that the Au^- ion will be the strongest Lewis base that can possibly be obtained with gold, thus yielding the most stabilising H-bond and X-bond energies. The H-bonded and X-bonded adducts of the Au^- ion can thus be thought of as theoretical precursors to our study. Therefore, we expect any anionic Au(I) complex to yield less stabilising interaction energies, as well as longer Au···H and Au···X distances *etc*.

We have selected the $[(Me)_2Au]^-$ ion as our model complex, since the CH_3 ligands are relatively small electron-donating ligands, so as to yield an overall greater negative charge on the gold atom.

Also, the computational cost of these adducts is significantly less than that for the large complexes commonly found in crystal structures. An anionic complex was selected so that we remain consistent with the total charge of the gold-containing atom/molecule. The aim is to find stable conformations where hydrogen and halogen bonding occur to yield insight into the capability of the $[(Me)_2Au]^-$ complex to act as a Lewis base and then to elucidate the properties of the $Au^I\cdots H$ and $Au^I\cdots X$ interactions.

We aim to show that the calculated geometrical changes and calculated AIM parameters of the hydrogen and halogen bonded adducts provide sufficient evidence that the noncovalent bonds formed are comparable to classical, known examples of hydrogen and halogen bonding, as defined by IUPAC. The Cu(I) and Ag(I) analogues of $[(Me)_2Au]^-$ will also be subject to investigation with regards to their ability to form hydrogen and halogen bonds. This should shed light on whether gold's behaviour in this respect is unique or whether it is typical of the group 11 elements.

We will also expand our study on H-bonds by investigating the influence of electron-withdrawing and donating-groups on the ability of an anionic Au(I) complex to act as an H-bond acceptor. Neutral Au(I) complexes will also be used to investigate whether Au(I) could still be a strong enough base to act as an H-bond acceptor, i.e. we aim to determine how weak a Au(I) Lewis base can be before it stops forming H-bonds. The model complexes chosen for this section contain an *N*-heterocyclic carbene (NHC) as a ligand along with an anionic ligand to yield a neutral complex. Due to time constraints, we could not investigate the ability of neutral Au(I) complexes to act as X-bond acceptors. Nevertheless, we hope that by showing that a particular complex could act as H-bond acceptor, it should also be considered that the same Au(I) complex would be able to act as an X-bond acceptor. In addition, we also intend to show that the basicity of the Au(I) can be changed depending on the ligand. Finally, our most ambitious aim is that this work will act as a stepping stone towards other studies where chemists harness the ability of gold as a directional supramolecular synthon, by providing examples of what criteria need to be met for the $Au^I\cdots H$ interaction to occur.

All the work presented in this dissertation is my own; Prof Dillen and Prof Esterhuysen aided in the editing of this document. Also, all the work presented here is in article format and ready to publish.

References

1. Steiner, T., *Angew. Chem. Int. Ed.*, 2002. **41**: p. 48-76.
2. Arunan, E., Desiraju, G.R., Klein, R.A., Sadlej, J., Scheiner, S., Alkorta, I., Clary, D.C., Crabtree, R.H., Dannenberg, J.J., Hobza, P., Kjaergaard, H.G., Legon, A.C., Menucci, B., Nesbitt, D.J., *Pure Appl. Chem*., 2011. **83**(8): p. 1637-1641.
3. Martín, A., *J. Chem. Edu*., 1999. **76**(4): p. 578.
4. Rizzato, S., Bergès, J., Mason, S.A., Albinati, A., Kozelka, *J., Angew. Chem. Int. Ed*., 2010. **49**: p. 7440-7443.
5. Braga, D., Grepioni, F., Tedesco, E., Biradha, K., Desiraju, G. R., *Organometallics*, 1999. **16**: p. 1846-1856.
6. Brammer, L., *Dalton Trans.*, 2003(16): p. 3145-3157.
7. Zhao, D., Ladipo, F.T., Braddock-Wilking, J., Brammer, L., Sherwood, P., *Organometallics*, 1996. **15**(5): p. 1441-1445.
8. Kazarian, S. G., Hamley, P.A., Poliakoff, M., *J. Am. Chem. Soc.*, 1993. **115**.
9. Shubina, E.S., Krylov, A.N., Timofeeva, T. V., Struchkov, Y.T., Ginzburg, A. G., Loim, N. M., Epstein, L. M., *J. Organomet. Chem*. 1992. **434**.
10. Shubina, Y.S., Epstein, L.M.., *J. Mol. Struct.*, 1992. **265**.
11. Siddiqui, K.A. Tiekink, E.R.T., *Chem. Commun*., 2013. **49**(76): p. 8501-8503.
12. Schmidbaur, H., Raubenheimer, H.G., Dobrzanska, L., *Chem. Soc. Rev*., 2014. **43**(1): p. 345-380.
13. Kryachko, E.S., *J. Mol. Struct*., 2008. **880**(1–3): p. 23-30.
14. Thakur, T.S., Desiraju, G.R., *J. Mol. Struct.: THEOCHEM*, 2007. **810**(1–3): p. 143-154.
15. Koskinen, L., Jääskeläinen, S., Kalenius, E., Hirva, P., Haukka, M., *Cryst. Growth & Des*., 2014. **14**(4): p. 1989-1997.
16. Koch, R., *Dtsch. Med. Wochenschr*., 1890. **16**: p. 756.
17. Benedek, T.G., *J. Hist. Med. Allied Sci*., 2004. **59**(1): p. 50-89.
18. Wójcik, M., Lewandowski, W., Król, M., Pawłowski, K., Mieczkowski, J., Lechowski, R., Zabielska, K., *PLoS ONE*, 2015. **10**(4): p. e0124955.
19. Che, C.M., Sun, R.W.Y., *Chem. Commun*., 2011. **47**(34): p. 9554-9560.
20. Tiekink, E.R.T., *Inflammopharmacology*, 2008. **16**(3): p. 138-142.
21. Pricker, S., *Gold Bull*., 1996. **29**(2): p. 53-60.
22. Metrangolo, P., Neukirch, H., Pilati, T., Resnati, G., *Acc. Chem. Res*., 2005. **38**(5): p. 386-395.
23. Shields, Z.P., Murray, J.S., Politzer, P., *Int. J. Quant. Chem*., 2010. **110**(15): p. 2823-2832.
24. Brammer, L., Minguez Espallargas, G., Libri, S., *CrystEngComm*, 2008. **10**(12): p. 1712-1727.

25. Gonnade, R.G., Shashidhar, M.S., Bhadbhade, M.M., *J. Ind. Inst. Sci.*, 2007. **87**(2): p. 149-165.
26. Clark, T., Hennemann, M., Murray, J., Politzer, P., *J. Mol. Model*., 2007. **13**(2): p. 291-296.
27. Politzer, P., Lane, P., Concha, M., Ma, Y., Murray, J., *J. Mol. Model*., 2007. **13**(2): p. 305-311.
28. Mohajeri, A., Pakiari, A.H., Bagheri, N., *Chem. Phys. Lett*., 2009. **467**(4–6): p. 393-397.
29. Libri, S., Jasim, N.A., Perutz, R.N., Brammer, L., *J. Am. Chem. Soc.*, 2008. **130**(25): p. 7842-7844.
30. Lu, Y.-X., Zou, J.-W., Wang, Y.-H., Jiang, Y.-J., Yu, Q.-S., J. *Phys. Chem. A*, 2007. **111**(42): p. 10781-10788.
31. Smith, D.A., Brammer, L., Hunter, C.A., Perutz, R.N., *J. Am. Chem. Soc.*, 2014. **136**(4): p. 1288-1291.
32. Ruei-Yang Liau, H.E., Anette Schier, Hubert Schmidbaur, *Z. Naturforsch*., 2002. **57b**: p. 1085-1089.
33. Schneider, D., Schier, A., Schmidbaur, H., *Dalton Trans*, 2004(13): p. 1995-2005.
34. Koch W, Holthausen, M.C., *A Chemist's guide to Density Functional Theory*. Vol. 1. 2000: Wiley-VCH.
35. Riley, K.E., Hobza, P., *J. Phys. Chem. A*, 2007. **111**(33): p. 8257-8263.
36. Tsipis, A.C., *Coor. Chem. Rev*., 2014. **272**: p. 1-29.
37. Perdew, J.P. Schmidt, K., *AIP Conference Proceedings*, 2001. **577**(1): p. 1-20.
38. Grimme, S., *J. Comp. Chem*., 2006. **27**(15): p. 1787-1799.
39. Lusi, M., de Villiers, D., Esterhuysen, C., *Cryst. Growth & Des*., 2014. **14**(7): p. 3480-3484.
40. Dunning, T.H., *J. Chem. Phys*, 1989. **90**(2): p. 1007-1023.
41. Figgen, D., Rauhut, G., Dolg, M., Stoll, H., *Chem. Phys*., 2005. **311**(1–2): p. 227-244.
42. Bader, R.F.W., *Acc. Chem. Res*., 1985. **18**(1): p. 9-15.
43. Popelier, P., *Atoms In Molecules; An Introduction*2000, UMIST, Manchester, UK: Prentice Hall. 164.
44. Nakanishi, W., Hayashi, S., Narahara, K., *J. Phys. Chem. A*, 2008. **112**(51): p. 13593-13599.
45. Johnson, E.R., Keinan, S., Mori-Sánchez, P., Contreras-García, J., Cohen, A.J., Yang, W., *J. Am. Chem. Soc.*, 2010. **132**(18): p. 6498-6506.
46. Johansson, M.P., Swart, M., *Phys. Chem. Chem. Phys*., 2013. **15**(27): p. 11543-11553.

2. Gold setting the "gold standard" among transition metals as a hydrogen bond acceptor – a theoretical investigation.

2.1. Abstract

In this theoretical study we investigate the ability of the Au(I) centre to act as a hydrogen-bond acceptor when bound to two methanide ligands, in order to provide theoretical evidence that Au(I) can act as a Lewis base and form hydrogen bonds. We first explore the accepted hydrogen-bond acceptor: the auride anion and a range of its hydrogen-bonded adducts in order to characterise the known $Au^{-}\cdots H$ interaction based on geometrical and Atoms in Molecules (AIM) parameters, and simultaneously test the auride anion's ability to act an acceptor for several hydrogen bond donors ranging in acidity. The calculations were performed utilising the B3LYP, TPSS and MP2 methods and the aug-cc-pVTZ-pp and cc-pVTZ-pp basis sets with HF, HCN, HCCH, H_2O, NH_3 and CH_4 as the selected hydrogen bond donors. The dimethylaurate anionic (DMA) complex yields calculated geometrical and AIM parameters comparable to those for the auride anion, varying in strength from -2.4 kcal/mol to -16.0 kcal/mol at the MP2/aug-cc-pVTZ-pp level of theory, yielding compelling evidence that the DMA anionic complex can act as a hydrogen-bond acceptor, with strong hydrogen bonds to HF and relatively weak hydrogen bonds with HCN, HCCH, H_2O, NH_3 and CH_4. AIM results and NCI plots provide additional insight into these interactions.

2.2. Introduction

Transition metals are unusual since they can act as both Lewis acids and Lewis bases (see ref [1] and references therein). One example of a metal acting as a Lewis acid occurs during "agostic" interactions, which are observed when there is charge transfer from the C-H bond to the metal centre. On the other hand, transition metals in low oxidation states may act as hydrogen-bond (H-bond) acceptors, thus behaving as Lewis bases. Martín [1] points out that these metal centres (Pt, Co, Rh, Ir,Ni) forming H-bonds are in the d^8 and d^{10} electron configurations. Differences between agostic and H-bonding interactions result in "different structural and spectroscopic features."

In 2013, Siddiqui and Tiekink [2] noted that when traditional hydrogen bonding is absent other noncovalent interactions start playing an increasingly important role. Their Cambridge Structural Database (CSD) analysis of C-H···M interactions in $(\cdots HCNM)_2$ synthons revealed that the distance between H and M, where M is a transition metal, is between

2.4 and 3.0 Å for Ni and Cu within the $(\cdots HCNM)_2$ synthons, while square planar complexes outnumber tetrahedral complexes, consistent with steric hindrance. They predict that the $(\cdots HCNM)_2$ synthon would most likely be less stabilising than the OH···Pt hydrogen bond that was calculated by Rizzato and co-workers [3] to be 3.9 kcal/mol in strength. Siddiqui and Tiekink conclude with the statement "$(\cdots HCNM)_2$ synthons can and do form in Ni and Cu complexes and lead to well-defined supramolecular architectures ranging from 0-D to 2-D."

Work by Zhao *et al.* [4] on N-H···Co hydrogen bonds showed that if the basicity of the Co centre is raised, by changing the ligands coordinating to the metal centre, it increases the strength of the H-bond. The authors utilised IR frequencies to show that the change in ν(CO) is consistent with the metal centre acting as a Lewis base. ^{1}H NMR studies revealed these adducts exist in nonpolar solvents and the dependence of the N-H···Co distances, observed in the solid state structures, on the basicity of the metal centre. Zhao *et al.* [4] also listed solution IR studies [5-7] by other authors that showed evidence of alcohols H-bonding to d^8 Co, Rh and Ir centres and also to d^6 Fe, Ru and Os metal centres. These metals were also identified by Brammer [8] who lists seven characteristic features of X-H···M hydrogen bonds, three of which are that "the metal atom is electron rich (typically a late transition metal) with filled d-orbitals suitably orientated to facilitate the hydrogen bond", the proton is acidic in nature and the intermolecular interaction has a geometry that is close to 180º.

Siddiqui and Tiekink [2] write "In crystal structures containing heavy elements, both transition and main group metals, new intermolecular interactions are increasingly being recognised as being important in directing supramolecular assembly…" Although they state that weak C-H···M intra-/intermolecular agostic, anagostic and hydrogen bond type interactions and their nature are well understood, the authors note that the role this C-H···M interaction plays in supramolecular aggregation patterns is relatively unexplored.

This is important since X-H···M intermolecular interactions can be used in the protonation and deprotonation of metal centres as well as oxidative addition of D-H groups (D = N, O).

In 2003, Brammer [8] wrote an article entitled "Metals and hydrogen bonds" where he points out that metals can play a considerable to varied role in the formation of hydrogen bonds, be it directly or indirectly. He highlights an example where platinum acts as an H-bond acceptor and that these D-H···M interactions can be viewed as Lewis acid-Lewis base interactions, where the metal act as a Lewis base.

In an extensive review on the auride anion written by Jansen [9] in 2008, he notes that the auride anion is intrinsically stable in vacuum and that gold has the highest first electron affinity of all the metals and rivals that of halogens. The auride anion has been prepared in

liquid ammonia [10] and ethylenediamine [11]. In 2008, Kryachko [12] published a theoretical study on the auride anion and its ability to form H-bonds, in order to perform a thorough comparison between experimental findings and theoretical results. In his study he showed that a single auride anion can act as H-bond acceptor to two H-bond donors simultaneously. The donors investigated were HF, H_2O and NH_3. Kryachko writes "…gold does enter the manifold of the hydrogen bond as a novel proton acceptor" and points out work by others [12] where it was shown that the auride anion behaves like the heavier halides, i.e. Br^- and I^-. We would like to highlight the fact that Kryachko also wrote the following: "We believe the present work initiates future studies on molecular complexes with nonconventional X-H···Au hydrogen bonds." This is true since this served as an incentive for the work described here. We investigated the most basic example of gold acting as a hydrogen bond acceptor, i.e. the auride anion [12], and what we believe to be a comparable example, namely the dimethylauride (DMA) anion.

Furthermore, in a recent review article written by Schmidbaur *et al.* [13] the authors make some convincing arguments as to why they think the Au(I) centre can act as a Lewis base with regards to the properties of Au(I) and its complexes. Firstly, Au(I) has the lowest oxidation number with only two ligands in a linear array making the metal atom readily accessible to approaching H-bond donors. Secondly, gold clusters and nanoparticles are becoming increasingly important for diagnostics and therapy and are ever more frequently investigated by research groups in order to determine bonding interactions between gold ions and peptides or other DNA bases, where they may exhibit specific docking properties. Lastly, they point out that gold is the most electronegative transition metal, due to relativistic effects. Schmidbaur *et al.* [13] refer to quantum mechanical calculations that suggest that relativistic effects are particularly relevant with regards to some basic thermodynamic and structural characteristics of gold, including electron affinity. The authors also mention observations of agostic interactions where there is an Au···H-C contact. However, the bonding mechanism of agostic interactions is the exact opposite of H-bonding, i.e. agostic interactions exhibit charge transfer from the $\sigma_{C\text{-}H}$ to the metal, while H-bonding involves charge transfer from the metal to the σ^* of the H-bond donor. This was shown by critical Natural Bond Orbital (NBO) analyses performed by Thakur and Desiraju [14] on various metal complexes, which indicated that agostic and H-bonding interactions can be distinguished by analysing the E2 delocalisation energy. The authors explicitly state that "Electron deficiency at the metal centre is an essential criterion for agostic behaviour." In addition, they concluded that NBO

can distinguish between agostic and H-bonding when difficulties arise with classification utilising geometrical parameters.

Very little experimental work is available for Au(I) acting as H-bond acceptor. Our preliminary CSD results are consistent with findings by Schmidbaur *et al.* [13] that there are contacts between H atoms and Au(I) atoms, but this does not necessarily imply a H-bond has been formed. However, there are two crystal structures (published in 2014) where an $Au^{I}\cdots H$ hydrogen bond was noted [15]. In both, the Au(I) complexes have a *N*-methylbenzothiazole-2-thione (mbtt) ligand and a halogen ligand consisting of either a chloride and bromide yielding neutral Au(I) complexes. The authors performed AIM analyses on these two crystal structures, which will be discussed later in this article. The observation of the $Au^{I}\cdots H$ hydrogen bond is surprising since their calculated interaction energy of -7 kJ/mol is relatively low compared to the results shown here.

Work by Dem'yanov and Gschwind [16] on the dimethylcuprate(I) anion showed that Cu(I) forms hydrogen bonds to C-H hydrogen bond donors, which are weak van de Waals (vdW) type interactions. Atoms in Molecules (AIM) analyses unveiled an atomic interaction line joining the Cu(I) centre to the neighbouring hydrogen atom on methane or propane that points towards the metal centre. Methane and propane thus form complexes with the dimethylcuprate anion with similar dissociation energies of approximately 1.0 kcal/mol. As a result, we deemed it appropriate to also briefly investigate the ability of the Ag(I) and Cu(I) analogues to DMA to act as H-bond donors for comparison.

The main aim, however, is to prove that Au(I) can act as a H-bond acceptor to a variety of H-bond donors. We do so by providing convincing theoretical evidence, such as geometrical and AIM parameters in conjunction with NCI plots, that this $Au^{I}\cdots H$ interaction exhibits all the characteristics of a classic H-bond according to the IUPAC definiton and is comparable to that in the H-bonded adducts of the auride anion.

We start our theoretical investigation with the auride anion and its ability to form H-bonds with a selected series of model H-bond donors, in order to benchmark our method against Kryachko's. We then move on to H-bond adducts of the DMA anionic complex, where the properties of the H-bonds formed by the auride anion are compared to those with DMA. In addition, the H-bond acceptor abilities of the Cu(I) and Ag(I) analogues to DMA are investigated to determine if H-bond formation is unique to Au(I) and how the stabilisation of these adducts compare to DMA. Finally, we investigate the role of relativistic effects on the H-bond capabilities of the auride anion and DMA anionic complex, since it has been noted previously [13] that relativistic effects can have an effect on certain properties of gold.

2.3. Methodology

All calculations were performed in the gas phase utilising the Gaussian 09 rev B.01 [17] software package. No symmetry constraints were enforced by including the "NoSymm" keyword for all geometry optimisations, which were performed with counterpoise corrections to avoid the basis set superposition error (BSSE) [18, 19]. Frequencies were calculated to confirm that optimised structures were energy minima.

The interaction energy was calculated by:

$$E_{INT} = E_{AB}^{BSSE} - (E_A + E_B)$$

The individual geometries (A and B) of the H-bonded adduct (AB) were utilised to calculate the individual fragment's monomeric potential energy. The magnitude of the elongation of the H-X bonds upon H-bond formation was calculated by subtracting the optimsed H-X bond length in the donor (HX) from the length in the H-bonded adduct [$(HX)_B$]: $\Delta R = (HX)_B - (HX)$. The Hartree-Fock (HF) energy and the E2 energy (MP2 correlation energy) were extracted from a single-point energy calculation of the optimised geometry, with no counterpoise corrections, at the MP2/aug-cc-pVTZ-pp level of theory. The HF and E2 energies of fragments A and B were extracted from the H-bonded adduct. The respective HF_{INT} and $E2_{INT}$ energies were calculated as follows.

$$X_{INT}(X = HF\ or\ E2) = E_{AB}^{X} - (E_A^X + E_B^X)$$

The B3LYP [20-22] and TPSSTPSS (hereafter TPSS) [23] Density Functionals (DFs) were utilised in combination with the aug-cc-pVTZ-pp [24] basis set for describing the metals (Au, Cu and Ag) with the effective core potential (ECP) designed by Friggen *et al.*[25], while the remaining atoms (H, C, F, O, N) were described by the same basis set (the aug-cc-pVTZ [26, 27]). Furthermore, the wave function theory (WFT) method MP2 [28, 29] was utilised in combination with the cc-pVTZ-pp (hereafter designated as MP2*) and the aug-cc-pVTZ-pp (hereafter MP2) [24] basis sets with an ECP [25] for the Au, Ag and Cu atoms, to decrease computational cost and account for relativistic effects. Again, the cc-pVTZ and aug-cc-pVTZ basis sets were used to describe the H, C, F, O, N atoms during the MP2* and MP2 optimisations, respectively. All the basis sets were downloaded from the EMSL basis set exchange website [30, 31]. In order to model gold with no relativistic effects, the ECP60MHF [32] basis set was utilised in combination with the ECP60MHF_MP2 ECP [33], while the aug-cc-pVTZ basis set was used to describe the remaining atoms. The optimised geometries were visually investigated utilising the ChemCraft [34] suite.

The Atoms In Molecules analyses were performed utilising AIMAll [35] version 14.06.21. The electron density [ρ_b (ea_0^{-3})] and Laplacian of the electron density $\nabla^2(\rho_b)$ (ea_0^{-5}) at the intermolecular Bond Critical Point (BCP) situated between Au and H, were obtained as is from AIMAll. The total electronic energy density (H_b) was calculated as $[H_b\ (au)] = -1 * K\ (au)$. The b subscript indicates that it is a property of the BCP situated between Au and H. Wave functions were obtained as *.wfx files for the optimised geometries performed at the MP2/aug-cc-pVTZ-pp level of theory utilising the Gaussian software suite. The Non-Covalent Interaction (NCI) plots, as proposed by Johnson *et al.* [36], were calculated from the same wave function and were graphically displayed utilising AIMAll. The Reduced Electron Density Gradient (RDG) isosurfaces were calculated with a resolution of 0.04 au. The isosurface visualisation of the RDG surface was calculated at a value of 0.5 au and with minimum and maximum electron densities of 0.0001 and 0.05 ea_0^{-3}, respectively. The maximum density was changed to 0.03 ea_0^{-3} for the NCI analyses of the Ag(I) and Cu(I) structures due to higher density artifacts emerging around the BCP situated between the metal and coordinating atom. The RDG surfaces were visualised by mapping the "Sign(HessRho_EigVal_2)*Rho" values onto them. The colour scale ("Range Method") was the "-Maximum Magnitude to +Minimum Magnitude". Red indicates a negative or greater negative sign(λ_2)×ρ value and blue the positive value of sign(λ_2)×ρ and are scaled according to the largest absolute values. Therefore, each colour scheme has been scaled in proportion to itself; for further information the value of sign(λ_2)×ρ has been included for each example.

The Electrostatic Surface Potential (ESP) isosurfaces were calculated, utilising AIMAll, at a surface defined at an electron density of 0.001 au, with the ESP projected onto the isodensity surface. The colour scale ("Range Method") of the ESP surface was selected as the "Minimum to Maximum" to emphasise fine structural details on the surface. The ESP analysis was performed at the B3LYP/aug-cc-pVTZ-pp and MP2/aug-cc-pVTZ-pp levels of theory.

2.4. Results and Discussion

Optimisation of H-bond adducts between the auride anion, Au^-, and H-bond donors, HF, HCN, HCCH, H_2O, NH_3 and CH_4 showed that in all cases stable minimum energy structures were obtained (Figure 1).

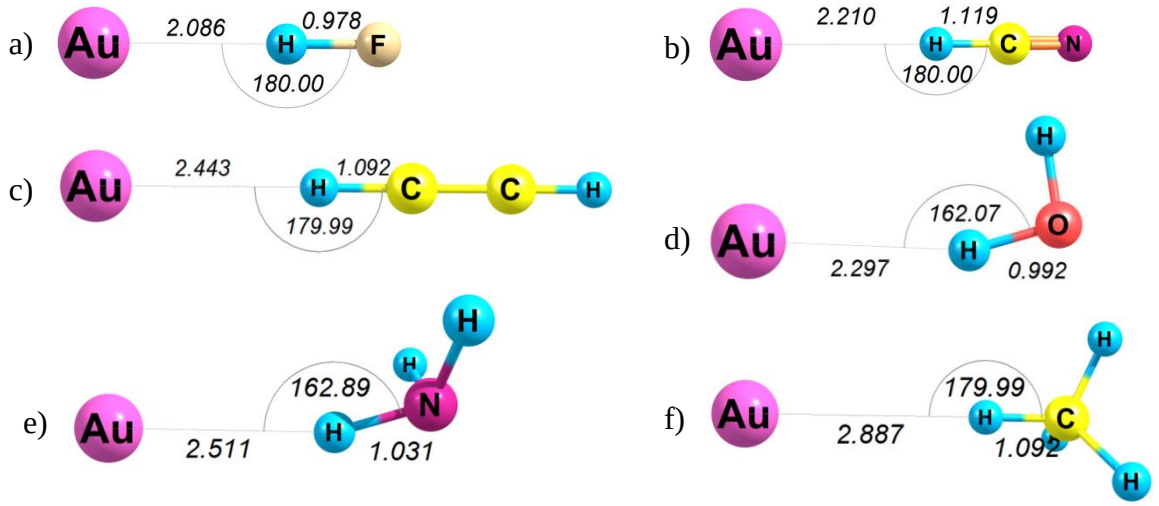

Figure 1 – Optimised geometries of the auride anion H-bonded to a) HF, b) HCN, c) HCCH, d) H_2O, e) NH_3 and f) CH_4 at the MP2/aug-cc-pVTZ-pp level of theory.

Interaction energies and important optimised geometrical parameters for the Au···H contacts are listed in Table 1 for all six H-bonded adducts. For comparison, we define the sum of the vdW radii of H-bonded gold adducts to be 2.86 Å, based on vdW radii of 1.66 Å for Au and 1.2 Å for the hydrogen atom [37].

Interaction energies [E_{INT}] for the various adducts are listed in Table 1. We consider the MP2* (MP2/cc-pVTZ-pp) level of theory as the benchmark, since previous work by us [38] and others [39] have shown that MP2* yields a good balance between electrostatic and dispersion interactions. Furthermore, the MP2 method with large basis sets, such as aug-cc-pVTZ-pp, is known to overestimate dispersion-type interactions [38], even though the calculated E_{INT} at the B3LYP/aug-cc-pVTZ-pp level of theory is closest to the experimental result of E_b^{ZPVE} = 10.38 kcal/mol, with E_b^{ZPVE} being the zero-point vibrational energies calculated by anion photoelectron spectroscopy measurements [40]. This is likely due to cancellation of errors since B3LYP's inability to model dispersion-type interactions is well known [38], hence it may yield poorer E_{INT} values for other H-bonded adducts with a greater dispersion component investigated later in this paper.

Kryachko [12] calculated the dissociation energies corrected for zero-point vibrational energy of 20.3 kcal/mol, 11.9 kcal/mol, 6.0 kcal/mol for the auride anion H-bonded to HF, H_2O and NH_3, respectively, which are comparable to our calculated E_{INT} values of -19.9 kcal/mol, -12.97 kcal/mol and -7.63 kcal/mol at the MP2* level of theory, for the same H-bonded adducts (we use the convention where the stabilising interactions are negative).

Furthermore, the reported Au···H distances of 2.156 Å, 2.444 Å and 2.960 Å for HF, H_2O and NH_3 H-bonded to Au^- [12] also compare relatively well to the MP2* values given in

Table 1. Kryachko found the Au···H-F angle to be 178.2º, compared to our 180º. In addition, he found the Au···H-O and Au···H-N angles to be 156-157º, which are comparable to values of 161-164º listed in Table 1. We conclude that our results for the H-bonded auride anion are both consistent with and comparable to those of Kryachko. The Au···H distances for Au^- H-bonded to HF, HCN, H_2O and NH_3 are all within the sum of the vdW radii (2.86 Å) for all levels of theory. Also, we see that the lowest E_{INT} value, obtained with the DF B3LYP, yields the largest Au^-···H distance with a value of 3.22 Å. It is interesting to note that the *d*(Au···H) distances calculated by DFs are substantially more elongated than those obtained with MP2, with values ranging from 2.89 Å for MP2 to 3.22 Å for B3LYP.

Most of the H-bonded adducts exhibit almost perfectly linear (HF, HCN, HCCN, CH_4) and nearly linear (NH_3, H_2O) Au···H-X angles, between 160º and 170º. This agrees with the study by Brammer in 2003 [8], who found that H-bonds to metal centres should be close to 180º. Interestingly, only the NH_3 and H_2O H-bond donors deviate from linearity, but this is consistent with the results by Kryachko [12].

Table 1 – Interaction energies (E_{INT}) in kcal/mol, intermolecular distance [*d*(Au···H)] in Å, bonding angles (Au···H-X) in º and H-X distances in Å for the optimised geometries of the H-bonded auride anion adducts at four different levels of theory.

Method	H-bond donor	E_{INT} (kcal/mol)	*d*(Au···H) (Å)	Au···H-X (deg)	H-X (Å)
B3LYP	HF	-19.96	2.16	180.0	0.98
TPSS		-23.24	2.06	180.0	1.00
MP2*		-19.89	2.15	180.0	0.96
MP2		-23.41	2.09	180.0	0.98
B3LYP	HCN	-16.52	2.36	180.0	1.11
TPSS		-18.93	2.22	180.0	1.13
MP2*		-19.55	2.25	180.0	1.11
MP2		-21.59	2.21	180.0	2.21
B3LYP	HCCH	-6.24	2.67	180.0	1.08
TPSS		-7.58	2.50	180.0	1.10
MP2*		-9.10	2.49	180.0	1.09
MP2		-10.30	2.44	180.0	1.09
B3LYP	H_2O	-11.63	2.40	161.9	0.99
TPSS		-13.15	2.29	165.1	1.01
MP2*		-12.97	2.37	161.7	0.98
MP2		-15.09	2.30	162.1	0.99
B3LYP	NH_3	-6.03	2.69	161.8	1.03
TPSS		-7.07	2.53	164.1	1.04
MP2*		-7.63	2.58	163.9	1.03
MP2		-8.86	2.51	162.9	1.03
B3LYP	CH_4	-1.18	3.22	179.9	1.09
TPSS		-1.65	3.04	180.0	1.10
MP2*		-2.47	2.93	180.0	1.09
MP2		-2.93	2.89	180.0	1.09

When considering the E_{INT} values in Table 1, we note that they decrease in the order HF > HCN > H_2O > HCCH > NH_3 > CH_4, such that Au^- forms strong H-bonds to HF, HCN and H_2O while the other H-bond donors yield weakly H-bonded adducts. The $Au^-\cdots H$ distances follow the same trend as the E_{INT} values, where the $Au^-\cdots H$ distances are inversely proportional to E_{INT} i.e. the more stabilising the interaction energy, the shorter the Au···H distance.

In order to investigate the nature of this interaction AIM analysis was performed. The molecular graphs of the optimised H-bonded auride adducts are shown in Figure 2 and the properties of the $Au^-\cdots H$ BCPs are given in Table 2.

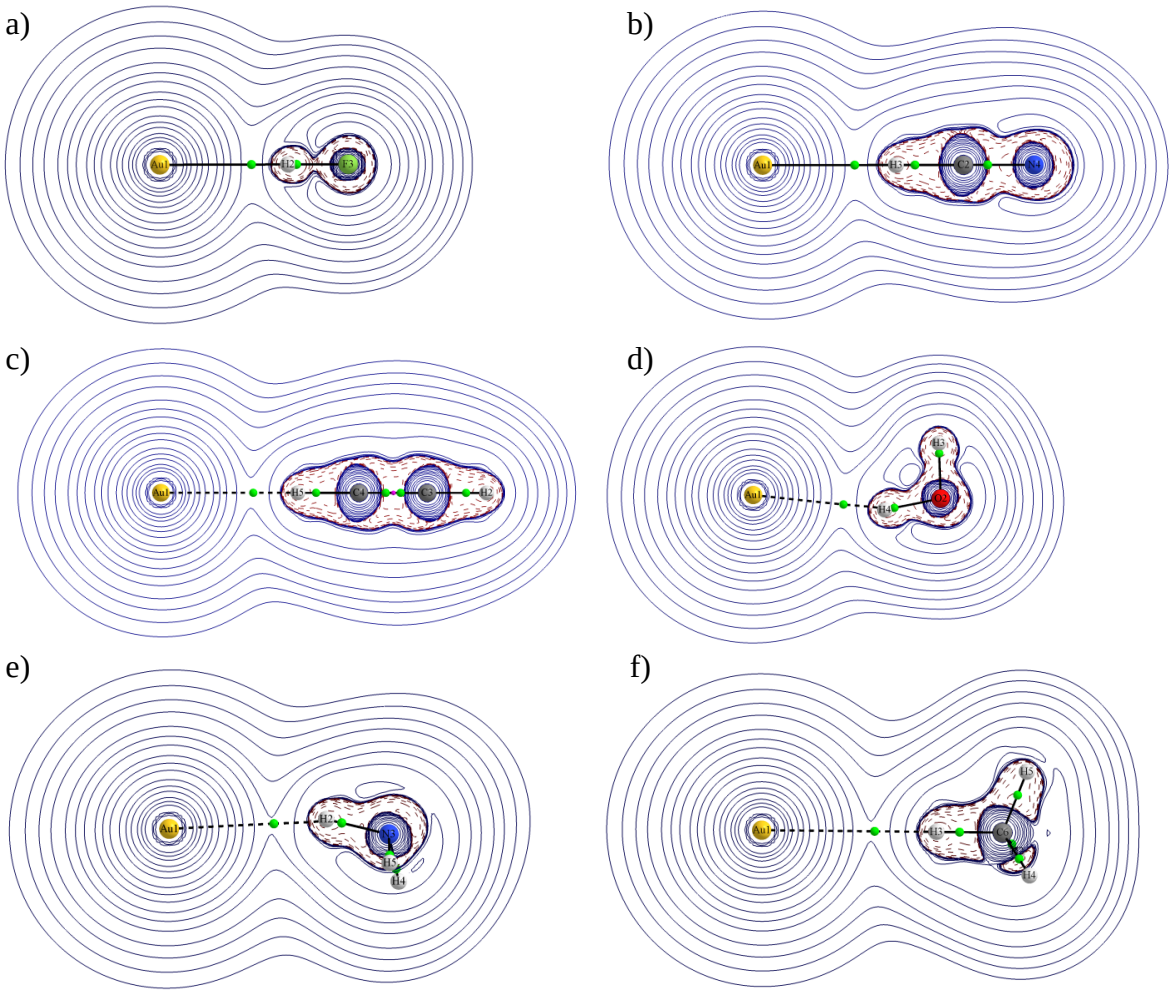

Figure 2 – Two dimensional contour plots for the $\nabla^2\rho$ (ea_0^{-5}) of the H-bonded optimised geometries in the gas phase of the auride anion with a) HF b) HCN c) HCCH d) H_2O e) NH_3 and f) CH_4 at the MP2/aug-cc-pVTZ-pp level of theory. The BCPs are shown as green spheres with the atomic interaction lines represented by the solid and dotted lines.

When the images in Figure 2 are considered, we can conclude that each adduct exhibits an Atomic Interaction Line (AIL) connecting the Au to H with a BCP separating the two neighbouring atoms. Even for the CH_4, with an intermolecular distance that falls outside the defined vdW distance at all four levels of theory (2.89 Å – 3.22 Å), we still see an atomic interaction line connecting the two fragments (see Figure 2 (f)). This suggests that the auride anion has a larger vdW radius than we have defined and that Au^- can form H-bonds with intermolecular distances up to 3 Å.

Table 2 – The electron density [ρ_b (ea_0^{-3})], the Laplacian of the electron density [$\nabla^2(\rho_b)$ (ea_0^{-5})] and the total electronic energy density [H_b (au)] of six optimised H-bonded Au^- adducts at the MP2/aug-cc-pVTZ-pp level of theory.

H-bond donor	$\boldsymbol{\rho_b}$ $\boldsymbol{(ea_0^{-3})}$	$\boldsymbol{\nabla^2(\rho_b)}$ $\boldsymbol{(ea_0^{-5})}$	$\boldsymbol{H_b}$ **(au)**
HF	0.039	0.043	-0.0117
HCN	0.031	0.057	-0.0055
HCCH	0.019	0.045	-0.0008
H_2O	0.025	0.052	-0.0031
NH_3	0.017	0.041	-0.0003
CH_4	0.009	0.022	0.0005

In 2008, Nakanishi *et al*. [41] listed AIM parameters for various types of interactions, where the values in Table 3 were identified as indicative of H-bond and van der Waals interactions.

Table 3 – Defined ranges for electron density [ρ_b (ea_0^{-3})], the Laplacian of the electron density [$\nabla^2(\rho_b)$ (ea_0^{-5})] and the total electronic energy density [H_b (au)] for interactions of the vdW, H-bond and charge transfer in hypervalent trigonal bipyramidal adducts (CT-TBP) type interactions extracted from Nakanishi *et al*. [41]

Interaction type	$\boldsymbol{\rho_b}$ $\boldsymbol{(ea_0^{-3})}$	$\boldsymbol{\nabla^2(\rho_b)}$ $\boldsymbol{(ea_0^{-5})}$	$\boldsymbol{H_b}$ **(au)**
vdW	$0.00 < \rho_b < 0.01$	$0.00 < \nabla^2(\rho_b) < 0.04$	$0.00 < H_b < 0.002$
H-bond	$0.01 < \rho_b < 0.04$	$0.04 < \nabla^2(\rho_b) < 0.12$	$-0.004 < H_b < 0.002$
CT-TBP	$0.03 < \rho_b < 0.12$	$-0.01 < \nabla^2(\rho_b) < 0.1$	$-0.06 < H_b < -0.003$

Comparing the calculated ρ_b values for the $Au^-\cdots H$ interactions in Table 2 to those in Table 3, the Au···H BCPs fall within the range expected for H-bonds for all H-bonded adducts, except for the CH_4 adduct. The calculated parameters at the $Au^-\cdots CH_4$ BCP are substantially lower than for the other H-bond donors and the interaction can therefore be classified as a vdW type interaction. This is not surprising since the C-H bond is not very polarisable, hence the H atom is not very acidic.

The calculated H_b values are, however, not as clear cut, with only the BCPs for the Au^- H-bonded to HCCH, H_2O, NH_3 and CH_4 falling within the defined range for H-bonds and the H_b value for Au^- H-bonded to HF and HCN falling within the CT-TBP range. It is likely that the H_b values are unreliable due to the ECP of the basis set, which results in incorrect values of any energetic properties, e.g. H_b, since it accounts for electrons as a singular potential and it seems that most, but not all, of the electron density is recovered [42], when ECPs are employed to describe an atom.

Nevertheless, the AIM results for the $Au^-\cdots H$ interactions suggest that they are indeed H-bonds, other than CH_4, which yields an adduct that resembles a vdW type interaction.

In order to gain further insight into the nature of the $Au^{-}\cdots H$ interactions and to explain their linearity, NCI plots were calculated and are shown in combination with a two-dimensional contour plot of $\nabla^2(\rho_b)$ in Figure 3 for Au^{-} H-bonded to the six model H-bond donors.

a)

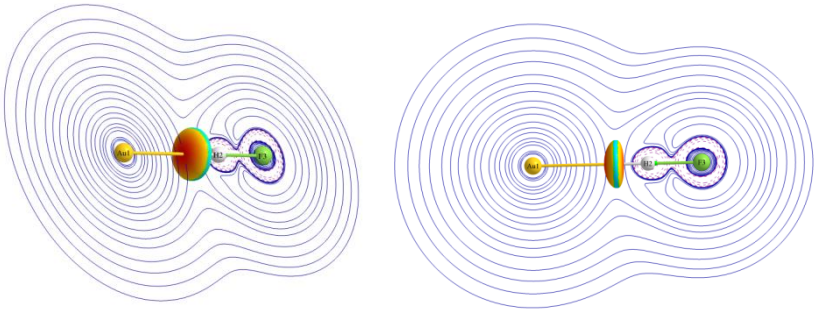

$Au^{-}\cdots HF$

Legend	Sign(λ_2)×ρ (au)
Red	-0.04794
Blue	0.02728

b)

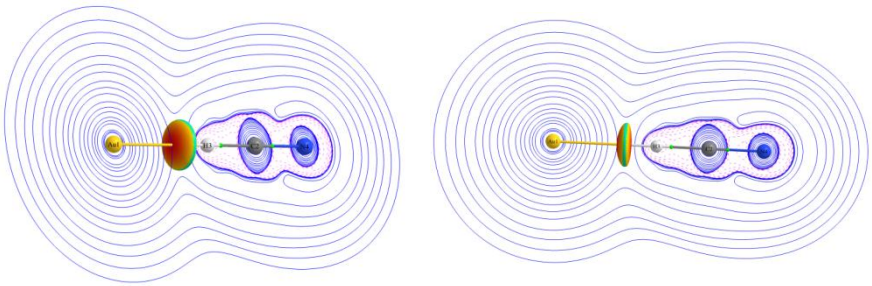

$Au^{-}\cdots HCN$

Legend	Sign(λ_2)×ρ (au)
Red	-0.03676
Blue	0.02153

c)

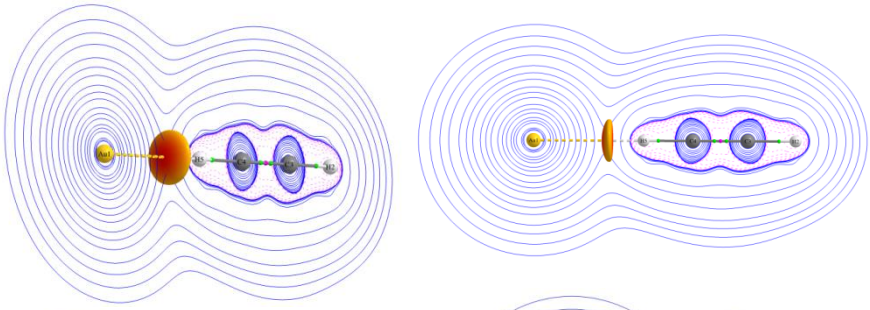

$Au^{-}\cdots HCCH$

Legend	Sign(λ_2)×ρ (au)
Red	-0.02095
Blue	-0.01347

d)

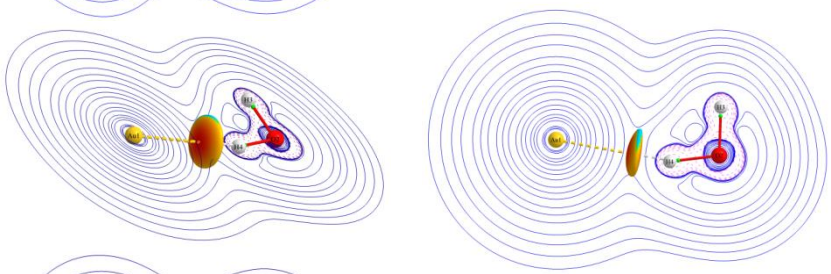

$Au^{-}\cdots H_2O$

Legend	Sign(λ_2)×ρ (au)
Red	-0.02835
Blue	0.01785

e)

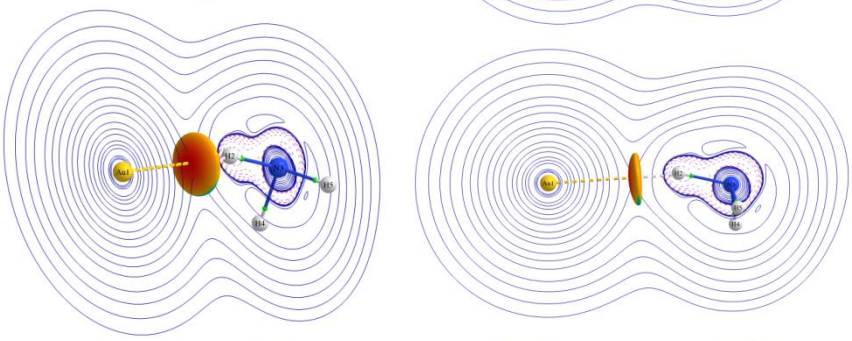

$Au^{-}\cdots NH_3$

Legend	Sign(λ_2)×ρ (au)
Red	-0.01828
Blue	0.01166

f)

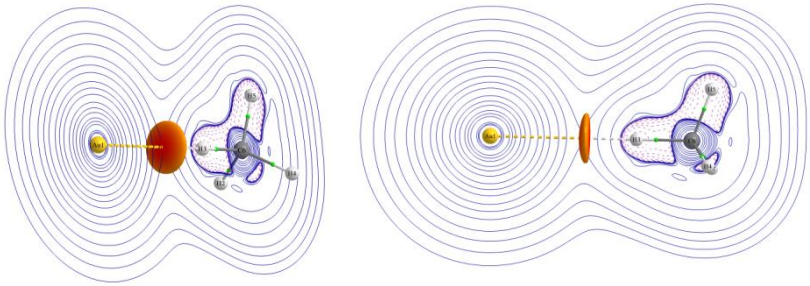

$Au^{-}\cdots CH_4$

Legend	Sign(λ_2)×ρ (au)
Red	-0.00917
Blue	-0.00655

Figure 3 – NCI plots and two-dimensional contour plots of the $\nabla^2\rho$ (ea_0^{-5}) calculated for the auride anion H-Bonded to six H-bond donors: a) HF, b) HCN, c) HCCH, d) H_2O, e) NH_3 and f) CH_4. The sign(λ_2)×ρ (au) values are indicated in the tables next to each image. Red indicates the minimum value (attractive), yellow indicates values less than zero, green indicates zero, cyan greater than zero and blue indicates the maximum value (repulsive).

The colouring in Figure 3 indicates the sign of λ_2, which can be utilised to distinguish between bonded ($\lambda_2<0$) and non-bonded ($\lambda_2>0$) interactions. Since only the negative sign(λ_2) $\times\rho$ values represent attractive intermolecular interactions, the values shown in red are of interest. The dispersion-bound methane dimer was shown to have a negative sign(λ_2) $\times\rho$ value that is close to zero [36]. Similarly, Au^- H-bonded to CH_4, shown in Figure 3f, has a sign(λ_2) $\times\rho$ value of -0.00917 au. Conversely, the $Au^-\cdots HF$ adduct has the greatest negative value for sign(λ_2) $\times\rho$. In addition, it seems that there is a relationship between the calculated sign(λ_2) $\times\rho$ and the calculated E_{INT}: the more negative the value for sign(λ_2) $\times\rho$, the stronger the E_{INT} value. The trend for the absolute values of sign(λ_2) $\times\rho$ HF > HCN > H_2O > HCCH > NH_3 > CH_4, corresponds exactly to the E_{INT} trend.

2.5. DMA anionic complex $[(\mathbf{Me})_2\mathbf{Au}]^-$

The optimised geometries of the DMA complex with the six H-bond donors are shown in Figure 4, while selected geometrical parameters are given in Table 4.

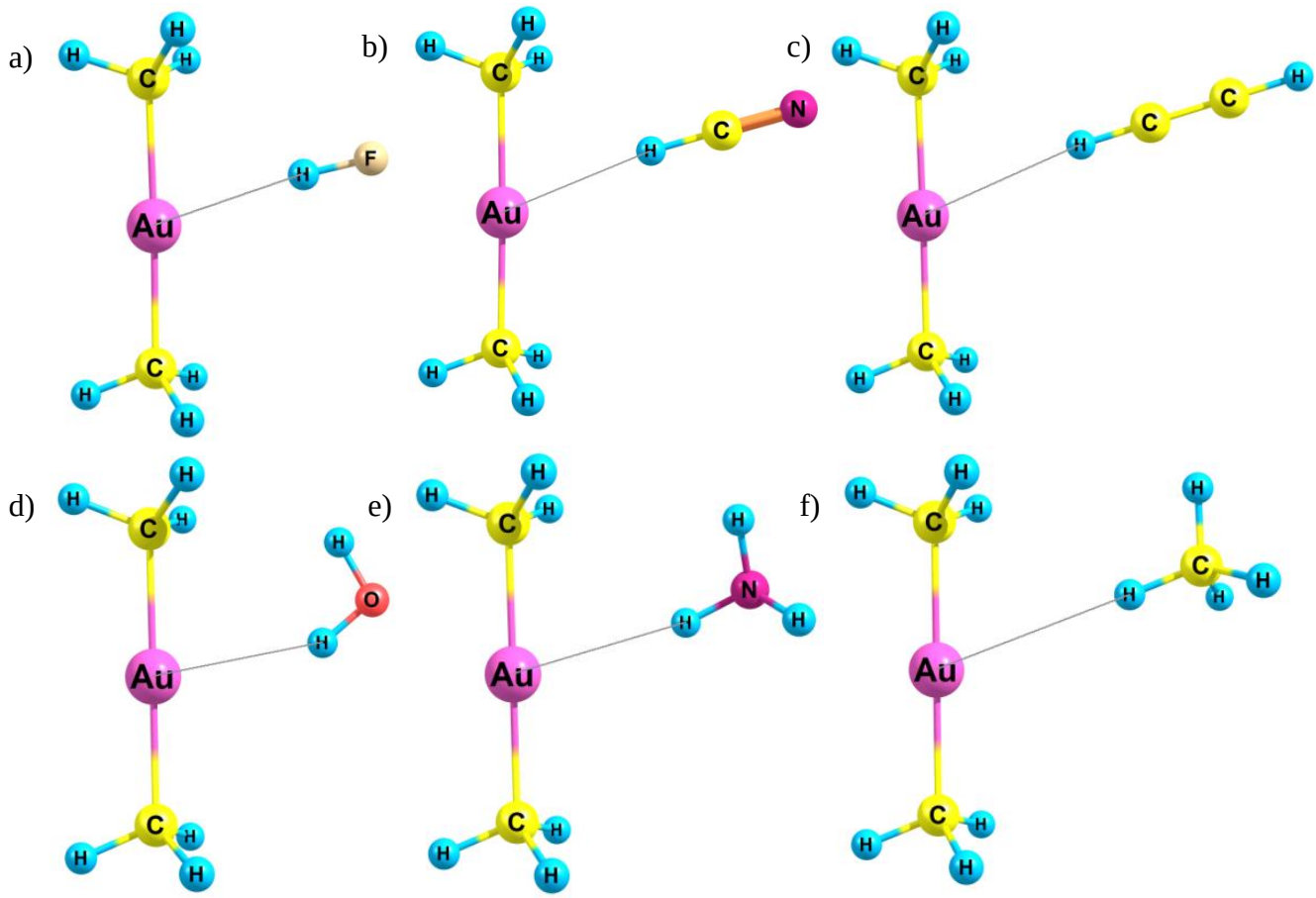

Figure 4 – Optimised geometries of $[(Me)_2Au]^-$ H-bonded to a) HF, b) HCN, c) HCCN, d) H_2O, e) NH_3 and f) CH_4 at the MP2/aug-cc-pVTZ-pp level of theory.

Table 4 – The E_{INT} values in kcal/mol, Au-CH_3 bond lengths in Å, intermolecular distances *d*(Au···H) in Å, bonding angles (Au···H-X) (º) and the H-X distances in Å of $[(Me)_2Au]^-$ H-bonded to HF, HCN, HCCH, H_2O, NH_3 and CH_4 optimised using the B3LYP, TPSS and MP2 methods with the aug-cc-pVTZ-pp and cc-pVTZ-pp basis sets.

Method	H-bond donor	E_{INT} (kcal/mol)	Au-CH_3 (Å)	*d*(Au···H) (Å)	Au···H-X (º)	H-X (Å)
B3LYP	HF	-15.32	2.117	2.205	179.9	0.960
TPSS		-17.34	2.111	2.124	179.9	0.979
MP2*		-14.58	2.060	2.260	175.2	0.945
MP2		-16.00	2.061	2.222	174.4	0.954
B3LYP	HCN	-13.57	2.115	2.437	174.1	1.094
TPSS		-14.79	2.110	2.299	177.4	1.111
MP2*		-15.95	2.065	2.407	173.4	1.090
MP2		-16.17	2.065	2.388	173.5	1.092
B3LYP	HCCH	-5.05	2.117	2.717	174.2	1.077
TPSS		-5.76	2.111	2.580	176.2	1.086
MP2*		-6.99	2.062	2.611	173.2	1.078
MP2		-7.48	2.063	2.580	173.5	1.079
B3LYP	H_2O	-9.50	2.123	2.510	154.7	0.977
TPSS		-10.48	2.116	2.374	159.5	0.992
MP2*		-10.51	2.063	2.529	149.7	0.971
MP2		-11.52	2.064	2.468	151.3	0.976
B3LYP	NH_3	-4.81	2.120	2.729	160.0	1.023
TPSS		-5.45	2.112	2.596	162.4	1.033
MP2*		-4.61	2.061	2.677	160.1	1.021
MP2		-6.89	2.062	2.621	158.6	1.023
B3LYP	CH_4	-0.90	2.119	3.184	179.5	1.089
TPSS		-1.21	2.111	3.087	179.2	1.094
MP2*		-2.05	2.060	2.983	178.8	1.088
MP2		-2.40	2.061	2.915	179.2	1.089

As before, we consider the MP2* level of theory to yield the most balanced results between dispersion and electrostatic forces. The most stable H-bonded adduct is found to be when the H-bond donor is HCN (-15.95 kcal/mol), with HF (-14.58 kcal/mol) yielding a similar amount of stabilisation. As before, the weakest H-bond is that formed in the CH_4 adduct, with an E_{INT} of -2.05 kcal/mol. If we compare all of the E_{INT} values calculated at the MP2* level, the order of decreasing E_{INT} is HCN > HF > H_2O > HCCH > NH_3 > CH_4; different to the trend seen for the H-bonded Au^- ion with respect to HCN and HF. This difference could be method dependent, since only MP2 yields a more stable H-bond for HCN than for HF, for the DFs the trend is identical to the previously discussed auride anion as a function of the H-bond donors. In general, when different trends emerge for DFTs and MP2 it is a result of either DFTs overestimating the electrostatic contribution, or underestimating the contribution of

dispersion contribution, or the MP2 method overestimating the dispersion-type interactions. The method-dependent trend in E_{INT} values could be a combination of these factors.

Alkorta and co-workers [43] point out that H-bonds with binding energies between -2.4 and -12 kcal/mol can be considered as weak H-bonds, with strong H-bonds between -12 and -24 kcal/mol. Taking this classification into consideration, we see that HF and HCN H-bond donors yield strong H-bonds, while the remaining H-bond donors form weak H-bond adducts with the DMA anionic complex.

There is a weakening of the hydrogen bond strength of 20 % to 60 % when the E_{INT} values of $[(Me)_2Au]^-$ are compared to those of the H-bonded Au^- analogues (shown in Table 1). The largest decrease in E_{INT} is for NH_3 binding to $[(Me)_2Au]^-$, but for the remainder of the adducts the small percentages by which E_{INT} decreases are surprising considering Au(I) is in a formal +1 oxidation state in $[(Me)_2Au]^-$, as compared to -1 for Au^-.

In order to put the H-bond stabilisation obtained for $[(Me)_2Au]^-$ into perspective we refer to the work performed by Alkorta *et al*.[44], who calculated E_{INT} values of -11.26 kcal/mol and -9.59 kcal/mol for $(CO)_4Co^-$ H-bonded to HF and HCN at the B3LYP/6-311++G** level of theory, respectively. The E_{INT} values obtained using the B3LYP method for the DMA anionic complex H-bonded to HF and HCN are approximately 4 kcal/mol more stabilising than the $(CO)_4Co^-$ complex H-bonded to the same H-bond donors. This added H-bond stabilisation of the Au(I) centre could be due to the relative basicity of the respective metal centres. For the $(CO)_4Ni^-$ analogue the Ni···H interaction is so weak for the HCN adduct that no stationary point was obtained. Alkorta *et al*. [44] point out that this is the likely reason for H-bonding to this anion not having been observed experimentally. In our case the E_{INT} values suggest that Au^{I}···H interactions should be more frequently observed experimentally. In order to determine whether the close Au^{I}···H contacts shown in Figure 4 are indeed H-bonds, AIM analysis was performed (see Figure 5 and Table 5).

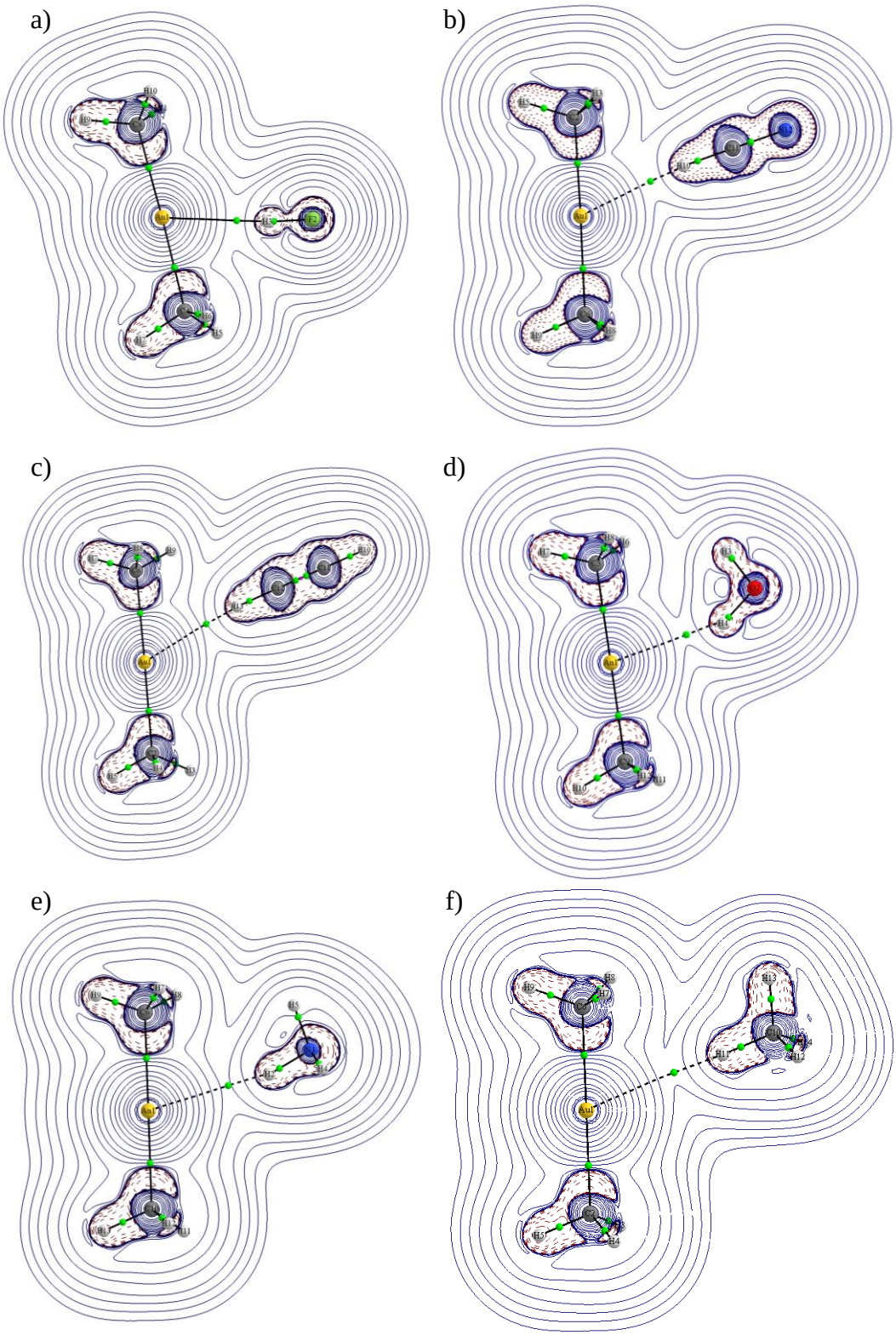

Figure 5 – Molecular graphs and two-dimensional contour plots of $\nabla^2\rho$ (ea_0^{-5}) of the optimised geometries of $[(Me)_2Au]^-$ H-bonded to a) HF, b) HCN, c) HCCH, d) H_2O, e) NH_3 and f) CH_4 at the MP2/aug-cc-pVTZ-pp level of theory.

The most important feature of the molecular graphs in Figure 5 is the fact that there is an AIL connecting Au with H for all six H-bonded adducts. Furthermore, the presence of a BCP between the Au and H atoms agrees with the IUPAC definition of the H-bond [45].

Table 5 – The HF_{INT}, $E2_{INT}$, the electron density [ρ_b ($e a_0^{-3}$)], the Laplacian of the electron density [$\nabla^2(\rho_b)$ ($e a_0^{-5}$)] and the total electronic energy density [H_b (au)] of the optimised geometries of the H-bonded adducts of $[(Me)_2Au]^-$ at the MP2/aug-cc-pVTZ-pp level of theory.

H-bond donor	HF_{INT} (kcal/mol)	$E2_{INT}$ (kcal/mol)	ρ_b ($e a_0^{-3}$)	$\nabla^2(\rho_b)$ ($e a_0^{-5}$)	H_b (au)
HF	-11.17	-6.35	0.028	0.048	-0.0052
HCN	-12.01	-5.84	0.021	0.051	-0.0012
HCCH	-3.57	-5.39	0.014	0.039	0.0004
H_2O	-7.20	-5.67	0.017	0.046	-0.0003
NH_3	-2.94	-5.12	0.013	0.037	0.0005
CH_4	0.35	-3.71	0.008	0.022	0.0007

The HF_{INT} and $E2_{INT}$ interaction energies obtained from the MP2 calculations are included in Table 5 to gain further insight into the nature of this intermolecular interaction, since HF_{INT} represents the electrostatic contribution and $E2_{INT}$ represents the contribution of electron correlation/dispersion-type interactions to the total E_{INT}. The HF_{INT} values for the HF, HCN and H_2O adducts illustrate that the electrostatic contributions are larger than those from dispersion ($E2_{INT}$); the interactions are therefore electrostatically dominated. Interestingly, we observe that the $E2_{INT}$ term remains relatively constant, suggesting that although a dispersion component is present in all the hydrogen bonds, it provides a relative constant stabilisation; it is the electrostatic component that plays the most important role in the strength of the hydrogen bond. For instance, the low HF_{INT} value for $Au^{I}\cdots CH_4$ indicates that this interaction can be said to be solely a result of dispersion-type interactions.

If we consider the ρ_b values for all six H-bonded adducts of $[(Me)_2Au]^-$, a trend of decreasing electron density emerges that is identical to what was found above for the H-bonded adducts of Au^- (HF > HCN > H_2O > HCCH > NH_3 > CH_4). Surprisingly, the trend in ρ_b does not correlate with the trend in E_{INT} as a function of the H-bond donor; the reason for this could also be the tendency of MP2 to overestimate the dispersion contribution. As before, the values for ρ_b are characteristic of H-bonds, except for the CH_4 interaction, which is typical of a vdW-type interaction and correlates to the small HF_{INT} contribution to E_{INT}.

We see that only the $\nabla^2(\rho_b)$ values for HF, HCN and H_2O fall within the expected range for H-bonds with the $\nabla^2(\rho_b)$ values for HCCH and NH_3 being slightly less than the range

defined for H-bonds, but comparable. The AIM parameters and E_{INT} values suggests that the $Au^I\cdots H$ interaction for HCCH and NH_3 borders between a pure H-bond and a vdW-type interaction.

The H_b values fluctuate but indicate that all interactions are hydrogen bonds, except for the $Au^I\cdots HF$ interaction which is indicated as stronger than an H-bond.

The values obtained here compare well to those of other H-bonds to transition metal centres [16, 44]. For instance, the copper analogue $[(Me)_2Cu]^-$ H-bonded to CH_4 yielded values of 0.0075 $e a_0^{-3}$, 0.0193 $e a_0^{-5}$ and 0.0007 au for ρ_b, $\nabla^2(\rho_b)$ and H_b, respectively, i.e. comparable but weaker than for $[(Me)_2Au]^-$. The authors also performed an AIM analysis for the copper analogue H-bonded to propane and calculated values of 0.0088 au for ρ_b, 0.0208 au for $\nabla^2(\rho_b)$ and 0.0005 au for H_b. Selected AIM results for HF and HCN interacting with $(CO)_4Co^-$ and $(CO)_4Ni$ listed in Table 6 [44], are also similar to the results given in Table 5.

Table 6 - The electron density [ρ_b ($e a_0^{-3}$)], the Laplacian of the electron density [$\nabla^2(\rho_b)$ ($e a_0^{-5}$)] and the total electronic energy density [H_b (au)] of Co and Ni complexes at the B3LYP/6-311++G** level of theory [44].

Metal complex	H-bond donor	ρ_b ($e a_0^{-3}$)	$\nabla^2(\rho_b)$ ($e a_0^{-5}$)	H_b (au)
$(CO)_4Co^-$	HF	0.0195	0.0306	-0.0004
	HCN	0.0109	0.0207	0.0006
$(CO)_4Ni$	HF	0.0121	0.0273	0.0011

The ρ_b values indicate H-bonds, whereas the $\nabla^2(\rho_b)$ values fall short of the range defined for H-bonds. As before, the H_b values are inconclusive.

As mentioned earlier, there are two experimental examples of the $Au^I\cdots H$ interaction in the solid state; the AuCl(mbbt) and AuBr(mbbt) complexes (see SI of ref [15]) obtained by Koskinen *et al*. [15] Their AIM results yielded ρ_b and $\nabla^2(\rho_b)$ values of 0.0609 $e a_0^{-3}$ and 0.7054 $e a_0^{-5}$, and 0.0599 $e a_0^{-3}$ and 0.6885 $e a_0^{-5}$ for the chlorine and bromine analogue, respectively. These values are substantially larger than what we have calculated for a $C\text{-}H\cdots Au^I$ type interaction. In addition, they calculated an $Au^I\cdots H$ interaction energy of -1.7 kcal/mol and is similar to our value for $CH_4\cdots Au^I$, but does not agree with the magnitude of the calculated AIM parameters. This is most likely due to their utilisation of experimental coordinates derived from diffraction, since the H-atom positions are notoriously poorly defined in X-ray diffraction. We suspect that optimisation of the H-atom positions would yield lower AIM values, comparable to our results for ρ_b and $\nabla^2(\rho_b)$ in Table 5, as well as a slightly higher H-bond interaction energy. Furthermore, the authors observed additional

H···S, H···Br, S···Br and H···H atomic interaction lines which may aid in decreasing the Au···H contact distance.

The largest differences between the Au^{-} and $[(Me)_2Au]^{-}$ adducts are the Au···H-X angles which deviate more from linearity for $[(Me)_2Au]^{-}$adducts. It appears that the reason for this may be the formation of an interaction between the H-bond donor and the methanide ligands that could be too weak to be indicated by a AIL and BCP. We therefore decided to perform an NCI analyses.

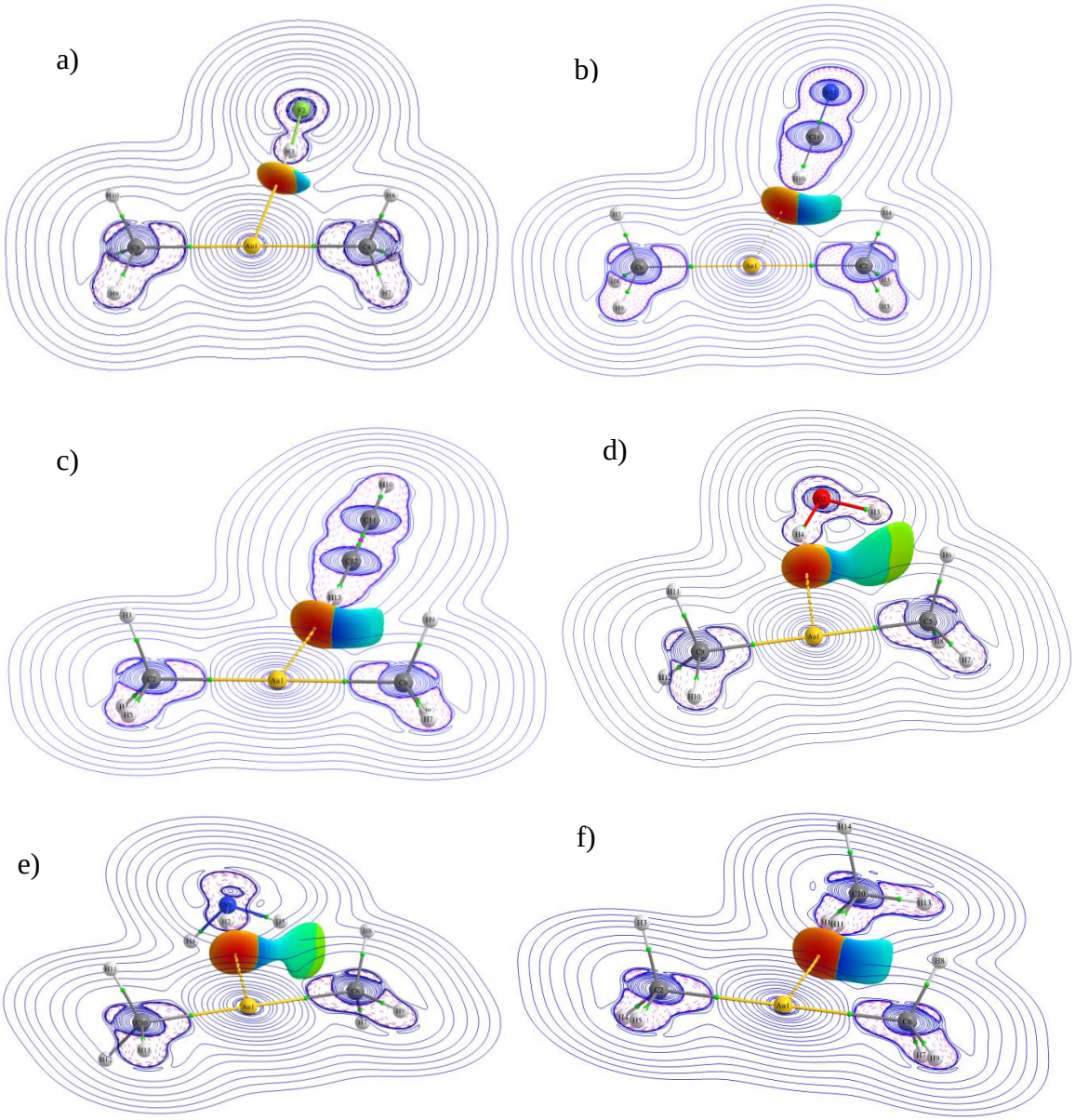

Figure 6 – Two-dimensional contour plots of $\nabla^2\rho\ (ea_0^{-5})$ with the NCI plots included of $[(Me)_2Au]^-$ H-bonded to a) HF, b) HCN, c) HCCH, d) H_2O, e) NH_3 and f) CH_4 calculated at the MP2/aug-cc-pVTZ-pp level of theory. Red and yellow indicates a negative sign(λ_2) $\times\rho$ value, green indicates a sign(λ_2) $\times\rho$ value of zero and blue shows the regions that have a positive sign(λ_2) $\times\rho$ value. Red areas identify the stabilising interactions and blue, destabilising interactions.

Surprisingly, the NCI plots shown in Figure 6 suggest that the H-bond donors are not stabilised by interactions with the carbon of the methanide ligand; on the contrary the interaction appears to be slightly repulsive, with the occasional stabilisation provided by dispersion-type interactions indicated as lime green regions. The majority of the stabilisation is provided by the Au(I) centre, agreeing with the molecular graphs shown in Figure 5, where an atomic interaction line connects the H-bond donor to the Au(I) centre.

We need to mention one geometrical parameter that is method dependent: the C-Au···H angle. The two selected DFs yielded C-Au···H angles close to 90º, while the MP2 method yielded values of approximately 73º, see Figure 7.

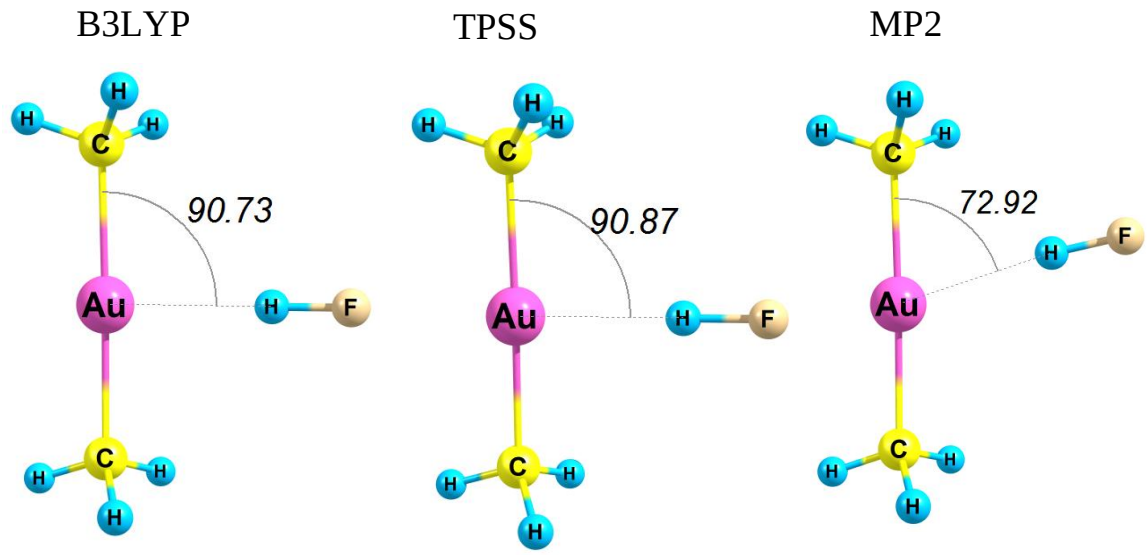

Figure 7 – Optimised geometries of $[(Me)_2Au]^-$ H-bonded to HF with the C-Au···H angle indicated in º, utilising various methods in combination with the aug-cc-pVTZ-pp basis set.

Whether this is method dependent or basis-set dependant is debateable. However, we believe the electrostatic surface potential (ESP) isosurface defined at 0.001 au explains why different optimised geometries are obtained (Figure 8).

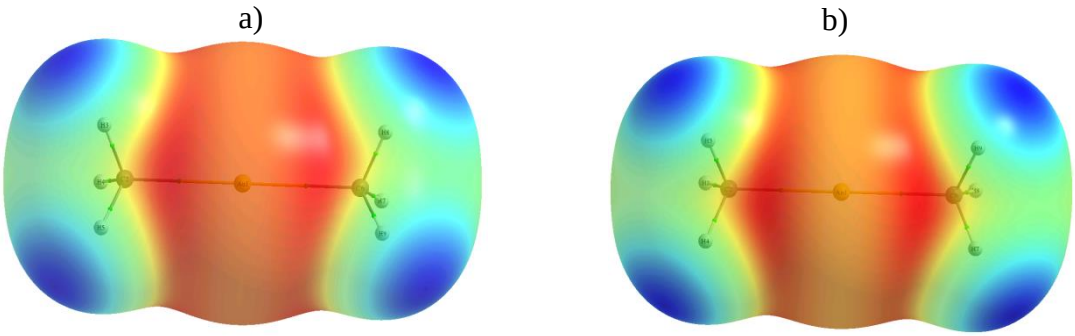

Figure 8 – ESP surfaces of the DMA anionic complex obtained using the a) B3LYP and b) MP2 methods with the aug-cc-pVTZ-pp basis set. Colour scheme (a) red = -0.18237 and blue = -0.13428 and (b) red = -0.18608 and blue = -0.13451 au.

When HF forms an H-bonded adduct to $[(Me)_2Au]^-$, the most favourable position would be where the H-atom of the HF arranges itself in such a manner to achieve greatest stabilisation. The results shown in Table 5 suggest that electrostatics play the greatest role in stabilising the interaction. This position would be dependent on the red regions corresponding with the

highest negative ESP in Figure 8. If the red regions calculated with the B3LYP and the MP2 methods are compared, we conclude that B3LYP yields a more negative surface potential that is more delocalised than the MP2 method, with the MP2 yielding negative regions localised between the gold and carbon atoms. Another possibility to consider is the fact that MP2 more accurately accounts for dispersion type interactions than DFTs and the orientation of the H-bond donor could also be a result of these interactions. Thus, we conclude that the differences in the Au-C···H angles correspond mostly to the method-dependent localisation of the ESP and also possibly to weaker dispersion interactions.

2.6. Comparison of the H-bonded adducts of Au^- to $[(Me)_2Au]^-$

Boyd and Choi [46] have shown that there is a linear relationship between the interaction energy and the electron density at the intermolecular BCP of an H-bond. The same is true for the Au···HX hydrogen bonds studied here, with linear trends for a wide range of E_{INT} values for both the Au^- and $[(Me)_2Au]^-$ H-bonded adducts (Figure 9). The most noticeable difference between the two groups of adducts is that the maximum density at the intermolecular BCP is higher for Au^-, as might be expected considering the greater negative E_{INT} values for Au^- H-bonded adducts, along with shorter Au···H distances. The maximum ρ_b value is obtained when the H-bond donor is HF, coinciding with the most stabilising E_{INT} values.

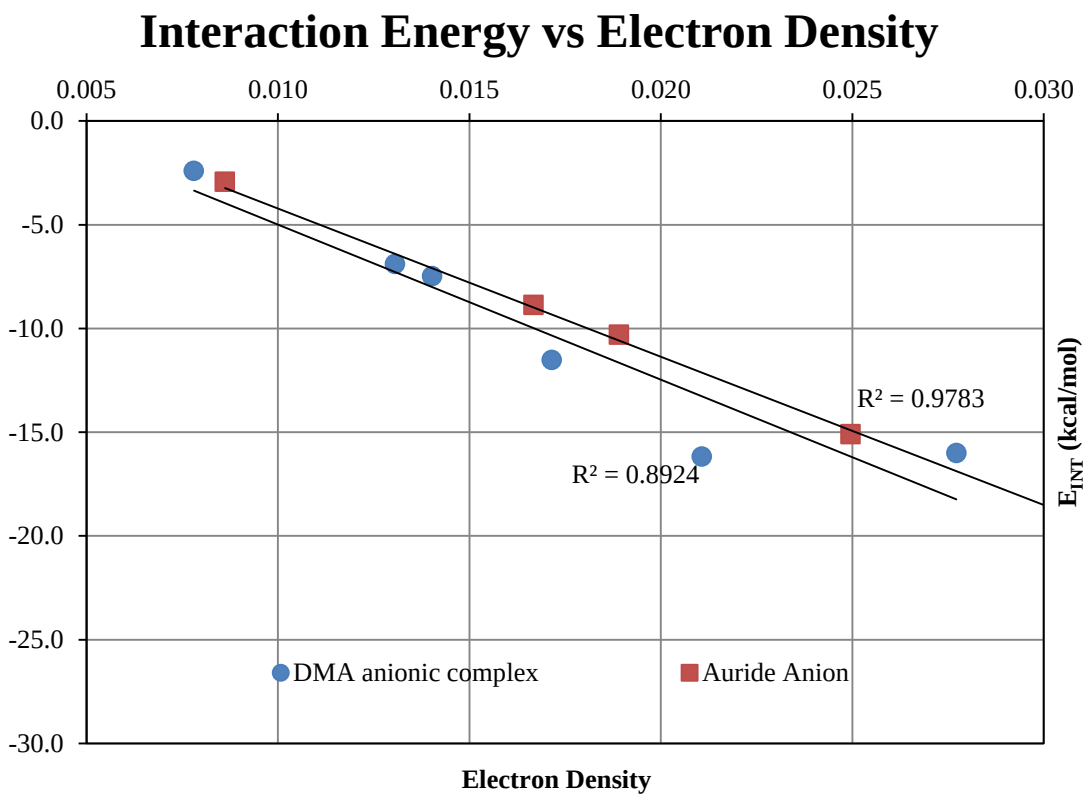

Figure 9 – Graphical representation of the interaction energies (E_{INT}) of the auride anion and the DMA anionic complex with various H-bond donors plotted against the electron density in ea_0^{-3} calculated at the MP2/aug-cc-pVTZ-pp level of theory.

Table 7 - Elongation of the H-X bond when bonded to the auride and the DMA anion at the MP2/aug-cc-pVTZ level of theory.

	Au^-	$[(Me)_2Au]^-$
	ΔR (Å)	**ΔR (Å)**
HF	0.056	0.030
HCN	0.055	0.028
HCCH	0.030	0.017
H_2O	0.031	0.015
NH_3	0.019	0.011
CH_4	0.005	0.003

According to the criteria for H-bond formation listed in Kryachko's paper [12] and the IUPAC definition [45], elongation of the H-X bond usually occur upon adduct formation, implying that ΔR should be positive. However, as mentioned by IUPAC [45], examples where the H-X bond shortens upon H-bond formation resulting in a blue shifted IR frequency of that bond. As we can see from the values listed in Table 8, bond elongation occurs for both the Au^- and $[(Me)_2Au]^-$ ions upon H-bond formation. Interestingly, when the H-bond

donors bind to the auride anion, HF and HCN elongate by approximately 6.1 %, HCCH and H_2O elongate by approximately 3.3 %, NH_3 elongates by 2 % and CH_4 elongates by 0.6 %. We observe that this trend of H-X elongation in decreasing order from HF to CH_4 remains for $[(Me)_2Au]^-$, confirming DMA as an H-bond acceptor, although elongation is consistently 50 % less when compared to adduct formation with the auride anion. This decrease in relative H-X bond elongation upon H-bond formation is expected, since the auride anion yields stronger H-bond adducts, based on the E_{INT} values.

Another characteristic feature of H-bond formation, according to Brammer [8] and IUPAC [45] is a decrease in the H-X stretching frequency. The uncorrected IR stretching frequencies of the H-bond donors (experimental and calculated) before and after adduct formation with Au^- and $[(Me)_2Au]^-$ are shown in Table 8.

Table 8 – The unscaled IR stretching frequencies for HF, HCN, HCCH, H_2O, NH_3 and CH_4 with Au^- and $[(Me)_2Au]^-$ and theoretical and experimental IR frequencies for the isolated H-bond donors at the MP2/aug-cc-pVTZ-pp level of theory.

	Calculated H-X stretching frequency			
H-Donor	**$Au^-\cdots$H-X**	**$[(Me)_2Au]^-\cdots$H-X**	**H-X**	**Exp.**
HF	2971.62	3444.75	4122.88	3953[a]
HCN	2682.86	3057.04	3465.70	3438.5[b]
HCCH	3026.66	3226.56	3431.58	3372[c]
H_2O	3289.75	3604.12	3948.04	3942[b]
NH_3	3274.23	3549.07	3649.93	3577[d]
CH_4	3147.44	3171.46	3204.71	3252[b]

[a]From ref [47]

[b]From ref [48]

[c]From ref [49]

[d]From ref [50]

As expected, the bond elongation corresponds to a decrease in the H-X IR stretching frequencies thus indicating a weakening of the H-X bond. We note that the greater the elongation, the lower the H-X stretching frequency of that bond, with the observed maximum decrease for HF when H-bonded to the Au^- or $[(Me)_2Au]^-$ ions. This again confirms that HF forms the strongest H-bonds to Au^- and DMA.

2.7. Comparison of Cu(I), Ag(I) and Au(I) analogues

Previous work by Dem'yanov and co-workers [16] showed that the Cu(I) analogue of DMA can act as H-bond acceptor to C-H-type H-bond donors; however, these H-bonds are weak and a result of dispersion-type interactions. In light of this, we deemed it worthy to further

demonstrate the significance of gold's ability to form H-bonds when compared to the Cu and Ag analogues. We therefore undertook the geometry optimisations of $[(Me)_2Cu]^-$ and $[(Me)_2Ag]^-$ with HF as the selected H-bond donor. AIM and NCI analyses were performed to gain further insight. The HF hydrogen-bond donor was selected since we have shown above that it has the most acidic proton and would be most likely to form an H-bond where electrostatic interactions are dominant. Our aim is not to perform an in-depth and extensive theoretical comparison, but rather to highlight significant differences. A schematic representation of the geometrical parameters listed in Table 9 is given in Figure 10.

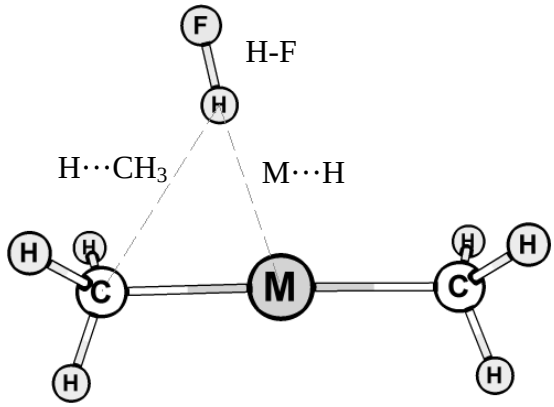

Figure 10 – Schematic representation of the H-bonded adduct and the geometrical parameters selected for comparison.

Table 9 – The interaction energy (E_{INT}) in kcal/mol, intermolecular distance (M···H and H···CH_3 in Å) and H-F bond length in Å for $[(Me)_2M]^-$ (M = Au^{I}, Cu^{I} and Ag^{I}) at the MP2/aug-cc-pVTZ-pp level of theory.

	E_{INT} (kcal/mol)	***d*(M···H) (Å)**	***d*(H···CH_3) (Å)**	**H-F (Å)**
$[(Me)_2Au]^-$ ··H-F	-16.00	2.222	2.548	0.954
$[(Me)_2Ag]^-$···H-F	-15.66	2.413	2.070	0.952
$[(Me)_2Cu]^-$· ·H-F	-15.76	2.282	2.097	0.953

The calculated E_{INT} values and *d*(M···H) distances listed in Table 9 are similar, and one could believe that all three metal analogues form strong M···H bonds due to the short *d*(M···H) distances and stabilising E_{INT} values. However, this is not true, as can be seen in Figure 11, where the AIM results show that the Cu^{I} and Ag^{I} analogues have atomic interaction lines connecting the H atom of HF to the carbon atom on the methanide ligand. Furthermore, the colour scheme of the NCI plot displays the directionality and the cause of complexation: the carbon atom acts as H-bond acceptor, driven by electrostatic interactions. We can therefore think of the carbon atom, in the cases of $[(Me)_2Cu]^-$ and $[(Me)_2Ag]^-$, as a competing H-bond acceptor or binding site. As we can see, Au^{I} is unique in this regard since the atomic

interaction line, shown at the top of Figure 11 (a), connects the Au(I) centre to the H-bond donor atom. It is interesting to note that even though we probed for a C···H-F interaction for the DMA anionic complex by providing an input geometry where the HF is within 2 Å of the C-atom, the HF moved away from the carbon atom towards Au(I). We postulate that the dimethyl cuprate and argentate anionic complexes can only form weak H-bonds to C-H-type H-bond donors. Possible reasons for this will be explained later in this chapter. It is interesting to note that Dem'yanov and Gschwind [16] utilised B3LYP and the MP2 method in combination with two basis sets in the analysis of weak H-bond formation of $[(Me)_2Cu]^{-}\cdots CH_4$. They found that B3LYP yielded a $Cu^{I}\cdots H$ AIL with both basis sets employed, with MP2 only yielding an AIL with one of the basis sets. Another factor we cannot overlook is that Au is known for large relativistic effects [51], which could also explain why these H-bonds occur. This renders the $[(Me)_2Cu]^{-}$ and $[(Me)_2Ag]^{-}$ ionic complexes fundamentally different to $[(Me)_2Au]^{-}$ as H-bond acceptors.

a)

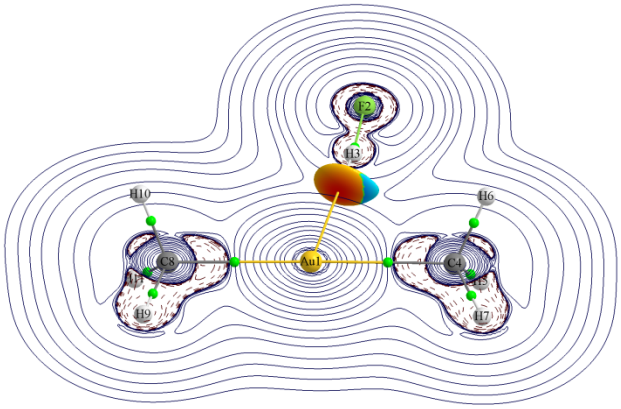

b)

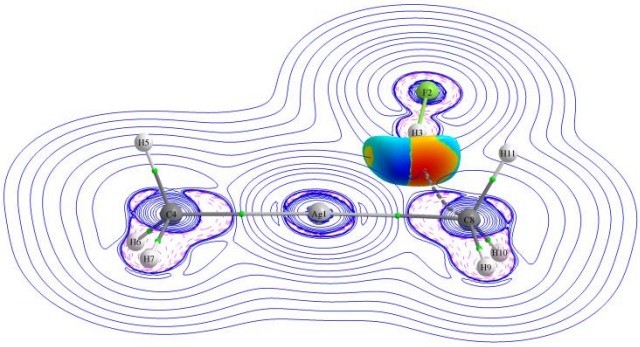

c)

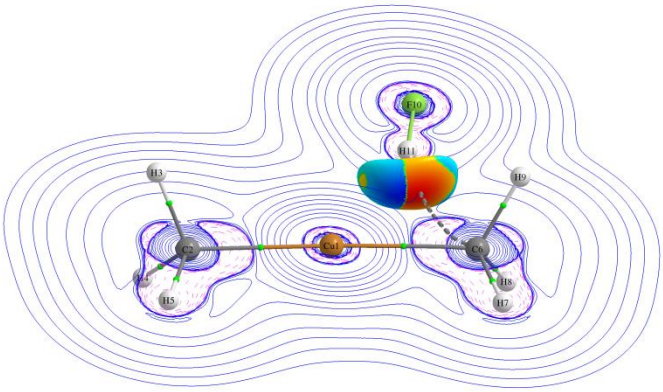

Figure 11 – Two-dimensional contour plots of the $\nabla^2\rho$ (ea_0^{-5}) with the NCI plots of the dimethyl Au(I), Ag(I) and Cu(I) anionic analogues (a, b and c, respectively) H-bonded to HF at the MP2/aug-cc-pVTZ-pp level of theory. Red indicates attractive interactions and blue repulsive interactions. The BCPs are represented by green spheres.

We therefore decided to investigate how relativistic effects influence the ability of the Au^- and $[(Me)_2Au]^-$ ions to act as H-bond acceptors. Again, we selected HF as the model H-bond donor. The AIM results are summarised in Table 10.

Table 10 – The interaction energies (E_{INT} kcal/mol), *d*(Au···H) interatomic distance in Å, the Au···H-F angle (°) and the H-F bond length (Å) of the $Au^{-}\cdots HF$ and $[(Me)_2Au]^{-}\cdots HF$ adducts at the B3LYP and MP2 methods without relativistic effects by utilisation of the ECP60MHF basis set and ECP to describe the gold atom. The electron density [ρ_b (ea_0^{-3})], the Laplacian of the electron density [$\nabla^2(\rho_b)$ (ea_0^{-5})] and the total electronic energy density [H_b (au)] were calculated with the MP2 method and basis sets used for the optimisation.

Au^{-}	**E_{INT} (kcal/mol)**	***d*(Au···H) (Å)**	**Au···H-F (deg)**	**H-F (Å)**	**ρ_b (ea_0^{-3})**	**$\nabla^2(\rho_b)$ (ea_0^{-5})**	**H_b (au)**
B3LYP	-15.06	2.50	180.0	0.96	-	-	-
MP2	-16.25	2.44	180.0	0.95	0.018	0.029	-0.0017
$[(Me)_2Au]^{-}$ wih HF	**E_{INT} (kcal/mol)**	***d*(Au···H) (Å)**	***d*(H···CH_3) (Å)**	**H-F (Å)**	**ρ_b (ea_0^{-3})**	**$\nabla^2(\rho_b)$ (ea_0^{-5})**	**H_b (au)**
B3LYP	-15.88	2.553	1.999	0.961			
MP2	-15.19	2.538	2.062	0.951	0.024	0.048	-0.0026

The E_{INT} values, geometrical parameters and AIM results for Au^{-} H-bonded to HF without taking relativistic effects into account are listed in Table 10. Comparison of the calculated E_{INT} values of the $Au^{-}\cdots HF$ adduct show that it becomes less stabilising by approximately 6.0 kcal/mol. Furthermore, the ρ_b and $\nabla^2(\rho_b)$ values are almost half the values listed in Table 2, where relativistic effects were taken into account, while the calculated H_b value is also substantially smaller. Despite the weakening of the interaction the AIM parameters still fall within the expected ranges for H-bonding as summarised in Table 3.

The effect is even more obvious for the H-bonded $[(Me)_2Au]^{-}\cdots HF$ adduct, where the H-bond disappears completely with the omission of relativistic effects (Table 10 and Figure 12). The calculated E_{INT} values for DMA in Table 10 are comparable to those listed in Table 4 for $[(Me)_2Au]^{-}$ H-bonded to HF but correspond to a C···H interaction. According to Figure 12 the $Au^{I}\cdots H$ interaction is now repulsive. Furthermore, if we look closely at the geometrical parameters in Table 10, we observe that all the listed geometrical parameters are almost identical to those of the Cu(I) and Ag(I) analogues listed in Table 9. This similarity between non-relativistic Au(I) and the Ag(I) and Cu(I) analogues (with relativistic effects included) suggests that the large relativistic effect is what sets Au(I) apart from its group 11 analogues. The ESPs of the $[(Me)_2Cu]^{-}$, $[(Me)_2Ag]^{-}$ and the nonrelativistic $[(Me)_2Au]^{-}$ complexes are shown in Figure 13.

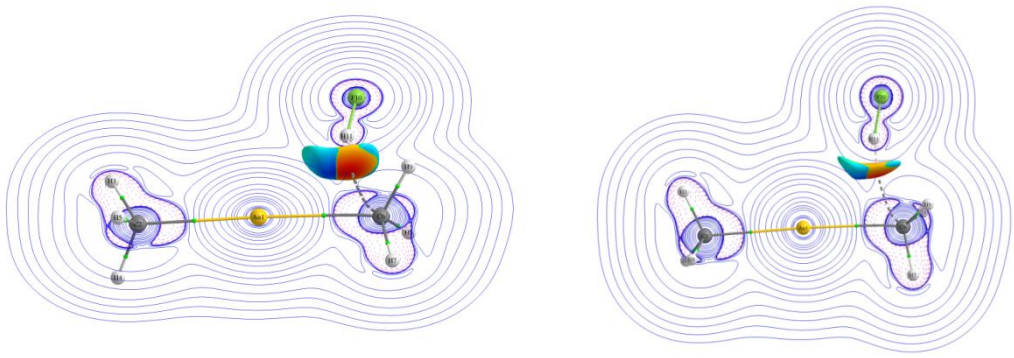

Figure 12 – Two-dimensional contour plot of $\nabla^2\rho$ (ea_0^{-5}) with the NCI plot of the optimised geometry of the $[(Me)_2Au]^-$ complex H-bonded to HF obtained utilising MP2 with the non-relativistic ECP60MHF basis set describing Au and aug-cc-pVTZ for the other atoms.

To further elucidate the differences between the Cu(I) and Ag(I) analogues of the DMA anionic complex, the ESPs will be compared, along with that of the $[(Me)_2Au]^-$ complex where relativistic effects are omitted, since these three examples did not yield an M···H interaction.

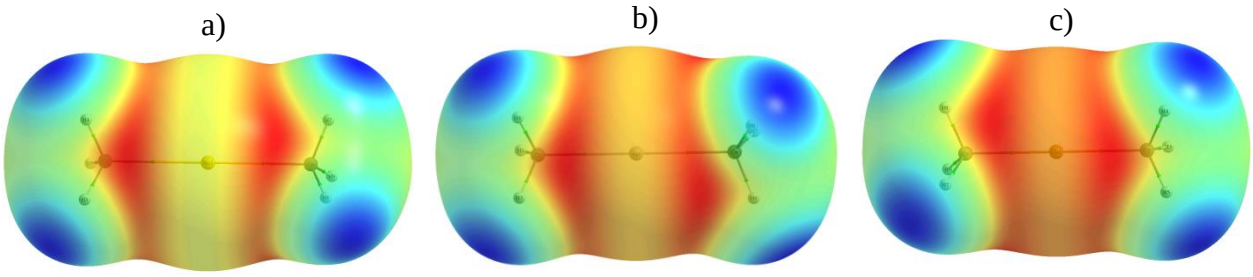

Figure 13 – Electrostatic surface potentials of the a) Au^{I}, b) Ag^{I} and c) Cu^{I}, and complexes at the electron density isosurface with a value of 0.001 au calculated at the B3LYP/aug-cc-pVTZ-pp level of theory.

The red regions are the greater negative areas of the molecule that will "interact" with approaching H-bond donor molecules. As we can see, the red regions are localised around the carbon atoms. These ESP of the isosurfaces illustrate the region where the maximum electrostatic interaction with the HF occur, explaining why none of these complexes yield an AIL connecting the metal centre to the H-bond donor. The most noticeable difference between the ESP plots of the relativistic and non-relativistic DMA [Figure 13 (a)] anionic complex is the torus around the gold atom which is bright yellow, as compared to the image shown in Figure 8 (a) and illustrates why the H-bond formed differs from the relativistic and non-relativistic models. Earlier, we showed that the ESPs are method dependent, here we now show that they are also basis set dependent. However, one fact is clear; the formation the H-bond to the metal centre can be predicted by mapping the ESP on the isosurface of the metal complex.

2.8. Conclusions

To summarise, we have shown that Au^- can act as an H-bond acceptor to six different H-bond donors with E_{INT} values, at the MP2/aug-cc-pVTZ-pp level of theory, ranging from -2.93 kcal/mol to -23.41 kcal/mol, for CH_4 and HF, respectively. The ability of Au^- to act as H-bond acceptor is known and our values agree with previous work performed by Kryachko [12].

We have also shown that the $[(Me)_2Au]^-$ ion can act as an H-bond acceptor with E_{INT} values ranging from -2.4 kcal/mol to -16.17 kcal/mol for the CH_4 and HCN H-bond donors, respectively. Similar trends were seen with regards to the E_{INT} dependency on the H-bond donor for both the auride anion and the DMA anionic complex, with HCN being the exception when H-bonded to $[(Me)_2Au]^-$ calculated utilising the MP2 method. Furthermore, the E_{INT} values calculated at the B3LYP/aug-cc-pVTZ-pp yield consistently comparable results to our MP2* benchmark with the TPSS/aug-cc-pVTZ-pp level of theory generally overestimating the E_{INT} values.

Most importantly, hydrogen bonds formed with both the Au^- and $[(Me)_2Au]^-$ ions conformed to the expected characteristics of H-bonds defined by IUPAC [45], where the Au···H distances are within the sum of vdW radii, there is a H-X bond elongation upon adduct formation, a decrease in the IR stretching frequency of the H-X bond and an AIL connecting Au to H accompanied by a BCP separating these two atoms. Furthermore, the AIM parameters agree with what is expected for H-bonds [41], as well as what has been found for H-bonds formed by other TMs [44]. In addition, our results for the $[(Me)_2Au]^-$ ion are consistent with values calculated by Koskinen *et al.* [15] obtained from the experimentally observed Au^{I}···H contact.

The NCI plots enabled us to conclude that the H-bond stabilisation occurs due to an interaction with the Au(I) centre and not with the neighbouring carbon atom.

The H-bond acceptor abilities of the $[(Me)_2Cu]^-$ and $[(Me)_2Ag]^-$ ions were also investigated where it was found that these two analogues do not form M···H interactions due to stronger competing C···H-F interactions. The H-bond acceptor ability was attributed to the difference in the topology of the ESPs.

The influence of relativistic effects on H-bond formation was also investigated, with the Au^- ion yielding an E_{INT} value 6 kcal/mol less stabilising when relativistic effects are omitted, while for the $[(Me)_2Au]^-$ ion no Au^{I}···H interaction was present. The ESP isosurface

revealed that the nonrelativistic basis set altered the ESP in such a way that the electrostatic potential of the gold became less negative, so that is was unable to act as a H-bond acceptor.

Our results suggest that the H-bond ability of the Cu(I), Ag(I) and Au(I) centres can be determined by calculating the ESP of the metal complex.

Most importantly, we have shown that Au(I) can indeed act as a good H-bond acceptor that binds to various neutral H-bond donors, and is more stabilising than other known examples where TMs act as H-bond acceptors.

References

1. Martín, A., *J. Chem. Edu.*, 1999. **76**(4): p. 578.
2. Siddiqui, K.A. Tiekink, E.R.T., *Chem. Commun*., 2013. **49**(76): p. 8501-8503.
3. Rizatto, S., Bergés, J., Mason, S.A., Albinati, A., Kozelka, J., *Angew. Chem. Int. Ed.*, 2010. **49**: p. 7440.
4. Zhao, D., Ladipo, F.T., Braddock-Wilking, J., Brammer, L., Sherwood, P., *Organometallics*, 1996. **15**(5): p. 1441-1445.
5. Kazarian, S. G., Hamley, P.A., Poliakoff, M., *J. Am. Chem. Soc*., 1993. **115**.
6. Shubina, E.S., Krylov, A.N., Timofeeva, T. V., Struchkov, Y.T., Ginzburg, A. G., Loim, N. M., Epstein, L. M., *J. Organnomet. Chem.*, 1992. **434**.
7. Shubina, Y.S., Epstein, L.M., *J. Mol. Struct.*, 1992. **265**.
8. Brammer, L. *Dalton Trans.*, 2003(16): p. 3145-3157.
9. Jansen, M., *Chem. Soc. Rev*., 2008. **37**(9): p. 1826-1835.
10. Peer, W.J. Lagowski, J.J., *J. Am. Chem. Soc.*, 1978. **100**(19): p. 6260-6261.
11. Jagannathan, R., Wallace, D.B., Lagowski, J.J., *Inorganic Chemistry*, 1985. **24**(1): p. 113-114.
12. Kryachko, E.S., *J. Mol. Struct.*, 2008. **880**(1–3): p. 23-30.
13. Schmidbaur, H., Raubenheimer, H.G., Dobrzanska, L., *Chem. Soc. Rev.*, 2014. **43**(1): p. 345-380.
14. Thakur, T.S. Desiraju, G.R., *J. Mol. Struct.: THEOCHEM*, 2007. **810**(1–3): p. 143-154.
15. Koskinen, L., Jääskeläinen, S., Kalenius, E., Hirva, P., Haukka, M., *Cryst. Growth & Des*, 2014. **14**(4): p. 1989-1997.
16. Dem'yanov, P.I. Gschwind, R.M., *Organometallics*, 2006. **25**(24): p. 5709-5723.
17. Frisch, M.J., Trucks, G.W., Schlegel, H.B., Scuseria, G.E., Robb, M.A., Cheeseman, J.R., Scalmani, G., Barone, V., Mennucci, B., Petersson, G.A., Nakatsuji, H., Caricato, M., Li, X., Hratchian, H.P., Izmaylov, A.F., Bloino, J., Zheng, G., Sonnenberg, J.L., Hada, M., Ehara, M., Toyota, K., Fukuda, R., Hasegawa, J., Ishida, M., Nakajima, T., Honda, Y., Kitao, O., Nakai, H., Vreven, T., Montgomery, J.A., Peralta, J.E., Ogliaro, F., Bearpark, M., Heyd, J.J., Brothers, E., Kudin, K.N., Staroverov, V.N., Kobayashi, R., Normand, J., Raghavachari, K., Rendell, A., Burant, J.C., Iyengar, S.S., Tomasi, J., Cossi, M., Rega, N., Millam, J.M., Klene, M., Knox, J.E., Cross, J.B., Bakken, V., Adamo, C., Jaramillo, J., Gomperts, R., Stratmann, R.E., Yazyev, O., Austin, A.J., Cammi, R., Pomelli, C., Ochterski, J.W., Martin, R.L., Morokuma, K., Zakrzewski, V.G., Voth, G.A., Salvador, P., Dannenberg, J.J., Dapprich, S., Daniels, A.D., Farkas, Foresman, J.B., Ortiz, J.V., Cioslowski, J., Fox, D.J., *Gaussian 09, Revision B.01*. 2009.
18. Boys, S.F., Bernardi, F., *Mol. Phys.*, 1970. **19**(4): p. 553-566.
19. Simon, S., Duran, M., Dannenberg, J.J., *J. Chem. Phys.*, 1996. **105**(24): p. 11024-11031.

20. Becke, A.D., *J. Chem. Phys.*, 1993. **98**(7): p. 5648-5652.
21. Lee, C., Yang, W., Parr, R.G., *Phys. Rev. B*, 1988. **37**(2): p. 785-789.
22. Miehlich, B., Savin, A., Stoll, H., Preuss, H., *Chem. Phys. Lett.*, 1989. **157**(3): p. 200-206.
23. Tao, J., Perdew, J.P., Staroverov, V.N., Scuseria, G.E., *Phys. Rev. Lett.*, 2003. **91**(14): p. 146401.
24. Peterson, K.A., Puzzarini, C., *Theor. Chem. Acc.*, 2005. **114**(4-5): p. 283-296.
25. Figgen, D., Rauhut, G., Dolg, M., Stoll, H., *Chem. Phys.*, 2005. **311**(1–2): p. 227-244.
26. Kendall, R.A., Dunning, T.H., Harrison, R.J., *J. Chem. Phys.*, 1992. **96**(9): p. 6796-6806.
27. Dunning, T.H., *J. Chem. Phys*., 1989. **90**(2): p. 1007-1023.
28. Møller, C., Plesset, M.S., *Phys. Rev.*, 1934. **46**(7): p. 618-622.
29. Binkley, J.S., Pople, J.A., *Int. J. Quantum. Chem.*, 1975. **9**(2): p. 229-236.
30. Feller, D., *J. Comp. Chem*., 1996. **17**(13): p. 1571-1586.
31. Schuchardt, K.L., Didier, B.T., Elsethagen, T., Sun, L., Gurumoorthi, V., Chase, J., Li, J., Windus, T.L., *J. Chem. Inf. Model*., 2007. **47**(3): p. 1045-1052.
32. Wesendrup, R., Schwerdtfeger, P., Unpublilshed, 1999.
33. Schwerdtfeger, P., Dolg, M., Schwarz, W.H.E., Bowmaker, G.A., Boyd, P.D.W., *J. Chem. Phys.*, 1989. **91**(3): p. 1762-1774.
34. Zhurko, G.A., Zhurko, .D.A., *ChemCraft*, 2012.
35. Keith, T.A., *AIMAll* 2012 TK Gristmill Software.
36. Johnson, E.R., Keinan, S., Mori-Sánchez, P., Contreras-García, J., Cohen, A.J., Yang, W., *J. Am. Chem. Soc*., 2010. **132**(18): p. 6498-6506.
37. Bondi, A., *J. Phys. Chem.*, 1964. **68**(3): p. 441-451.
38. Groenewald, F., Esterhuysen, C., Dillen, J., *Theor. Chem. Acc.*, 2012. **131**(10): p. 1-12.
39. Riley, K.E., Hobza, P., *J. Phys. Chem. A*, 2007. **111**(33): p. 8257-8263.
40. Zheng, W., Li, X., Eustis, S., Grubisic, A., Thomas, O., de Clercq, H., Bowen, K., *Chem. Phys. Lett.*, 2007. **444**(4–6): p. 232-236.
41. Nakanishi, W., Hayashi, S., Narahara, K., *J. Phys. Chem. A*, 2008. **112**(51): p. 13593-13599.
42. Keith, T.A. Frisch, M.J., *J. Phys. Chem. A*, 2011. **115**(45): p. 12879-12894.
43. Alkorta, I. Elguero, J., *Chem. Soc. Rev.*, 1998. **27**(2): p. 163-170.
44. Alkorta, I., Rozas, I., Elguero, J., *J. Mol. Struct.*: *THEOCHEM*, 2001. **537**(1–3): p. 139-150.
45. Arunan, E., Desiraju, G.R., Klein, R.A., Sadlej, J., Scheiner, S., Alkorta, I., Clary, D.C., Crabtree, R.H., Dannenberg, J.J., Hobza, P., Kjaergaard, H.G., Legon, A.C., Menucci, B., Nesbitt, D.J., *Pure. Appl. Chem.*, 2011. **83**(8): p. 1637-1641.
46. Boyd, R.J., Choi, S.C., *Chem. Phys. Lett.*, 1986. **129**(1): p. 62-65.
47. Bowers, M.T., Kerley, G.I., Flygare, W.H., *J Chem. Phys.*, 1966. **45**(9): p. 3399-3414.
48. Choi, C.H., Kertesz, M., *J. Phys. Chem.*, 1996. **100**(41): p. 16530-16537.
49. Murphy, W.F., Holzer, W., Bernstein, H.J., *Appl. Spectrosc.*, 1969. **23**(3): p. 211-218.

50. Fan, L., Ziegler, T., *J. Chem. Phys*., 1992. **96**(12): p. 9005-9012.

51. Pyykkö, P., *Angew Chem Int. Edit.*, 2004. **43**(34): p. 4412-4456.

3. Theoretical investigation on the inductive effects of ligands on the Lewis basicity of the Au(I) centre within anionic complexes

3.1. Abstract

Previous theoretical work has shown that the Au(I) metal centre can act as a hydrogen bond acceptor when bonded to two methanide ligands, yielding an anionic Au(I) complex. Here we explore the change in the Au(I) centre's Lewis basicity by changing the ligands with electron-withdrawing and electron-donating groups. We are particularly interested in how the change in the Lewis basicity affects geometrical parameters such as Au···H distances, Au···H-R angles, interaction energies (E_{INT}), Atoms in Molecules (AIM) parameters and Noncovalent Interaction (NCI) plots. Furthermore, we will use these geometrical and AIM parameters to characterise the Au^{I}···H interactions and their respective trends. Calculated E_{INT} values can change by 6.8 kcal/mol simply by varying the ligands coordinated to Au(I). Furthermore, our results suggest charge transfer from the Au(I) metal centre upon H-bond formation was noted in all cases, with one exception. Slight deviations from the expected trends if conventional inductive effects are considered were observed. The deviations occurred with regards to the E_{INT} values and could be explained upon further investigation of the NCI plots.

3.2. Introduction

It is known that transition metals can act as hydrogen bond acceptors and a large amount of research has been performed on this topic [1-12]. We will, however, only briefly highlight some of these results that are of relevance to this study.

Au^{-} and also Au^{0} have been shown to act as H-bond acceptors with H-bond donors such as HF, H_2O and NH_3 [11]. It was found that the Au···H-R angles for H_2O and NH_3 forming a H-bond to Au^{-} are less linear (~157º) than that obtained for HF (~180º). This was also found for the $[(Me)_2Au]^{-}$ complex bonded to the same H-bond donors and seem characteristic of the Au^{I}···H interaction [13].

Very recently, Schmidbaur and co-workers [12] postulated that Au(I) metal centres have the ability to act as H-bond acceptors, based upon unusual atomic properties of the gold atom. The authors state that solid state structures available within the Cambridge Structural Database exhibit no true H-bond to gold, with most Au^{I}···H contacts arising from weak Au^{I}···H-C interactions, which have crystallographers puzzled dating back as far as the early

1960s. The most recent and profound development in the search of the $Au^{I}\cdots H$ interaction occurred in 2014 with the work of Koskinen *et al.* [2], who obtained two crystal structures with this elusive $Au^{I}\cdots H$ interaction present. The authors reported a stabilisation energy of -1.7 kcal/mol, calculated with QTAIM charge density analysis, which is typical for dispersion type interactions and is expected for an $Au^{I}\cdots H$-C contact. Most importantly, the AIM analyses yielded an atomic interaction line connecting Au(I) to H and accompanied by a Bond Critical Point (BCP) is a clear indication of the formation of an H-bond as indicated by the IUPAC definition [14]. The authors [2] state that the $Au^{I}\cdots H$ interaction "play(s) a dominant role in the construction of the supramolecular structures". This statement is based upon the fact that the Au···H contact is the only directing interaction along the *c*-axis, and we consider this a fair deduction. However, we do remain a bit sceptical of the fact that this weak Au···H interaction can have such a significant influence in determining the packing arrangement. We agree with the authors that the $Au^{I}\cdots H$ interaction is important but if the AIM molecular graphs, found in the supplementary information, are considered other atomic interaction lines are present and could also have influenced the packing arrangement just as much as the $Au^{I}\cdots H$ interaction. The study was concluded with an enticingly profound statement: "These results show that even though the C-H···Au^{I} contacts are weak and often overshadowed by stronger interactions, they should not be ignored when considering the supramolecular ensembles of gold complexes."

Our current and previous work illustrate that the $Au^{I}\cdots H$ interaction can yield stabilisation energies comparable to conventional moderate to strong H-bonds. We have shown that the $[(Me)_2Au]^-$ ion can H-bond to a six different H-bond donors, ranging in strength from -2.05 to -15.95 kcal/mol at the MP2/cc-pVTZ-pp level of theory. Depending on the interaction energy, the Au···H distances ranged from 2.260 Å to 2.983 Å with AILs connecting the Au(I) atom to the H atom even though the sum of vdW radii is 2.86 Å. This suggests that this should be considered when structures are interpreted with possible Au···H contacts present.

To familiarise ourselves with general geometrical and AIM parameters where transition metals act as H-bond acceptors a few examples will be discussed. This will illustrate the significance our results by comparing it to known transition metals H-bonded adducts.

Zhao *et al*. [6] showed that as the basicity of the Co centre is increased, the N-H···Co interaction becomes more stabilising. This was confirmed by variable temperature ^{1}H and ^{13}C NMR studies in solution along with crystallographic data. They also performed *ab initio* SCF calculations of the potential energy surface varying the N-H···Co distance for the $Co(CO)_4^-$

and $Co(CO)_3PPh_3^-$ anions H-bonded to the Me_3NH^+ cation and showed the latter anion has a minimum energy conformation situated around 1.9 Å from Co. Poliakoff and co-workers [15] showed that Co, Rh, Ir can H-bond to an alcohol and found the O-H···M interaction energies to be comparable to conventional H-bond strengths. Furthermore, they showed that as the basicity of the metal centre increases, by either introducing an electron-donating ligand or by changing the metal centre, the O-H···M H-bond strength increased. Alkorta *et al*. [1], reported interaction energies at the B3LYP/6-311++G** level for $[Co(CO)_4]^-$ H-bonded to HF and HCN of -11.26 kcal/mol and -9.59 kcal/mol, respectively. The authors performed Atoms In Molecules (AIM) analyses that yielded ρ_b and $\nabla^2(\rho_b)$ values of 0.0195 $e a_0^{-3}$ and 0.0306 $e a_0^{-5}$ as well as 0.0109 $e a_0^{-3}$ and 0.0207 $e a_0^{-5}$, for HF and HCN, respectively, H-bonded to $[Co(CO)_4]^-$ ion. These results are characteristic of H-bonds and give us an idea what to expect for H-bonded transition metal complexes. In addition, the authors showed that when H-bonding occurs, the natural atomic charge of the Co centre becomes more positive indicating a loss of electrons; the atomic charge changed by 0.053 *e* and 0.037 *e* for the HF and HCN H-bonded adducts, respectively. Most interestingly, the Alkorta [1] concluded that the lack of formal charge on the Ni atom within the organometallic complex is responsible for the absence of H-bond formation.

Brammer [5] mentions that H-bonds are often discussed as static interaction and it is important to think of the D-H···M interactions in a dynamic way, such that they indicate an incipient proton transfer reaction. H-bond formation can also be seen as an oxidative addition of the D-H groups to the metal centre. Recently, Rizzato and co-workers [4] showed that Pt^{II} forms H-bonds to H_2O and that these interactions are dispersion-type interactions with a stabilisation energy of -3.9 kcal/mol. Furthermore, the authors concluded that they have reported "the first crystallographic evidence for a hydrogen-bonding-like interaction between a water molecule and a d^8 metal ion, based on neutron diffraction." The authors speculate that H-bonding may affect the solvolysis mechanism and could be the cause of the slow aquation rate constants previously reported for Pt^{II} complexes. Siddiqui and Tiekink [3] performed a CSD survey where they showed that Cu and Ni can also act as H-bond acceptors with specific angle ranges. They postulate that the stabilisation of these interaction would be less than 3.9 kcal/mol, as calculated for the OH···Pt H-bond in the inverse hydrated *trans*-$[PtCl_2(NH_3)(N\text{-glycine})]\cdot H_2O$ [4] complex.

The aim of this study is to extend the number of theoretical examples of H-bonded Au^I adducts and thus to obtain more geometrical and AIM parameters on this novel $Au^{I}\cdots H$

interaction. Since, we have previously shown $[(Me)_2Au]^-$ acts as a H-bond acceptor, we thought it would be logical to extend from this ion, which we know can act as one. This study addresses the influences of electron-withdrawing and electron-donating groups on the Lewis basicity of Au(I) and if this affects the H-bond formation. We hope the results would give us an idea of what is the maximum and minimum $Au^{I}\cdots H$ interaction energy strength for Au(I) when bonded to a negatively charged carbon atom, thus providing a range of interaction energies, geometrical and AIM parameters for Au(I) bonded to a anionic carbon donor atom. Furthermore, we hope the results shown here would aid in the understanding of the $Au^{I}\cdots H$ interaction and prerequisites needed for this interaction to occur, i.e. the less basic the Au(I) centre becomes, the more acidic the H-bond donor's proton must be for this interaction to occur. We are essentially implicitly probing the influence the properties of the negatively charged coordinating carbon atom has on the formation of the $Au^{I}\cdots H$ interaction. In addition, by introducing the fluoronated methanide ligands, we are also investigating the affect close-lying H-bond acceptors have on the formation and geometry of these interactions. According to conventional knowledge, the E_{INT} trend will follow the inductive ability of the ligand coordinated to Au(I) and will be investigated.

3.3. Methodology

All geometry optimisations were performed in the gas phase utilising the Gaussian 09 revB.01 [16] software package. No symmetry constraints were enforced during optimisations and all the geometry optimisations were performed in the gas phase. Frequencies were calculated to confirm that the structures are energy minima. All optimisations were performed with the counterpoise corrections [17, 18] to remove the basis-set superposition error (BSSE).

The interaction energy was calculated by:

$$E_{INT} = E_{AB}^{BSSE} - (E_A + E_B)$$

Where the E_A and E_B geometries were obtained from the optimised H-bonded adduct.

The elongation of the H-R bond (ΔR) upon H-bond formation of the H-bond donor was calculated by subtracting the H-bond donor bond length in the opimised monomer $[(HR)_{monomer}]$ from that of the adduct $[(HR)_{adduct}]$:

$$\Delta R = (HR)_{adduct} - (HR)_{monomer}.$$

The B3LYP [19-21] and TPSSTPSS (TPSS) [22] Density Functionals (DFs) were utilised in combination with the aug-cc-pVTZ-pp [23] basis set along with the effective core potential

(ECP) designed by Friggen *et al.*[24] used to describing the Au atom while the other atoms (H, C, F, O, N) were represented by the aug-cc-pVTZ [25, 26] basis set. All the basis sets utilised for this study were downloaded from the EMSL basis set exchange website. [27, 28] The optimised geometries were visually investigated utilising the ChemCraft [29] suite. The sum of the vdW radii for the Au···H interaction was selected to be 2.86 Å with the van der Waals (vdW) radii being 1.66 Å as defined by Bondi [30] with the vdW radii of H being 1.2 Å.

The Atoms In Molecules analyses were performed utilising AIMAll [31] version 14.06.21. The electron density ρ_b $(e a_0^{-3})$ at the intermolecular Bond Critical Point (BCP) and Laplacian of the electron density $\nabla^2(\rho_b)$ $(e a_0^{-5})$ were obtained as is from AIMAll. The b subscript indicates an intermolecular BCP situated between the two noncovalently interacting molecules. The wave functions were obtained as *.wfx files of the optimised geometries performed at the B3LYP/aug-cc-pVTZ-pp level of theory, utilising Gaussian 09 revB.01 [16]. The Noncovalent Interaction (NCI) plots, as proposed by Johnson *et al.* [32], were calculated from the same wfx file and were graphically displayed utilising the AIMAll software. The Reduced Electron Density Gradient (RDG) isosurfaces were calculated with a resolution spacing of 0.04 au. The isosurface regions of the RDG were calculated at a value of 0.5 au and with a minimum and maximum electron densities of 0.0001 and 0.05 $e a_0^{-3}$, respectively. The RDG surfaces were colour coded by mapping the "Sign(HessRho_EigVal_2)*Rho" [sign(λ_2) ×ρ] onto the RDG surface. The colour scale ("Range Method") was defined by the "-Maximum Magnitude to +Minimum Magnitude" method and takes the absolute value of the largest sign(λ_2) ×ρ value to assign colours accordingly. Red indicates a negative or greater negative sign(λ_2) ×ρ value and blue the positive value of sign(λ_2) ×ρ and are scaled according to the largest absolute values. The Δq values (difference in AIM charges) were calculated by

$\Delta q(Au) = q(Au)_{monomer} - q(Au)_{adduct}$.

The Interacting Quantum Atom approach could not be followed due to the influence of the ECPs on the atomic energies, similarly, the Total Electronic Energy Density (H) obtained from the AIM analyses was ignored for the same reason, since the author of AIMAll only mentions that only part of the electron density is recovered [33].

3.4. Results and Discussion

In our previous work [13] we investigated the ability of $[(Me)_2Au]^-$ (**1**) to H-bond to numerous H-bond donors, thus behaving as a Lewis base. Here we investigate the dependence of the gold atom's Lewis basicity and hence the E_{INT} values, on the substituents bonded to the carbon atom coordinated to Au(I) (See Figure 1). We selected $[(CMe_3)_2Au]^-$ (**2**) and $[(CF_3)_2Au]^-$ (**3**) complexes with electron-donating and electron-withdrawing ligands, respectively.

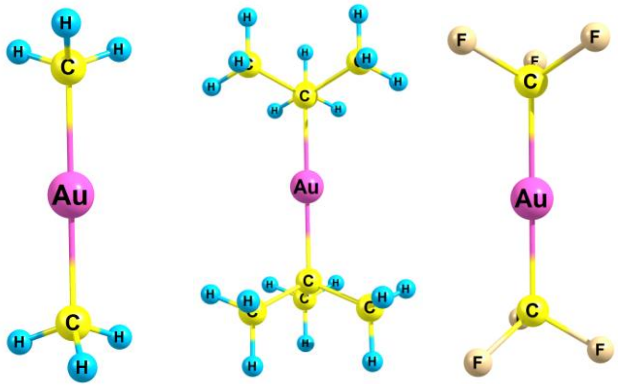

1 **2** **3**

Figure 1 – The three Au(I) complexes under investigation, i.e., $[(Me)_2Au]^-$ (**1**), $[(CMe_3)_2Au]^-$ (**2**) and the $[(CF_3)_2Au]^-$ (**3**).

The inductive ability of the ligands are such that the atomic charges on the Au(I) is expected to be **2** < **1** < **3**. Therefore, according to conventional wisdom, the E_{INT} values should be **2** < **1** < **3** for the same H-bond donor. Due to computational cost, the theoretical investigation was performed using two DFs, i.e. B3LYP and TPSS in combination with the aug-cc-pVTZ-pp basis sets that were used in prior studies [13]. We have previously concluded that the B3LYP method consistently yielded comparable results to the MP2/cc-pVTZ-pp benchmarks illustrating that these interactions can be modelled and investigated with computationally less expensive methods, with the TPSS method constantly overestimating the E_{INT} and thus therefore we consider the B3LYP/aug-cc-pVTZ-pp level of theory to be the more accurate DF. Previously published E_{INT} and geometrical parameters are given in Table 1. Again, the sum of van der Waals radii of Au and H is defined as 2.86 Å.

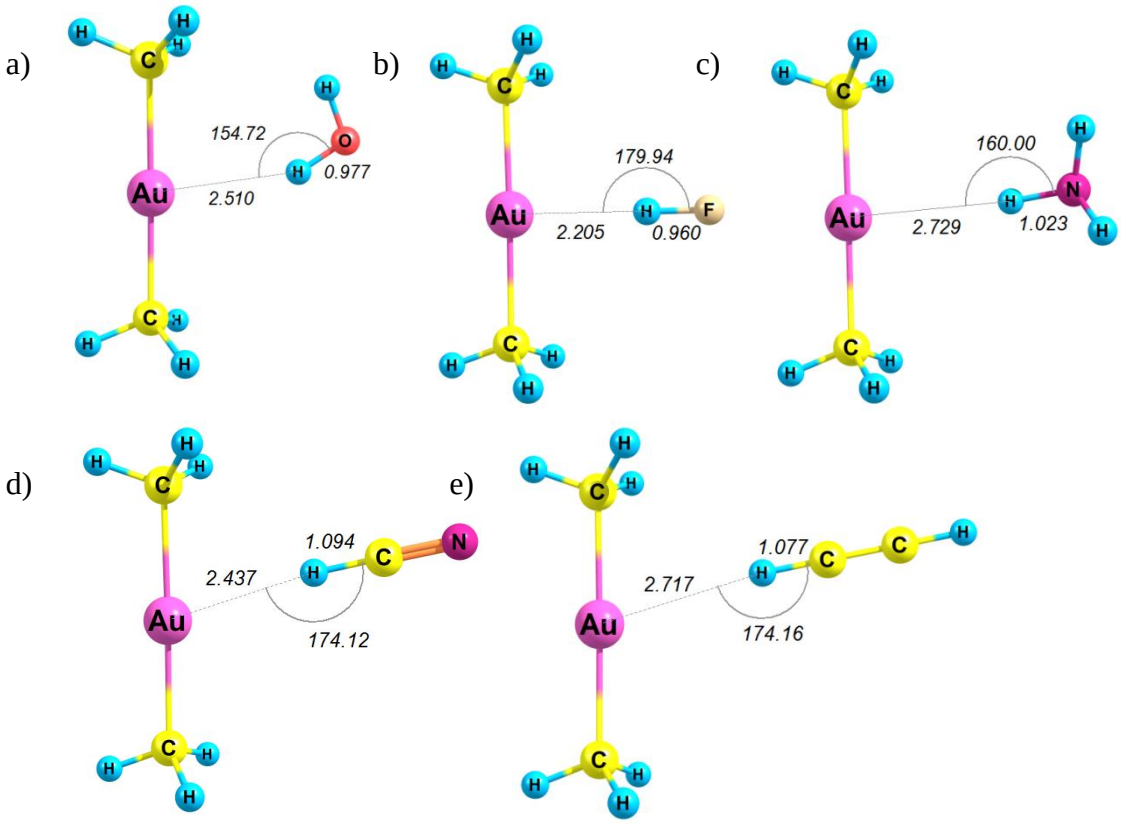

Figure 2 – Optimised geometries of **1** H-bonded to a) H_2O, b) HF, c) NH_3, d) HCN and e) HCCH donors at the B3LYP/aug-cc-pVTZ-pp level of theory.

The interaction energies and geometrical parameters of these adducts showed in Figure 2 are summarised in Table 1. These results will not be discussed extensively, since we have done so previously.

Table 1 – The E_{INT} (kcal/mol), *d*(Au···H) distances (Å), Au···H-R bonding angles (º), the H-R distances (Å) and the ΔR values (Å) for the optimised geometries of the complex **1** H-bonded to a number of H-bond donors, calculated at the B3LYP and TPSS levels of theory with the aug-cc-pVTZ-pp basis sets for all the atoms.

Method	**H-bond donor**	**E_{INT} (kcal/mol)**	***d*(Au···H) (Å)**	**Au···H-R (deg)**	**H-R (Å)**	**ΔR (Å)**
B3LYP	H_2O	-9.50	2.510	154.7	0.977	0.015
TPSS		-10.48	2.374	159.5	0.992	0.023
B3LYP	HF	-15.32	2.205	179.9	0.960	0.036
TPSS		-17.34	2.124	179.9	0.979	0.049
B3LYP	NH_3	-4.81	2.729	160.0	1.023	0.010
TPSS		-5.45	2.596	162.4	1.033	0.014
B3LYP	HCN	-13.57	2.437	174.1	1.094	0.029
TPSS		-14.79	2.299	177.4	1.111	0.041

B3LYP	HCCH	-5.05	2.717	174.2	1.077	0.015
TPSS		-5.76	2.580	176.2	1.086	0.020

Nevertheless, we note that the B3LYP E_{INT} values in order of decreasing stabilisation are HF > HCN > H_2O > HCCH > NH_3. Furthermore, the Au···H distances correlate to the E_{INT} values, which is also reflected in the ΔR values (defined as the lengthening of the R-H bond length upon H-bond formation). Thus, the higher the stabilisation, the shorter the Au···H distance becomes and the more elongated the H-R bond becomes. As previously seen for the H-bond adducts of the Au^- ion, we observe here that the Au···H-R angle deviates most from linearity for the H_2O and NH_3 H-bond donors. This suggests that an H-bond has indeed formed, but for confirmation AIM analyses were performed with the summarised results in Table 2.

Table 2 – The ρ_b ($e a_0^{-3}$) and the $\nabla^2(\rho_b)$ ($e a_0^{-5}$) of the optimised structures at the B3LYP/aug-cc-pVTZ-pp level of theory of the complex **1** H-bonded to H_2O, HF and HCN.

H-bond donor	$\boldsymbol{\rho_b}$ $\boldsymbol{(e a_0^{-3})}$	$\boldsymbol{\nabla^2(\rho_b)}$ $\boldsymbol{(e a_0^{-5})}$
H_2O	0.0179	0.0385
HF	0.0332	0.0404
HCN	0.0212	0.0434

The results in Table 2 show that just as the higher E_{INT} values correspond to shorter Au···H distances, they also correlate to higher ρ_b values. HF yields the most stable H-bonded adduct and H_2O the least stable, with interaction energies of -15.32 kcal/mol and -9.50 kcal/mol, respectively. In order to study the effect of greater electron donation, the optimised geometries of **2** H-bonded to H_2O, HF, NH_3, HCN and HCCH are shown in Figure 3 with the E_{INT} values and geometrical parameters summarised in Table 3.

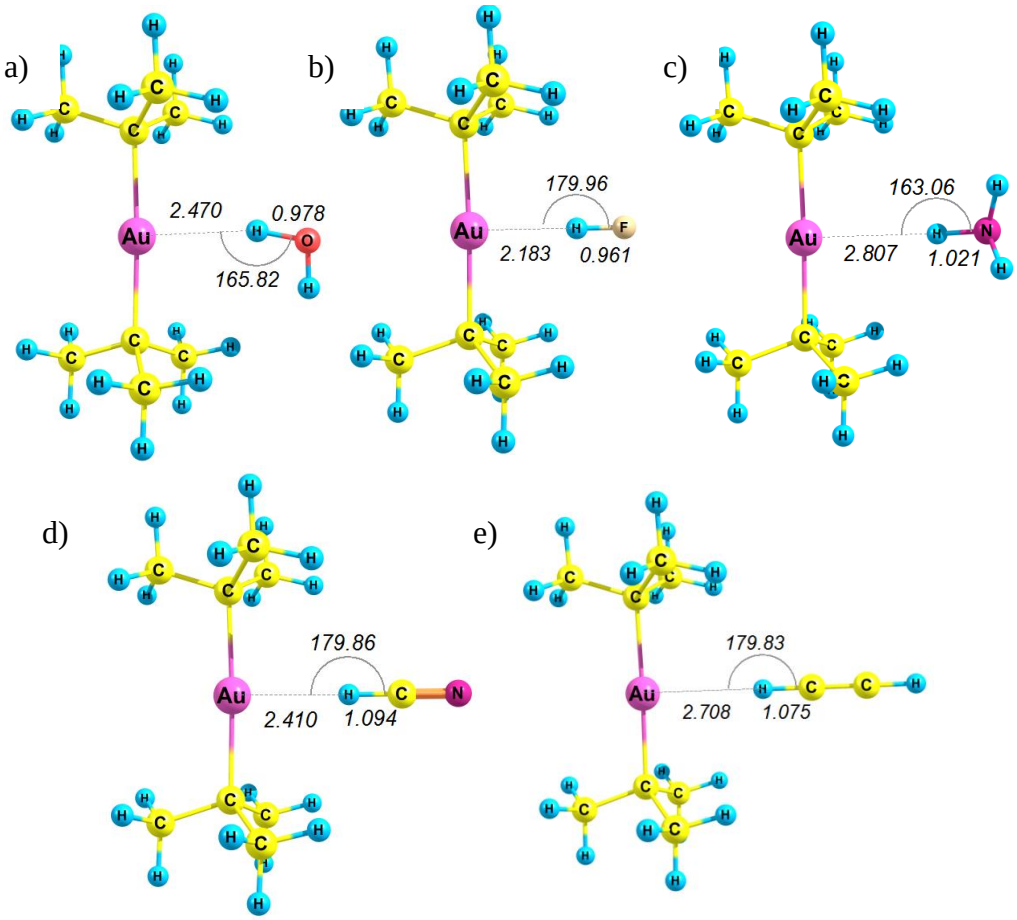

Figure 3 – Optimised geometries of **2** H-bonded to a) H_2O, b) HF, c) NH_3, d) HCN and e) HCCH at the B3LYP/aug-cc-pVTZ-pp level of theory.

At the B3LYP/aug-cc-pVTZ-pp level of theory, the order of decreasing stabilisation, E_{INT}, is HF > HCN > H_2O > HCCH > NH_3. The dependence of E_{INT} with regards to the H-bond donor is identical to that for complex **1**, but surprisingly, the E_{INT} values of **1** are more stabilising than those of **2**. These adducts containing **1** are generally about 1.5 kcal/mol more stable than those of **2**. At first, this seems counterintuitive since the Au(I) centre in complex **2** should be considered a stronger Lewis base than complex **1**, due to the inductive effects of the ligands, resulting in a stronger $Au^{I}\cdots H$ interaction. However, even though the H-bond E_{INT} values of **2** are less stabilising than **1**, the Au···H distances of these adducts (Figure 3) are generally shorter, with the **2**.NH_3 adduct being the exception. This trend of E_{INT} can be explained by the NCI plots shown in Figure 4. We also observe that the ΔR values of **2** are larger than **1**. The shortening of the Au···H distance, along with a larger ΔR value, suggest that the Au(I) atom in **2** is indeed a stronger Lewis base than in **1**.

Table 3 –E_{INT} (kcal/mol), intermolecular distance [*d*(Au···H)] (Å), bonding angle (Au···H-R) (º), H-R distance (Å) and ΔR (Å) for the optimised geometries of the complex **2** H-bonded to HF, HCN, HCCH, H_2O and NH_3 with B3LYP and TPSS using the aug-cc-pVTZ-pp basis set.

Method	H-bond donor	E_{INT} (kcal/mol)	*d*(Au···H) (Å)	Au···H-R (deg)	H-R (Å)	ΔR (Å)
B3LYP	H_2O	-7.35	2.470	165.8	0.978	0.017
TPSS		-8.46	2.352	168.4	0.993	0.025
B3LYP	HF	-13.69	2.183	180.0	0.961	0.037
TPSS		-15.77	2.108	179.9	0.980	0.050
B3LYP	NH_3	-3.49	2.807	163.1	1.021	0.008
TPSS		-4.11	2.661	165.3	1.031	0.012
B3LYP	HCN	-11.36	2.410	179.9	1.094	0.028
TPSS		-12.58	2.306	179.8	1.108	0.038
B3LYP	HCCH	-3.63	2.708	179.8	1.075	0.014
TPSS		-4.40	2.586	180.0	1.084	0.019

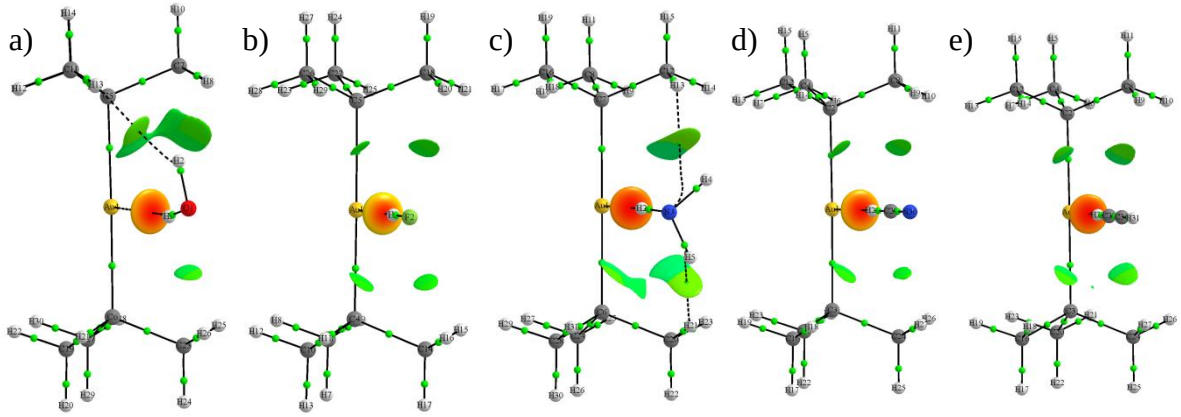

Figure 4 – Molecular graphs and NCI plots of complex **2** H-bonded to H_2O, HF, NH_3, HCN and HCCH at the B3LYP/aug-cc-pVTZ-pp level of theory. The red regions indicate stabilising interactions and the lime green regions dispersion type interactions. Atomic interaction lines are represented by the solid and dotted black lines and the BCPs are represented by green spheres.

The sign(λ_2)×ρ values of the NCI plots are summarised in Table 4, with the red regions coinciding with stabilising interactions and cyano/blue regions with repulsive nonbonding intermolecular interactions. The greater negative the sign(λ_2)×ρ value is, the more stabilising the interaction. The NCI plots thus give one a qualitative visual representation of the directionality of the intermolecular interactions and also their relative magnitudes. Furthermore, the molecular graphs in Figure 4 confirm the existence of a H-bond by the presence of an AIL connecting the H-bond donor to Au(I).

The NCI plots in Figure 4 reveal regions of repulsion (nonbonding interactions) indicated by a cyano/blue colour and weaker dispersion-type interactions shown in lime green. This effect

is noticeable for **2**.NH_3 and **2**.H_2O. The NCI plots suggest that there is repulsion between the negatively charged carbon atoms and the H-bond donor's heteroatoms and this is why the **2**.NH_3 adduct yield a larger Au···H distance compared to **1**.NH_3. The most apparent difference can be observed in the Au···H-R angles, with it being more linear for H-bonded adducts of **2** in order minimise repulsion. Furthermore, the repulsion between the coordinated ligands and the H-bond donor, as indicated in Figure 4, explains the destabilisation noted in the overall E_{INT} values of **2**.

Table 4 – The ρ_b ($e a_0^{-3}$), $\nabla^2(\rho_b)$ ($e a_0^{-5}$) and the sign(λ_2)×ρ values for the NCI plots of the complex **2** H-bonded to H_2O, HF, NH_3, HCN and HCCH of the optimised structures at the B3LYP/aug-cc-pVTZ-pp level of theory

	AIM Results		**sign(λ_2)×ρ values (au)**	
H-bond donor	$\boldsymbol{\rho_b}$ $\boldsymbol{(e a_0^{-3})}$	$\boldsymbol{\nabla^2(\rho_b)}$ $\boldsymbol{(e a_0^{-5})}$	**Min (Red)**	**Max (Blue)**
H_2O	0.020	0.039	-0.0220	0.0037
HF	0.035	0.040	-0.0433	0.0244
NH_3	0.010	0.024	-0.0112	0.0028
HCN	0.023	0.044	-0.0260	0.0032
HCCH	0.012	0.029	-0.0133	0.0025

If the minimum sign(λ_2)×ρ values shown in Table 4 are arranged in increasing order the trend is HF < HCN < H_2O < HCCH < NH_3, which is inversely proportional to the trend seen for E_{INT} and implies that the more stabilising E_{INT} is, the more negative the sign(λ_2)×ρ value. On the other hand, if we consider the maximum sign(λ_2)×ρ values, the opposite trend is obtained HCCH < NH_3 < HCN < H_2O < HF revealing the influence of the intermolecular repulsion (cyano regions in Figure 4 and are also referred to as nonbonding interactions). The lime green regions of the NCI plots reveal additional dispersion-type interactions present that are not always detected and represented by atomic interaction lines.

Similarly, the ρ_b values show the E_{INT} values: the more stabilising the value of E_{INT} the higher the electron density at the intermolecular BCP. Nakanishi *et al.*[34] have defined typical ranges for BCP parameters of H-bonding: $0.01 < \rho_b < 0.04$ and $0.04 < \nabla^2(\rho_b) < 0.12$. All the calculated ρ_b and $\nabla^2(\rho_b)$ values in Table 4 fall within these ranges except for the values for **2**.H_2O, **2**.NH_3 and **2**.HCCH which are less than the minimum value expected for H-bonds, namely 0.04 $e a_0^{-5}$. Nevertheless, the **2**.H_2O, **2**.NH_3 and **2**.HCCH adducts would only be considered a vdW-type interaction if both the ρ_b and $\nabla^2(\rho_b)$ values were less that the minimum value defined for H-bonds. Thus, we conclude that the $Au^{I}\cdots H$ interactions of **2** with H_2O, HF, NH_3, HCN and HCCH are H-bonds.

To this end, the interaction energies and geometrical parameters of the weakest Lewis base, complex **3** (shown in Figure 5) are summarised in Table 5. Only the H_2O, HF and HCN H-bond donors yielded stationary points where an $Au^{I}\cdots H$ interaction is present, while alternative interactions were found for NH_3 and HCCH. The reason for HCCH and NH_3 not forming stable conformations with an $Au^{I}\cdots H$ interaction present could be a result of two possibilities 1) The basicity of the Au(I) atom is insufficient and it can not act as Lewis base for the H-bond donors 2) the competing F···H interaction provides substantially more stabilisation than the $Au^{I}\cdots H$ interaction, i.e. the fluorine atom is a better H-bond acceptor than Au(I) and attracts the H-bond donor away from the Au atom.

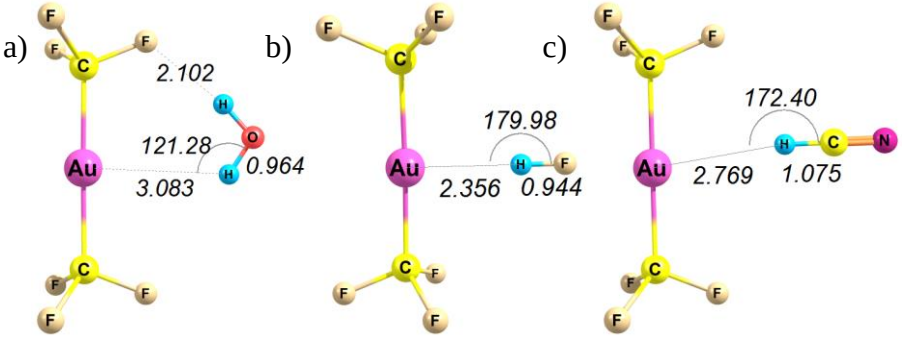

Figure 5 – Optimised geometries of **3** H-bonded to a) H_2O, b) HF and c) HCN at the B3LYP/aug-cc-pVTZ-pp level of theory.

Table 5 – The interaction energies (kcal/mol) and geometrical parameters of the H-bonded complex **3** to H_2O, HF and HCN calculated at the B3LYP and TPSS DFs with the aug-cc-pVTZ-pp basis sets.

Method	H-bond donor	E_{INT} (kcal/mol)	*d*(Au···H) (Å)	Au···H-R (deg)	H-R (Å)	ΔR (Å)
B3LYP	H_2O	-7.20	3.083	121.3	0.964	0.0024
TPSS		-7.33	2.977	119.8	0.972	0.0035
B3LYP	HF	-8.48	2.356	180.0	0.944	0.0195
TPSS		-9.76	2.251	179.9	0.959	0.0284
B3LYP	HCN	-8.54	2.769	172.4	1.075	0.0099
TPSS		-8.93	2.612	179.9	1.085	0.0147

If the E_{INT} values of complex **3** (Table 5) are arranged in order of decreasing H-bond stability, then: HCN > HF > H_2O. This trend is different to what we have seen for H-bonded adducts of complexes **1** and **2**, where the most stable H-bonded adducts were formed with HF. Surprisingly, complex **3** forms the most stable H-bonded adduct with HCN. This outcome can be explained by the molecular graphs and NCI plots in Figure 6.

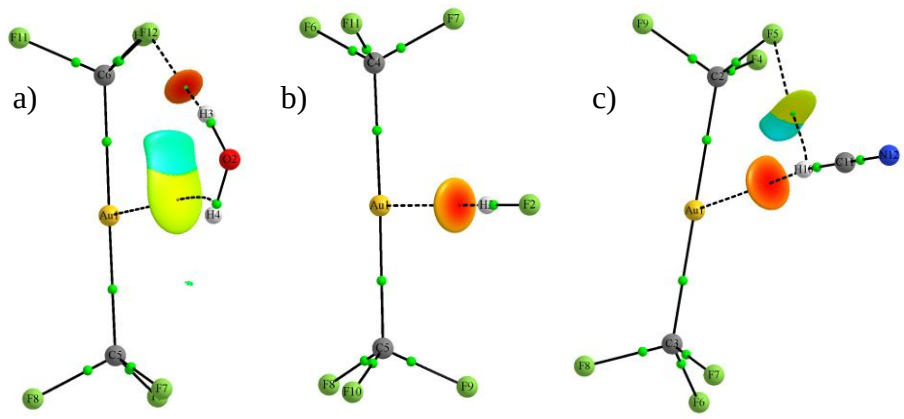

Figure 6 – Molecular graphs and NCI plots of the optimised geometries of **3** H-bonded to a) H_2O, b) HF and c) HCN at the B3LYP/aug-cc-pVTZ-pp level of theory. Atomic interaction lines are represented by the solid and dotted black lines, the BCPs are represented by green spheres and RCPs are represented by red spheres.

These molecular graphs reveal two H-bonds are present when complex **3** H-bonds to H_2O and HCN, the second being an H···F hydrogen bond. Only HF yields a single H-bond to the Au(I) centre confirmed by the molecular graph and the NCI plot. The lime green regions are characteristic of weaker, dispersion-type interactions, while red regions are relatively more stabilising interactions. This allows us to conclude that HCN forms a secondary dispersion-type interaction to fluorine, while for H_2O the F···H interaction is stronger and a second, weak dispersion-type interaction is formed with Au(I). The blue NCI regions indicate nonbonding areas. Table 6 contains the sign(λ_2)×ρ values that are visually represented as the colour of Figure 6, along with the AIM parameters of the BCPs.

Table 6 – The electron density [ρ_b (ea_0^{-3})], the Laplacian of the electron density [$\nabla^2(\rho_b)$ (ea_0^{-5})] and the sign(λ_2)×ρ values of the NCI plots of the optimised structures of complex **3** H-bonded to H_2O, HF and HCN at the B3LYP/aug-cc-pVTZ-pp level of theory.

	AIM results		**sign(λ_2)×ρ value (au)**	
H-bond donor	$\boldsymbol{\rho_b}$ $\boldsymbol{(ea_0^{-3})}$	$\boldsymbol{\nabla^2(\rho_b)}$ $\boldsymbol{(ea_0^{-5})}$	**Min (red)**	**Max (Blue)**
H_2O	0.0065	0.0172	-0.015	0.006
HF	0.0234	0.0396	-0.027	-0.017
HCN	0.0103	0.0254	-0.011	0.008

The ρ_b values in Table 6 for the HF and HCN H-bonded adducts fall within the expected values for H-bonds as defined by Nakanishi *et al.*[34] The ρ_b value of **3**.H_2O is indicative of a vdW-type interaction. The $\nabla^2(\rho_b)$ values are all less than those normally expected for H-bonds, where the range for H-bonds $0.04 < \nabla^2(\rho_b) < 0.12$ ea_0^{-5}. The AIM parameters in

Table 6 for HF and HCN allow us to conclude that these adducts resemble weak H-bond interactions, while the Au···H_2O atomic interaction line arises due to vdW-type interactions as suggested by both the AIM parameters and the NCI plots.

Table 7 – E_{INT} values and F···H distances for NH_3 and HCCH H-bonded to complex **3**

Method	H-bond donor	E_{INT} (kcal/mol)	*d*(F···H) (Å)
B3LYP	NH_3	-3.73	2.495
B3LYP	HCCH	-3.52	2.173

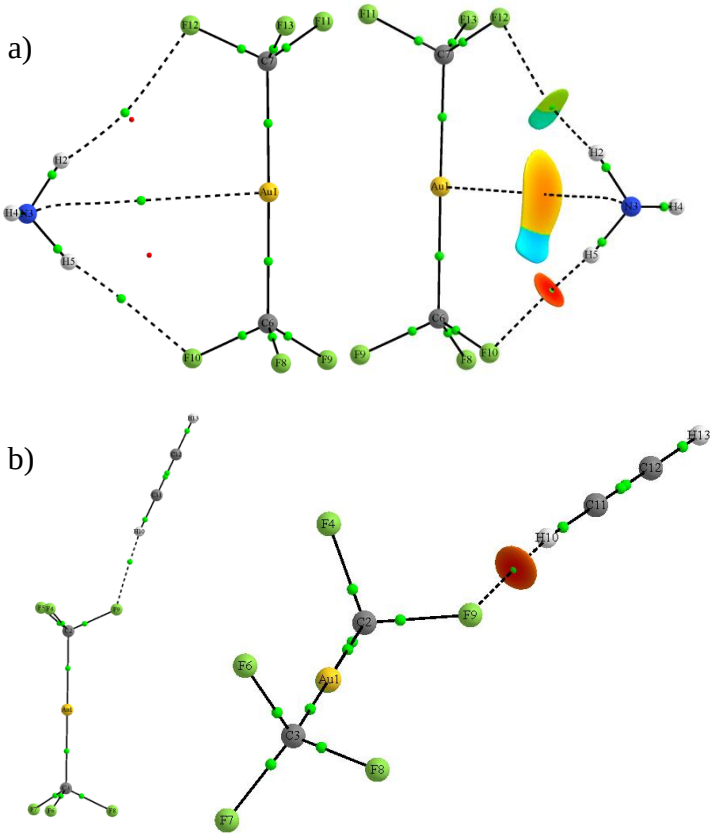

Figure 7 –Molecular graphs and NCI plots of the optimised geometries for adducts a) **3**.NH_3 and b) **3**.HCCH at the B3LYP/aug-cc-pVTZ-pp level of theory.

Figure 7 displays the stable H-bonded conformations found for monomer **3** when the NH_3 and HCCH H-bond donors are considered. No $Au^{I}\cdots H$ interactions are present due to competing F···H intermolecular interactions (Table 7). Surprisingly, we see an atomic interaction line connecting Au(I) to N, but the small negative sign(λ_2)×ρ values and BCP properties (listed in Table 8) indicate that all the interactions shown are vdW-type interaction arising from the F···H contacts forcing the N atom close enough to the Au(I) centre for an atomic interaction line to occur.

We classify these F···H interactions as competing interactions. One of our criteria for the $Au^{I}\cdots H$ interaction to be observed is that the competing interaction i.e. a close lying H-bond acceptor should be such that it does not pull the H-bond donor away from the gold atom.

Table 8 – The sign(λ_2)×ρ values of NH_3 and HCCH H-bonded to complex **3** The calculated E_{INT} values, the F··H distances, the electron density [ρ_b ($e a_0^{-3}$)] and the Laplacian of the electron density [$\nabla^2(\rho_b)$ ($e a_0^{-5}$)]

	sign(λ_2)×ρ (au)		**AIM parameters**	
H-bond donor	**Min (red)**	**Max (blue)**	**ρ_b ($e a_0^{-3}$)**	**$\nabla^2(\rho_b)$ ($e a_0^{-5}$)**
NH_3	-0.007	0.004	0.0063	0.0244
			0.00232	0.0088
			0.00459[a]	0.0124[a]
HCCH	-0.013	-0.010	0.0124	0.0514

[a] The BCP between Au(I) and N

The NCI plots in Figure 7 suggest that the nitrogen atom in NH_3 experiences repulsive interactions with the carbon atoms that are bonded to Au(I), represented by the light blue NCI regions. The most stabilising interaction of complex **3** H-bonded to NH_3 is the F···H contact, which we expect to contribute most to the E_{INT} value. This is also true for **3**.HCCH, where the F···H interaction is so strong that no stable conformation with the $Au^{I}\cdots H$ interaction were obtained. The ρ_b and $\nabla^2(\rho_b)$ values for HCCH indicates the intermolecular interaction is indeed a H-bond.

In order to gain insight into the relative basicity of the Au atoms, we utilised the atomic charges obtained from integration of the electron density across the atomic basin of the Au atoms for the complexes before and after H-bond formation. Only the examples where the H-bond donor formed H-bonds with all three complexes are included, namely HF, HCN and H_2O.

Table 9 –Interaction energies (E_{INT} in kcal/mol), AIM charges of the Au(I) atom for complexes **1**, **2** and **3** and their H-bonded adducts (Δq) to HF, HCN and H_2O at the B3LYP/aug-cc-pVTZ-pp level of theory.

Complex		**monomer**	**HF**	**HCN**	**H_2O**
$[(CH_3)_2Au]^-$ (**1**)	E_{INT}	-	-15.32	-13.57	-9.50
	Δq (e) Au	**-0.106**	0.177	0.196	0.025
$[(CMe_3)_2Au]^-$ (**2**)	E_{INT}	-	-13.69	-11.36	-7.35
	Δq (e) Au	**-0.069**	0.017	0.004	0.009
$[(CF_3)_2Au]^-$ (**3**)	E_{INT}	-	-8.48	-8.54	-7.20
	Δq (e) Au	**0.124**	0.007	-0.005	0.005

Surprisingly, complex **1** yields the greatest partial negative charge on the Au(I) atom, followed by the monomer **2** and **3**. This trend seen for the atomic charge of gold is surprising, since conventional chemistry would suggest that complex **2** would exhibit the greater partial negative charge on the Au(I) centre due to greater electron donating ability of the *tert*-butyl group over the methanide ligand. We suspect this is due to the longer Au-C bond length of **2** (2.16 Å) as compared to complex **1** (2.12 Å) at the B3LYP/aug-cc-pVTZ-pp level of theory. The elongation of the Au-C bond can only be explained by steric repulsion and would result in a less effective charge transfer from the carbon atom to the Au(I) centre.

Nevertheless, in all cases in Table 9, the Au(I) atom loses charge upon H-bond formation, with the HCN H-bonded to complex **3** being the exception, where the Au(I) atom gains electrons (0.005 *e*). It is interesting to note that even though complex **3** has a slightly positive partial charge it is still able to act as a H-bond acceptor and consistently loses charge when H-bond formation occurs, although we postulate that this could contribute to the fact that no Au···H interactions occur with the NH_3 and HCCH as H-bond donors.

Interestingly, complexes **1** and **3** exhibit identical trends, different to **2**, which can be ascribed to the steric influences by introducing "bulky" ligands. This is indicated by the NCI plots shown in Figure 3 where nonbonding/repulsive interactions arise between the heteroatoms of the H-bond donors and the carbon atoms on the ligands bonded to Au(I).

3.5. Conclusions

To conclude, the expected trend of E_{INT} as a function of the ligand's inductive ability is **2** > **1** > **3**. Our results indicate that this prediction is not necessarily true for E_{INT} and Δq values. Reasons for the deviations from the expected trend are also elegantly displayed by the cyano/blue NCI plot regions indicative of repulsion between atoms. However, inductive effects are most noticeable when the Au···H distances of the three complexes H-bonded to HF are compared, with values of 2.205, 2.183 and 2.356 Å for **1**, **2** and **3**, respectively.

Our AIM results indicate that the $Au^{I}\cdots H$ interactions can be classified as conventional H-bonds, or as vdW-type interactions when the H-bond is found to be relatively less stabilising. Furthermore, the calculated electron densities at the intermolecular BCPs along the Au···H atomic interaction line correlate with the Au···H distance for the three monomers H-bonded to HF with ρ_b having the largest value for complex **1**, followed by complex **2** and complex **3**. We only mention HF since it is the only H-bond donor that yield an AIL to the Au atom only. The minimum NCI values also correlate with the expected trend of inductivity with values of -0.0400, -0.0433, -0.027 au for complex **1**, **2** and **3**, respectively. To

summarise, the conventional understanding of inductive effects on a metal centre leads to expected trends for the Au···H distances, ρ_b and the sign(λ_2)×ρ, values but not necessarily for the E_{INT} values or charges, due to additional factors that can be explained by performing AIM and NCI analyses. Most importantly, all the $Au^{I}\cdots H$ interactions here exhibit geometrical and AIM parameters that are characteristic of H-bonding, as defined by IUPAC [14].

References

1. Alkorta, I., Rozas, I., Elguero, J., J. *Mol. Struct.: THEOCHEM*, 2001. **537**(1–3): p. 139-150.
2. Koskinen, L., Jääskeläinen, S., Kalenius, E., Hirva, P., Haukka, M., *Cryst. Growth & Des*, 2014. **14**(4): p. 1989-1997.
3. Siddiqui, K.A., Tiekink, Edward, R.T., *Chem. Commun.*, 2013. **49**(76): p. 8501-8503.
4. Rizzato, S., Bergès, J., Mason, S.A., Albinati, A., Kozelka, *J., Angew. Chem. Int. Ed*., 2010. **49**: p. 7440-7443.
5. Brammer, L., *Dalton. Trans*, 2003(16): p. 3145-3157.
6. Zhao, D., Ladipo, F.T., Braddock-Wilking, J., Brammer, L., Sherwood, P., *Organometallics*, 1996. **15**(5): p. 1441-1445.
7. Shubina, E.S., Krylov, A.N., Timofeeva, T.V., Struchkov, Y.T., Ginzburg, A.G., Loim, N.M., Epstein, L.M., *J. Organomet. Chem.*, 1992. **434**(3): p. 329-339.
8. Shubina, Y.S. Epstein, L.M., *J. Mol. Struct.*, 1992. **265**(3–4): p. 367-384.
9. Brammer, L., Zhao, D., Ladipo, F.T., Braddock-Wilking, J., *Acta Cryst B*, 1995. **51**(4): p. 632-640.
10. Martín, A., *J. Chem. Ed*., 1999. **76**(4): p. 578.
11. Kryachko, E.S., *J. Mol. Struct*., 2008. **880**(1–3): p. 23-30.
12. Schmidbaur, H., Raubenheimer, H.G., Dobrzanska, L., *Chem. Soc. Rev*., 2014. **43**(1): p. 345-380.
13. Groenewald, F. Esterhuysen C., Dillen, J., Raubenheimer, H., To be published.
14. Arunan, E., Desiraju, G.R., Klein, R.A., Sadlej, J., Scheiner, S., Alkorta, I., Clary, D.C., Crabtree R.H., Dannenberg, J.J., Hobza, P., Kjaergaard, H.G., Legon, A.C., Menucci, B., Nesbitt, D.J., *Pure Appl. Chem*., 2011. **83**(8): p. 1637-1641.
15. Kazarian, S.G., Hamley, P.A., Poliakoff, M., *J. Am. Chem. Soc. Rev*., 1993. **115**(20): p. 9069-9079.
16. Frisch, M.J., Trucks, G.W., Schlegel, H.B., Scuseria, G.E., Robb, M.A., Cheeseman, J.R., Scalmani, G., Barone, V., Mennucci, B., Petersson, G.A., Nakatsuji, H., Caricato, M., Li, X., Hratchian, H.P., Izmaylov, A.F., Bloino, J., Zheng, G., Sonnenberg, J.L., Hada, M., Ehara, M., Toyota, K., Fukuda, R., Hasegawa, J., Ishida, M., Nakajima, T., Honda, Y., Kitao, O., Nakai, H., Vreven, T., Montgomery, J.A., Peralta, J.E., Ogliaro, F., Bearpark, M., Heyd, J.J., Brothers, E., Kudin, K.N., Staroverov, V.N., Kobayashi, R., Normand, J., Raghavachari, K., Rendell, A., Burant, J.C., Iyengar, S.S., Tomasi, J., Cossi, M., Rega, N., Millam, J.M., Klene, M., Knox, J.E., Cross, J.B., Bakken, V., Adamo, C., Jaramillo, J., Gomperts, R., Stratmann, R.E., Yazyev, O., Austin, A.J., Cammi, R., Pomelli, C., Ochterski, J.W., Martin, R.L., Morokuma, K., Zakrzewski, V.G., Voth, G.A., Salvador, P., Dannenberg, J.J., Dapprich, S., Daniels, A.D., Farkas, Foresman, J.B., Ortiz, J.V., Cioslowski, J., Fox, D.J., *Gaussian 09, Revision B.01*. 2009.

17. Boys, S.F., Bernardi, F., *Mol. Phys*., 1970. **19**(4): p. 553-566.
18. Simon, S., Duran, M., Dannenberg, J.J., *J. Chem. Phys*., 1996. **105**(24): p. 11024-11031.
19. Becke, A.D., *J. Chem. Phys*., 1993. **98**(7): p. 5648-5652.
20. Lee, C., Yang, W., Parr, R.G., *Phys. Rev. B*, 1988. **37**(2): p. 785-789.
21. Miehlich, B., Savin, A., Stoll, H., Preuss, H., *Chem. Phys. Lett*., 1989. **157**(3): p. 200-206.
22. Tao, J., Perdew, J.P., Staroverov, V.N., Scuseria, G.E., *Phys. Rev. Lett*., 2003. **91**(14): p. 146401.
23. Peterson, K.A. Puzzarini, C., *Theo. Chem. Acc*., 2005. **114**(4-5): p. 283-296.
24. Figgen, D., Rauhut, G., Dolg, M., Stoll, H., *Chem. Phys*., 2005. **311**(1–2): p. 227-244.
25. Kendall, R.A., Dunning, T.H., Harrison, R.J., *J. Chem. Phys*., 1992. **96**(9): p. 6796-6806.
26. Dunning, T.H., *J. Chem. Phys*., 1989. **90**(2): p. 1007-1023.
27. Feller, D., J. *Comp. Chem*., 1996. **17**(13): p. 1571-1586.
28. Schuchardt, K.L., Didier, B.T., Elsethagen, T., Sun, L., Gurumoorthi, V., Chase, J., Li, J., Windus, T.L., *J. Chem. Inf. Model*., 2007. **47**(3): p. 1045-1052.
29. Zhurko, G.A., Zhurko, D.A., *ChemCraft*, 2012.
30. Bondi, A., *J. Phys. Chem*., 1964. **68**(3): p. 441-451.
31. Keith, T.A., *AIMAll* 2012 TK Gristmill Software.
32. Johnson, E.R., Keinan, S., Mori-Sánchez, P., Contreras-García, J., Cohen, A.J., Yang, W., *J. Am. Chem. Soc*., 2010. **132**(18): p. 6498-6506.
33. Keith, T.A. Frisch, M.J., *J. Phys. Chem. A*, 2011. **115**(45): p. 12879-12894.
34. Nakanishi, W., Hayashi, S., Narahara, K., *J. Phys. Chem. A*, 2008. **112**(51): p. 13593-13599.

4. Theoretical investigation of neutral Au(NHC)R (R = H^-, CH_3^-, Cl^-, OH^-) complexes forming $Au^I\cdots H$ hydrogen bonds to H_2O, NH_3 and HF

4.1. Abstract

In this theoretical study we investigate the ability of the selected neutral R-Au(I)-NHC (NHC = *N*-heterocyclic carbene) complexes [R = H^- (**1**), H_3C^- (**2**), Cl^- (**3**), HO^- (**4**)] to form hydrogen bonds to H_2O, HF and NH_3 H-bond donors. The optimised geometries were obtained at the B3LYP/aug-cc-pVTZ-pp, TPSS/aug-cc-pVTZ-pp, MP2/cc-pVTZ-pp and MP2/aug-cc-pVTZ-pp level of theory. Every hydrogen-bonded adduct investigated exhibits two hydrogen bonds, namely the Au···H interaction of interest and a secondary NH···XH interaction, to form a hydrogen-bonded ring with graph-set notation $R_2^2(6)$. The most stabilised adduct is **3.NH$_3$** with an interaction energy (E_{INT}) of -13.6 kcal/mol and the weakest interaction was **4.HF** with an E_{INT} of -9.03 kcal/mol at the MP2/cc-pVTZ level of theory. AIM analysis at the MP2/aug-cc-pVTZ-pp level of theory indicates the presence of bond critical points (BCPs) along the primary and secondary hydrogen bonds for all adducts investigated. The highest electron density accumulated at the Au···H BCP is 0.0268 $e a_0^{-3}$ for the complex **4**.**HF**. NCI plots identify three NCI regions: two coinciding with the primary and secondary hydrogen bonds, with the third corresponding to a repulsive region between the heteroatom of the hydrogen bond donor and the carbon atom of the carbene ligand coordinated to Au(I).

4.2. Introduction

Kazarian *et al.* [1] posed the question “Is Intermolecular Hydrogen-Bonding to Uncharged Metal Centres Of Organometallic Compounds Widespread in Solution?” and considered the examples of Co, Rh and Ir. They pointed out that the protonation of a metal centre is of importance, since it is widely recognised as a key step in organometallic chemistry, but is somewhat poorly understood even though H-bonding to the group 9 metals can be observed by IR and is quite widespread. Considering these examples where transition metals can act as H-bond acceptors, it is not unreasonable to expect that gold also has this capability since it is the most electronegative metal centre (see [2] and references therein), implying that it could be a strong Lewis base given the “correct” ligands.

Nevertheless, there is little experimental data available for $Au^I\cdots H$ interactions [2] other than two crystal structures conclusively exhibiting the $Au^I\cdots H$ interaction [3]. The complexes

consist of the *N*-methylbenzothiazole-2-thione (mbtt) ligand bonded to Au(I) in combination with two halogens, yielding Au(mbtt)X complexes, where X = Cl^- and Br^-. The authors do not mention why they think the $Au^I\cdots H$ interaction occurred, but they do postulate its importance in influencing the packing arrangement.

Our previous theoretical investigations [4] have shown that the Au(I) centre can act as a hydrogen bond (H-bond) donor when coordinating to two electron-donating ligands to yield anionic complexes. The ligands induce a partial negative charge on the gold atom, along with the required electrostatic surface potential topology, enabling the Au(I) centre to act as a Lewis base and thus as an H-bond acceptor to a wide variety of H-bond donors. We were further able to show that even neutral complexes could form weak H-bonds to H_2O. The examples presented in [4] and in this paper could be considered "frozen" states between the unprotonated and protonated Au(I) species.

To further understand this phenomenon we describe here a study of a range of Au(NHC)R (R = H^- (**1**), H_3C^- (**2**), Cl^- (**3**) and HO^-(**4**); NHC = *N*-heterocyclic carbene) complexes with a series of H-bond donors, namely H_2O, NH_3 and HF. Our main objective is to determine if an $Au^I\cdots H$ interaction forms and what its nature is as defined by geometrical and AIM parameters. In addition, with the range of complexes chosen we will be able to determine how the R group influences the formation of the $Au^I\cdots H$ interaction and its properties. The NHCs were selected since the synthesis of Au(NHC)X (X = Cl^-, Br^- and I^-) complexes in a one-step methodology is reportedly "straightforward", as described by Collado *et al.* [5]. The Au(NHC)H complex has been synthesised by Phillips *et al.*[6], while Nahra *et al*. [7] have recently proposed a novel route to obtain Au(NHC)OH complexes in multi-gram scale. We also included the Au(NHC)CH_3 complex as we recently showed [4] that the $[(Me)_2Au]^-$ complex forms strong H-bonds; the most stable H-bonded adducts to HF and HCN involve interaction energies of -14.58 kcal/mol and -15.95 kcal/mol, respectively, as a result of the influence of the H_3C^- ligand on the Au(I) centre.

Our investigation will be performed using two Density Funtional Theory (DFT) methods, where two different sets of basis sets will be utilised with the MP2 method. MP2 is known to overestimate the role of dispersion, however H-bond energies calculated with Density Functionals (DFs) are also not as trustworthy as those calculated with MP2 [8], which is why we perform the investigation at four different levels of theory. We consider the MP2* (defined as MP2/cc-pVTZ-pp) results to be the most accurate since MP2 (defined as MP2/aug-cc-pVTZ-pp) is known to overestimate dispersion interactions, while our previous

results [9] and those of others [10] have shown that MP2* provides a balance to the E_{INT} value. The DFs were included to serve as comparison to MP2* and if found accurate, to be utilised in larger systems. Since these systems are computationally expensive at high levels of theory, we deem it useful to test the DFs ability to model these interactions.

Geometrical parameters may be a measure of the strength of the H-bond, but care should be taken since the application of this estimation has limitations [8]. Topological parameters such as the electron density, Laplacian of the electron density and the energy density [H(*r*)] [11] can be useful to determine if the interaction is a H-bond [12-14].

Table 1 – Defined ranges for electron density [ρ_b ($e a_0^{-3}$)], the Laplacian of the electron density [$\nabla^2(\rho_b)$ ($e a_0^{-5}$)] and the total electronic energy density [H_b (au)] for van der Waals (vdW), hydrogen bonds (H-bond) and charge transfer in hypervalent trigonal bipyramidal adducts (CT-TBP) type interactions extracted from Nakanishi *et al*. [15]

Interaction type	$\boldsymbol{\rho_b}$ $\boldsymbol{(e a_0^{-3})}$	$\boldsymbol{\nabla^2(\rho_b)}$ $\boldsymbol{(e a_0^{-5})}$	$\boldsymbol{H_b}$ **(au)**
vdW	$0.00 < \rho_b < 0.01$	$0.00 < \nabla^2(\rho_b) < 0.04$	$0.00 < H_b < 0.002$
H-bond	$0.01 < \rho_b < 0.04$	$0.04 < \nabla^2(\rho_b) < 0.12$	$-0.004 < H_b < 0.002$
CT-TBP	$0.03 < \rho_b < 0.12$	$-0.01 < \nabla^2(\rho_b) < 0.1$	$-0.06 < H_b < -0.003$

In order to determine how similar these systems are theoretically to the "classical" H-bonds the topological parameters of these H-bonded adducts will be compared to those described by Nakanishi *et al.* [15], summarised in Table 1, who classified types of interactions based on the AIM parameters of the bond critical points (BCPs) along the intermolecular interaction line of the H-bond. The subscript *b* indicates that the value is for the intermolecular BCP.

A schematic representation of the series of adducts including the geometrical parameters discussed is shown in Figure 1.

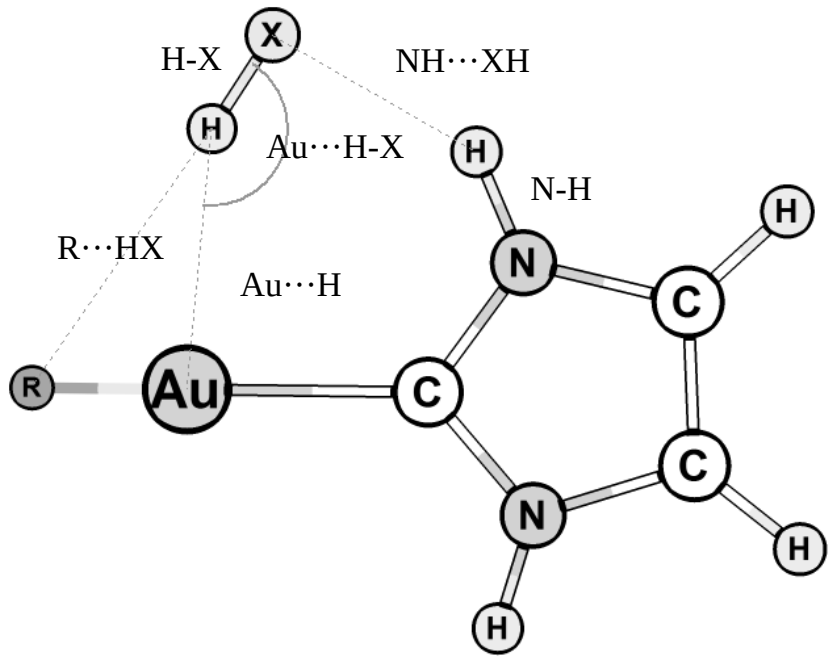

Figure 1 – Schematic representation of the H-bonded Au(I) NHC complexes with the R groups being H^-, CH_3^-, Cl^-, HO^-, and H-bond donors H_2O, HF and NH_3.

There are two H-bonds forming a ring with graph set notation $R_2^2(6)$ [16] and in order to distinguish between these we shall refer to the Au···H contact as the primary H-bond and the NH···XH contact as the secondary H-bond. Therefore, the Au(I) centre will be referred to as the primary H-bond acceptor. Furthermore, the HX molecule is acting as a primary H-bond donor and a secondary H-bond acceptor. The NH bond located on the NHC ligand will be referred to as the secondary H-bond donor. The R···HX distances are included in the tables below, because in some cases we view these interactions as competing H-bonds.

4.3. Methodology

All geometry optimisations were performed in the gas phase, with counterpoise corrections [17, 18], utilising the Gaussian 09 revB.01 [19] software package. During the optimisations no symmetry constraints were enforced and frequencies were calculated to verify that geometries were energy minima.

The counterpoise corrected interaction energy was calculated by:

$$E_{INT} = E_{AB}^{BSSE} - (E_A + E_B)$$

The energies of fragments A and B (E_A and E_B) were calculated with the individual geometries extracted from the AB adduct.

The B3LYP [20-22] and TPSSTPSS (TPSS) [23] Density Functionals were utilised in combination with the aug-cc-pVTZ-pp [24] basis set describing the Au atom in combination with the effective core potential (ECP) developed by Friggen *et al.*[25]. The other atoms (H, C, F, O, N) were represented by the aug-cc-pVTZ [26, 27] basis set. The MP2 [28, 29] method was employed in combination with the cc-pVTZ-pp (MP2*) and the aug-cc-pVTZ-pp (MP2) [24] basis set with the correct ECP [25] corresponding to the Au atom for each basis set. When the cc-pVTZ-pp or aug-cc-pVTZ-pp basis sets were employed to describe Au, the corresponding basis sets, cc-pVTZ and aug-cc-pVTZ, were utilised to describe the other atoms, as before with the DFs, to ensure all atoms are described by the same type of basis set. The TPSS/aug-cc-pVTZ-pp and MP2/aug-cc-pVTZ-pp interaction energies along with the geometrical parameters were omitted for the sake of brevity and can be found in the supplementary information. All basis sets were downloaded from the EMSL basis set exchange website [30, 31]. The ChemCraft [32] suite was the tool utilised for investigation of the output files.

The van der Waals (vdW) radii of N, O, F and Au were obtained from Bondi [33] and were selected as 1.55 Å, 1.43 Å, 1.47 Å and 1.66 Å, respectively. The vdW radius for the H-atom was selected as 1.2 Å. The sum of vdW radii for Au···H, F···H, N···H and O···H are therefore 2.86 Å, 2.67 Å, 2.75 Å and 2.63 Å, respectively.

The wave function files (wfx) obtained from Gaussian at the MP2/aug-cc-pVTZ-pp level of theory were analysed with the Atoms In Molecules (AIM) analysis program AIMAll [34] version 14.06.21. The electron density [ρ_b ($e a_0^{-3}$)] and the Laplacian of the electron density $\nabla^2(\rho_b)$ ($e a_0^{-5}$) at the intermolecular Bond Critical Points (BCPs), were obtained as is from AIMAll along with the total electronic energy density, $H_b\ (au) = -K\ (au)$. The *b* subscript indicates that it is a property at the intermolecular BCP of the H-bond. Noncovalent Interaction (NCI) plots developed by Johnson *et al.* [35] were also calculated from the wfx file and were graphically investigated and displayed utilising AIMAll. The Reduced Electron Density Gradient (RDG) isosurfaces were calculated with a resolution of 0.04 au. The isosurface visualisation of the RDG was calculated at a value of 0.5 au and with a minimum and maximum electron density of 0.0001 and 0.05 $e a_0^{-3}$, respectively. The RDG surfaces were visualised by mapping the "Sign(HessRho_EigVal_2)*Rho" onto them. The colour scale ("Range Method") chosen was the "-Maximum Magnitude to +Minimum Magnitude". Red indicates a negative or greater negative sign(λ_2)×ρ value and blue the positive value of sign(λ_2)×ρ and are scaled according to the largest absolute value.

4.4. Result and Discussion

The four Au(NHC)R complexes, investigated with [R = H^- (**1**), H_3C^- (**2**), Cl^- (**3**), HO^- (**4**)], can be divided into two groups, namely those with electron-donating R groups (complexes **1** and **2**), and those with electron-withdrawing groups (complexes **3** and **4**). We will discuss the interactions of these two groups with the three H-bond donors HF, H_2O and NH_3 separately, starting with those containing electron-donating groups. The optimised geometries for the H-bonded adducts of these complexes are shown in Figure 2. As can be seen, two H-bonds are formed for each adduct.

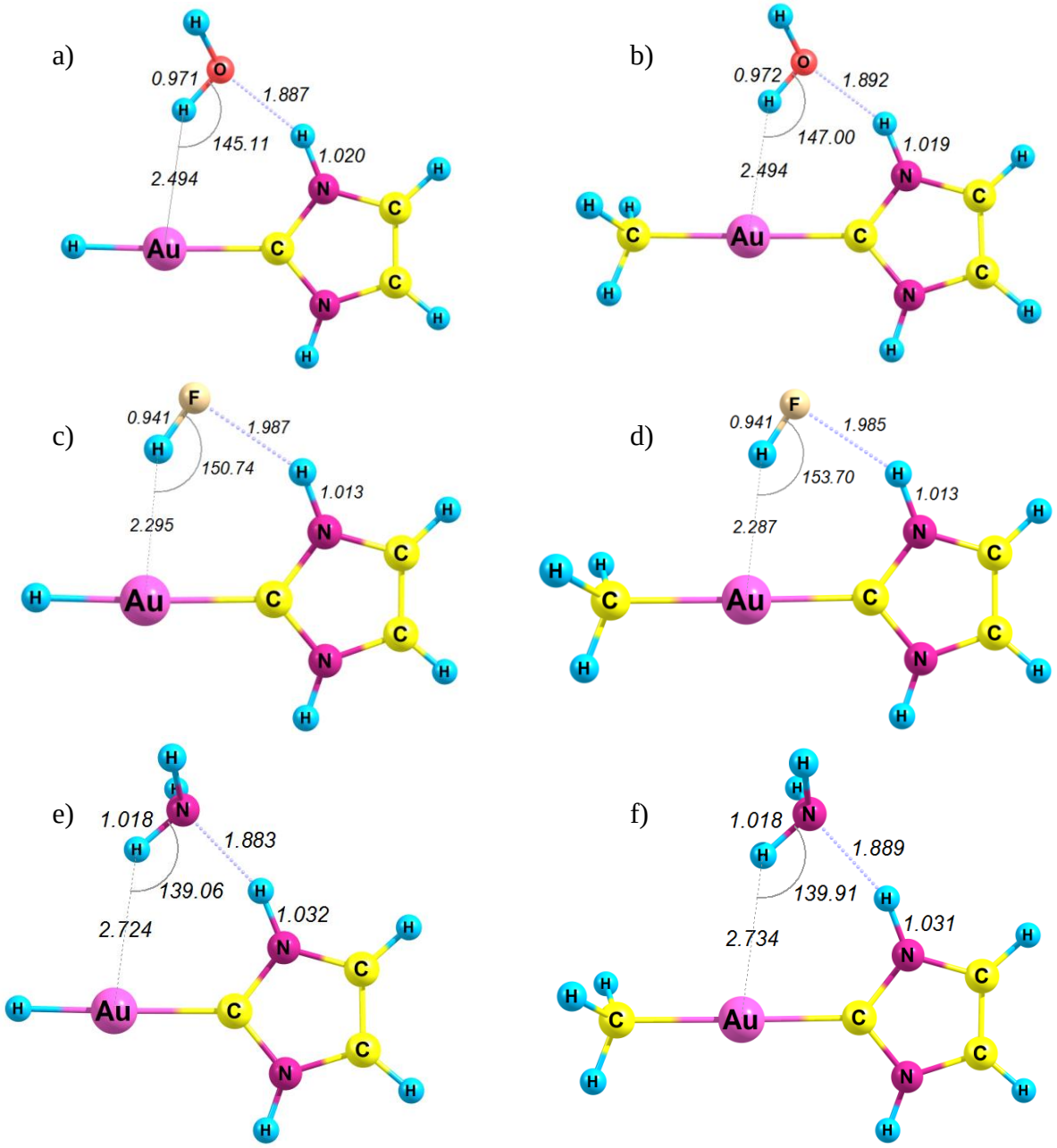

Figure 2 – Optimised geometries of complexes **1** H-bonded to a) H_2O, c) HF, e) $NH_3$and **2** H-bonded to b) H_2O, d) HF and f) NH_3 at the MP2/cc-pVTZ-pp level of theory. Distances and angles are in Å and º, respectively.

The interaction energies and the geometrical parameters of the adducts shown in Figure 2 are summarised in Table 2.

Table 2 –Interaction energies (E_{INT}) in kcal/mol, various geometrical parameters [Au···H distance (Å), Au···H-X angle (º), R···HX distance (Å), NH···XH distance (Å)], the H-N distance (Å), H-X distance (Å)] of the H-bonded adducts of complexes **1** and **2** to H_2O, HF and NH_3 at two levels of theory.

R = H^-			**Intermolecular Geometrical Parameters**					**H-bond Donors**	
Method	**H-bond donor**	**E_{INT} (kcal/mol)**	**Au···H (Å)**	**Au···H-X (º)**	**R···HX (Å)**	**NH···XH (Å)**	**% sum of vdW**	**H-N (Å)**	**H-X (Å)**
B3LYP	H_2O	-9.71	2.53	144.7	3.13	1.93	73.3	1.02	0.97
MP2*		-11.54	2.49	145.1	3.08	1.89	71.6	1.02	0.97
B3LYP	HF	-10.72	2.27	151.7	2.84	2.02	71.8	1.01	0.95
MP2*		-10.86	2.30	150.7	2.85	1.99	71.8	1.01	0.94
B3LYP	NH_3	-10.38	2.88	136.3	3.48	1.92	75.5	1.03	1.02
MP2*		-12.91	2.72	139.1	3.30	1.88	73.7	1.03	1.02
R = CH_3^-									
Method	**H-bond donor**	**E_{INT} (kcal/mol)**	**Au···H (Å)**	**Au···H-X (º)**	**R···HX (Å)**	**NH···XH (Å)**	**% sum of vdW**	**H-N (Å)**	**H-X (Å)**
B3LYP	H_2O	-9.40	2.54	146.7	3.49	1.93	79.5	1.02	0.97
MP2*		-11.25	2.49	147.0	3.41	1.89	77.7	1.02	0.97
B3LYP	HF	-10.61	2.25	154.8	3.21	2.01	77.9	1.01	0.95
MP2*		-10.73	2.29	153.7	3.21	1.99	77.9	1.01	0.94
B3LYP	NH_3	-10.03	2.88	136.8	3.79	1.92	81.4	1.03	1.02
MP2*		-12.53	2.73	139.9	3.61	1.89	79.6	1.03	1.02

It is interesting to note that NH_3 yields the most stable adduct to complex **1**, at the MP2* level of theory, with a value of -12.92 kcal/mol, followed by H_2O and HF with values of -11.54 kcal/mol and -10.86 kcal/mol, respectively. If, on the other hand, only the E_{INT} values obtained with B3LYP are considered **1.HF** appears to be the most stable adduct. This change in adduct stability as a function of the level of theory arises from the lack of dispersion contributions and/or the overestimation of the electrostatic contribution for B3LYP.

Interestingly, the Au···H distances do not correlate to the trend seen for E_{INT}. The Au···H distances are inversely proportional to the E_{INT} values. Nevertheless, all the Au···H distances are shorter than the sum of vdW radii of 2.86 Å, with **1.NH$_3$** at the B3LYP level of theory being the exception. If the Au···H distances are considered for complex **1**, we see that adduct **1.HF** yields the shortest Au···H distance, followed by H_2O and NH_3, with distances of 2.30, 2.49 and 2.72 Å, respectively.

Another geometrical parameter that is dependent on E_{INT} is the Au···H-X angle, where the deviation from linearity becomes more severe as the E_{INT} values increase: **1.NH$_3$** has an E_{INT} value of -12.91 kcal/mol with an Au···H-X angle of 139.1º.

Interestingly, when the NH···XH distances are compared for the three H-bonded adducts of **1**, we see that this distance correlates with the E_{INT} with **1.NH$_3$** yielding the shortest distance of 1.88 Å and is 68 % of the sum of vdW radii (2.75 Å). The **1.H$_2$O** and **1.HF** adducts are close second and third with a NH···XH distances that is 72 % and 74 % of the total sum of vdW radii (2.63 Å and 2.67), respectively. If the E_{INT} values in conjunction with the geometrical parameters of the secondary H-bond (NH···XH) are considered, we can postulate that the NH···XH interaction has a greater contribution to the total E_{INT} value than the Au^{I}···H interaction.

If the E_{INT} values of complex **2** are considered, the same trend as we saw with complex **1** persists, i.e. the NH_3 adduct yields the most stable H-bonded adduct, with an E_{INT} value of -12.53 kcal/mol, followed by **2.H$_2$O** and **2.HF** with E_{INT} values of -11.25 kcal/mol and -10.73 kcal/mol, respectively.

The Au···H distances for **2.H$_2$O** and **2.HF** are within the sums of the vdW radii, at both levels of theory, with the **2.NH$_3$** adduct yielding distances that are larger than 2.86 Å at the B3LYP level of theory. We also note that the Au···H-X angles deviate more from linearity as E_{INT} increases, yielding a relatively small angle of 139.9º observed for the most stable adduct, i.e. **2.NH$_3$**. Comparing the secondary H-bond distances, we note that both the most stable adduct, **2.NH$_3$**, as well as **2.H$_2$O**, consistently yield the same shortest NH···XH distance of 1.89 Å, corresponding to 74 % and 78 % of the respective sums of the vdW radii of 2.55 Å

and 2.43 Å. The shortening of the NH···XH distance correlates with the N-H values, where the relation is inversely proportional.

Complex **1** consistently yields more stable adducts than complex **2** for the same H-bond donors, although the Au···H distances remain relatively constant for complexes **1** and **2** for the same H-bond donor, ranging from 2.25 Å to 2.73 Å. On the other hand, the Au···H-X angles deviate most substantially from linearity with the smallest angle being 139.1º for **1.NH3**, with the largest angle being 153.7º for **2.HF**. All the angles are below 160º, with deviation from linearity explained by the presence of the NH···XH interaction so that the H-bond donor can maximise interactions with both the Au and NH group. According to Jeffrey [36] moderately strong H-bonds typically have E_{INT} values of 4-15 kcal/mol and angles of 130-180º.

The NH···XH, H-N and H-X distances also remain relatively constant for complex **1** and **2** for the same H-bond donor. Interestingly, if we compare the R···HX distances of complex **1** to complex **2** for the same H-bond donor, we see that the R···HX distances for **1** are shorter than for **2** corresponding to the E_{INT} values becoming more stabilising. For instance, the R···HX distance for **1.HF** is 2.85 Å and for **2.HF** the distance is 3.21 Å even though the Au···H distances differ by only 0.01 Å. The shortening of the R···HX distance also corresponds to a smaller Au···H-X angle (see Figure 2). These trends suggest that the R group attracts the H-bond donor, and could thereby contribute to the stabilisation of the adduct and hence E_{INT}.

In order to gain further insight into the ditopic H-bonds, AIM analysis was performed in conjunction with NCI plots (see Figure 3 and Table 3). Thus far, our geometrical data suggest that the secondary H-bond adds the most stability to the E_{INT} value and is the strongest H-bond with NH_3; the AIM analysis and NCI plots should verify this.

Minimum sign(λ_2)×ρ value -0.0300
Maximum sign(λ_2)×ρ value 0.0131

a)

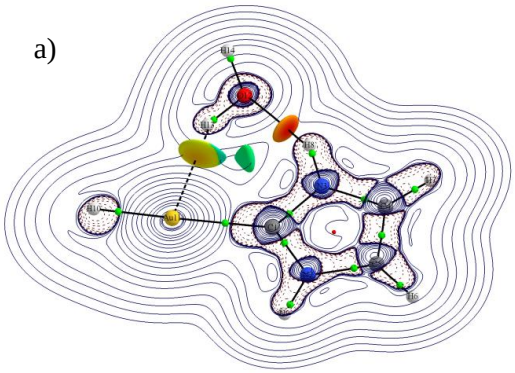

Minimum sign(λ_2)×ρ value -0.0296
Maximum sign(λ_2)×ρ value 0.0134

b)

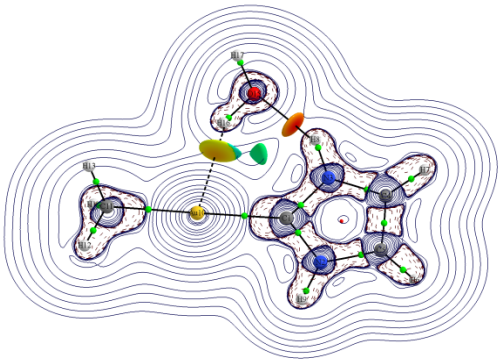

Minimum sign(λ_2)×ρ value -0.0292
Maximum sign(λ_2)×ρ value 0.0189

c)

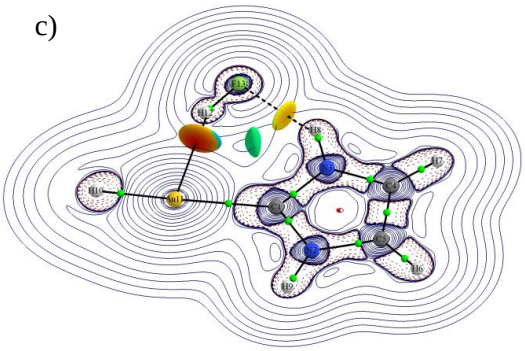

Minimum sign(λ_2)×ρ value -0.0305
Maximum sign(λ_2)×ρ value 0.0197

d)

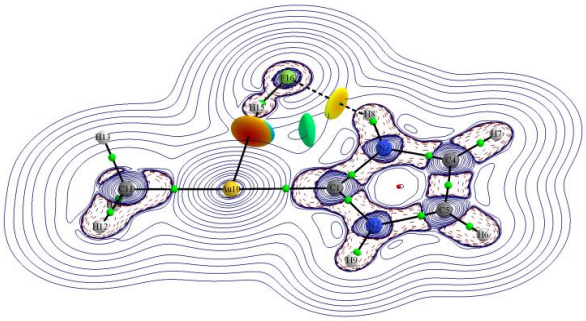

Minimum sign(λ_2)×ρ value -0.0408
Maximum sign(λ_2)×ρ value 0.0092

e)

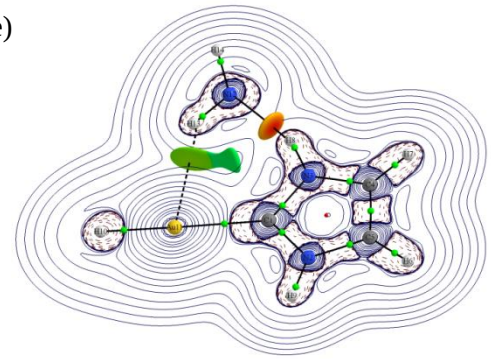

Minimum sign(λ_2)×ρ value -0.0399
Maximum sign(λ_2)×ρ value 0.0092

f)

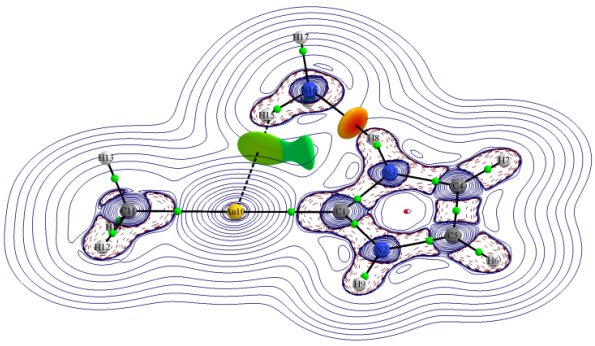

Figure 3 – The two-dimensional contour plot of $\nabla^2\rho$ (ea_0^{-5}) with the NCI plots shown as green to red areas on the images for complex **1** a) H_2O, c) HF, d) NH_3 and complex **2** H-bonded to b) H_2O, d) HF and f) NH_3. The red (minimum) regions indicate stabilising interactions, yellow/lime green regions indicate dispersion-type interactions and cyan/blue regions (maximum) coincide with repulsive intermolecular interactions. All values are in atomic units.

The most important characteristics of the molecular graphs in Figure 3 are the atomic interaction lines present for the Au···H and NH···XH interactions in all six H-bonded adducts of complexes **1** and **2**. These are indicative of overlap between atoms and can be interpreted as confirmation that a noncovalent interaction exists.

Most importantly, since the colouring shown in Figure 2 is based on a scale relative to the largest sign(λ_2)×ρ value for each respective adduct, the NCI plots enable one to make qualitative comparisons between the two H-bonds for each adduct. In terms of repulsion and attraction cyan/blue regions would normally represent nonbonding or repulsive interactions whereas the red, yellow and lime green regions indicate stabilising interactions. The lime green regions indicate sign(λ_2)×ρ values of weaker H-bonds, typically dispersion type interactions. Properties at the BCP indicate the type of interaction. Also, the NCI plots graphically display the nature of noncovalent interactions for each adduct; most importantly, they contrast the two H-bonds to confirm that the NH···XH interaction is generally more stabilising than the Au^{I}···H interaction. The exceptions are **1.HF** and **2.HF**, where it is clear that the Au^{I}···H interaction adds more stabilisation to E_{INT} than NH···XH. In addition, the NCI plots show that there is no detectable stabilisation between the H-bond donor and the anionic ligand coordinated to Au(I), while there seems to be a nonbonding/repulsion interaction between the heteroatom of the H-bond donor and the NHC carbon atom coordinated to Au(I).

Table 3 – Selected AIM parameters for the optimised structures of complex **1** and **2** H-bonded to H_2O, HF and NH_3 at the MP2/aug-cc-pVTZ-pp level of theory.

Complex **1**	**H-bond**	$\boldsymbol{\rho_b}$ $(\boldsymbol{e a_0^{-3}})$	$\boldsymbol{\nabla^2(\rho_b)}$ $(\boldsymbol{e a_0^{-5}})$	$\mathbf{H_b}$ **(au)**
H_2O	Au^{I}···H-X	0.018	0.049	-0.0002
	R-NH···X-H	0.028	0.104	0.0004
HF	Au^{I}···H-X	0.026	0.055	-0.0036
	R-NH···X-H	0.019	0.090	0.0032
NH_3	Au^{I}···H-X	0.012	0.036	0.0008
	R-NH···X-H	0.036	0.086	-0.0052
Complex **2**				
H_2O	Au^{I}···H-X	0.018	0.049	-0.0003
	R-NH···X-H	0.027	0.104	0.0005
HF	Au^{I}···H-X	0.027	0.054	-0.0041
	R-NH···X-H	0.019	0.091	0.0032
NH_3	Au^{I}···H-X	0.012	0.035	0.0008
	R-NH···X-H	0.035	0.085	-0.0048

There are no significant differences between the AIM parameters of complexes **1** and **2** H-bonded to the same H-bond donor, confirming that the $Au^{I}\cdots H$ interactions do not play the dominant role in the value of E_{INT}.

The ρ_b values of all the primary and secondary H-bonds in Table 3 are within the expected range for H-bonds, although the ρ_b values for NH···X-H interactions are higher than those of the $Au^{I}\cdots H$ interactions, except for HF where the ρ_b value for $Au^{I}\cdots H$ interaction is 37 % higher than that for NH···XH. The ρ_b values of the primary $Au^{I}\cdots H$ interaction decrease in the order HF (0.026 $e a_0^{-3}$) > H_2O (0.018 $e a_0^{-3}$) > NH_3 (0.012 $e a_0^{-3}$) and simultaneously increase for the secondary H-bond in HF (0.019 $e a_0^{-3}$) < H_2O (0.028 $e a_0^{-3}$) < NH_3 (0.036 $e a_0^{-3}$). These trends correlate with the NCI plots in shown Figure 2 and the geometrical parameters previously discussed.

The $\nabla^2(\rho_b)$ values listed in Table 3 are all positive, characteristic of noncovalent interactions, and falling within the range expected for H-bonds. Furthermore, we note that the $\nabla^2(\rho_b)$ value of the secondary H-bonds of **1.H_2O**, **1.NH_3**, **2.H_2O** and **2.NH_3** are almost twice those of the primary H-bond indicative of greater charge depletion.

All the H_b values in Table 3 calculated for the $Au^{I}\cdots H$ interactions fall within the ranges expected for H-bonds, except for **2.HF**, whereas only the H_b values of the NH···XH interaction in **1.H_2O** and **2.H_2O** fall within this defined range for H-bonds. This could be due to the presence of the ECP when calculating the kinetic energy. We will therefore not discuss the H_b values further since these values are known to fluctuate when ECPs are utilised as the electron density is not completely recovered [37, 38].

Next, we investigate the effect of electron-withdrawing groups coordinated to Au(I), see Figure 4, for optimised geometries of **3** and **4** with the three H-bond donors.

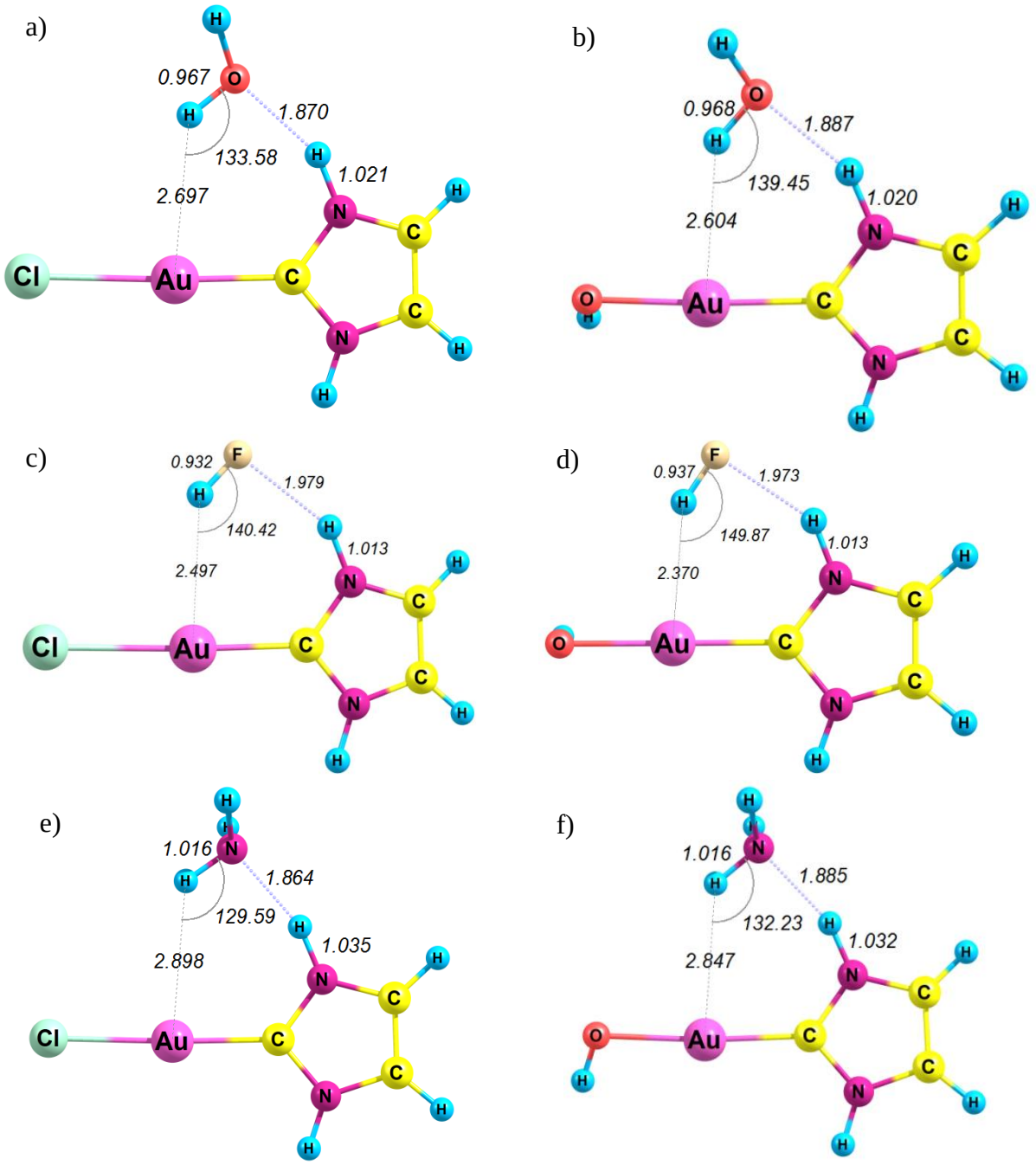

Figure 4 – Optimised geometries of complex **3** H-bonded to a) H_2O, c) HF , d) NH_3 and complex **4** H-bonded to b) H_2O, d) HF and f) NH_3 at the MP2/cc-pVTZ-pp level of theory. Distances and angles are in Å and °, respectively.

Table 4 – Interaction energies (E_{INT}) in kcal/mol, various intermolecular geometrical parameters [Au···H (Å), Au···H-X angle (º), R···HX (Å), NH···XH (Å)], the H-N (Å), H-X (Å) distances of the H-bond donors of the H-bonded adducts of complex **3** and complex **4** to H_2O, HF and NH_3 at two levels of theory.

R = Cl⁻			**Intermolecular Distances (Å)**					**H-bond donors**	
Method	**H-bond donor**	**E_{INT} (kcal/mol)**	**Au···H (Å)**	**Au···H-X (deg)**	**R···HX (Å)**	**NH···XH (Å)**	**% sum of vdW**	**H-N (Å)**	**H-X (Å)**
B3LYP	H_2O	-9.44	2.78	131.9	3.70	1.90	72.3	1.02	0.97
MP2*		-11.32	2.70	133.6	3.58	1.87	70.9	1.02	0.97
B3LYP	HF	-8.46	2.45	142.8	3.40	2.00	71.1	1.01	0.94
MP2*		-9.03	2.50	140.4	3.38	1.98	71.1	1.01	0.93
B3LYP	NH_3	-11.17	3.11	125.5	4.05	1.90	74.8	1.03	1.02
MP2*		-13.60	2.90	129.6	3.77	1.86	73.1	1.03	1.02
R = OH⁻									
Method	**H-bond donor**	**E_{INT} (kcal/mol)**	**Au···H (Å)**	**Au···H-X (deg)**	**R···HX (Å)**	**NH···XH (Å)**	**% sum of vdW**	**H-N (Å)**	**H-X (Å)**
B3LYP	H_2O	-9.34	2.68	136.7	3.38	1.92	73.14	1.02	0.97
MP2*		-11.23	2.60	139.5	3.32	1.89	71.69	1.02	0.97
B3LYP	HF	-9.65	2.31	152.8	3.22	1.99	71.77	1.01	0.95
MP2*		-9.88	2.37	149.9	3.20	1.97	71.70	1.01	0.94
B3LYP	NH_3	-10.54	3.01	128.8	3.65	1.92	74.68	1.03	1.02
MP2*		-12.81	2.85	132.2	3.49	1.88	73.70	1.03	1.02

If the E_{INT} values of the H-bonded adducts of **3** are considered we see that **3.NH$_3$** yields the most stable adduct with a value of -13.6 kcal/mol, with **3.H$_2$O** and **3.HF** yielding values of -11.32 kcal/mol and -9.88 kcal/mol, respectively, at the MP2* level of theory. The B3LYP DF follows the same trend with respect to adduct stability, with **3.NH$_3$** being the most stable. The Au···H distances for the **3.H$_2$O** and **3.HF** adducts are all within the sum of the vdW radii, with the Au···H distances for **3.NH$_3$** slightly longer than 2.86 Å at the MP2* level of theory. The Au···H distances are inversely proportional to the E_{INT} values, with an elongation upon increase in stabilisation; however, the NH···XH distances correlate with the interaction energies, with the **3.NH$_3$** adduct yielding a distance that is only 68 % of the sum of the vdW radii.

All the Au···H distances of H-bonded adducts of **4** are within the sum of the vdW radii, except for **4.NH$_3$** at the B3LYP level. This can be ascribed to the inability of B3LYP to model dispersion-type interactions, thus yielding a larger Au···H distance.

The trends in E_{INT} with respect to the H-bond donor are similar to what we saw for **3**, with **4.NH$_3$** yielding the most stable adduct with an E_{INT} of -12.81 kcal/mol, followed by **4.H$_2$O** and **4.HF**, with values of -11.23 kcal/mol and -9.88 kcal/mol. The **4.NH$_3$** adduct also exhibits the shortest NH···XH distance relative to the sum of the vdW radii for the NH···XH distance. This suggests that the secondary H-bond contributes the most stabilisation to the E_{INT} values. Interestingly, the E_{INT} values for adducts **4.H$_2$O** and **4.NH$_3$** are less stabilising than those for **3.H$_2$O and 3.NH$_3$**, but **4.HF** is a more stable adduct than **3.HF**. This difference in E_{INT} between **4.HF** and **3.HF** is due to the Au^{I}···H interaction, where the former complex exhibits a shorter Au···H distance (2.37 Å) than the latter (2.50 Å). Furthermore, **4.H$_2$O** and **4.NH$_3$** yield shorter Au···H distances than those of **3**. This is due to the increase in the Au^{I}···H interaction strength that increase the NH···XH distances slightly, which then decrease the percentage contribution the NH···XH interaction makes to the total stabilisation (E_{INT}). The H-N and H-X distances of the adducts of **4** are almost identical to those with **3**.

To gain a qualitative view of the two competing H-bonds, we turn to the NCI plots shown in Figure 5, along with a more quantitative analysis of the interactions with AIM results summarised in Table 5.

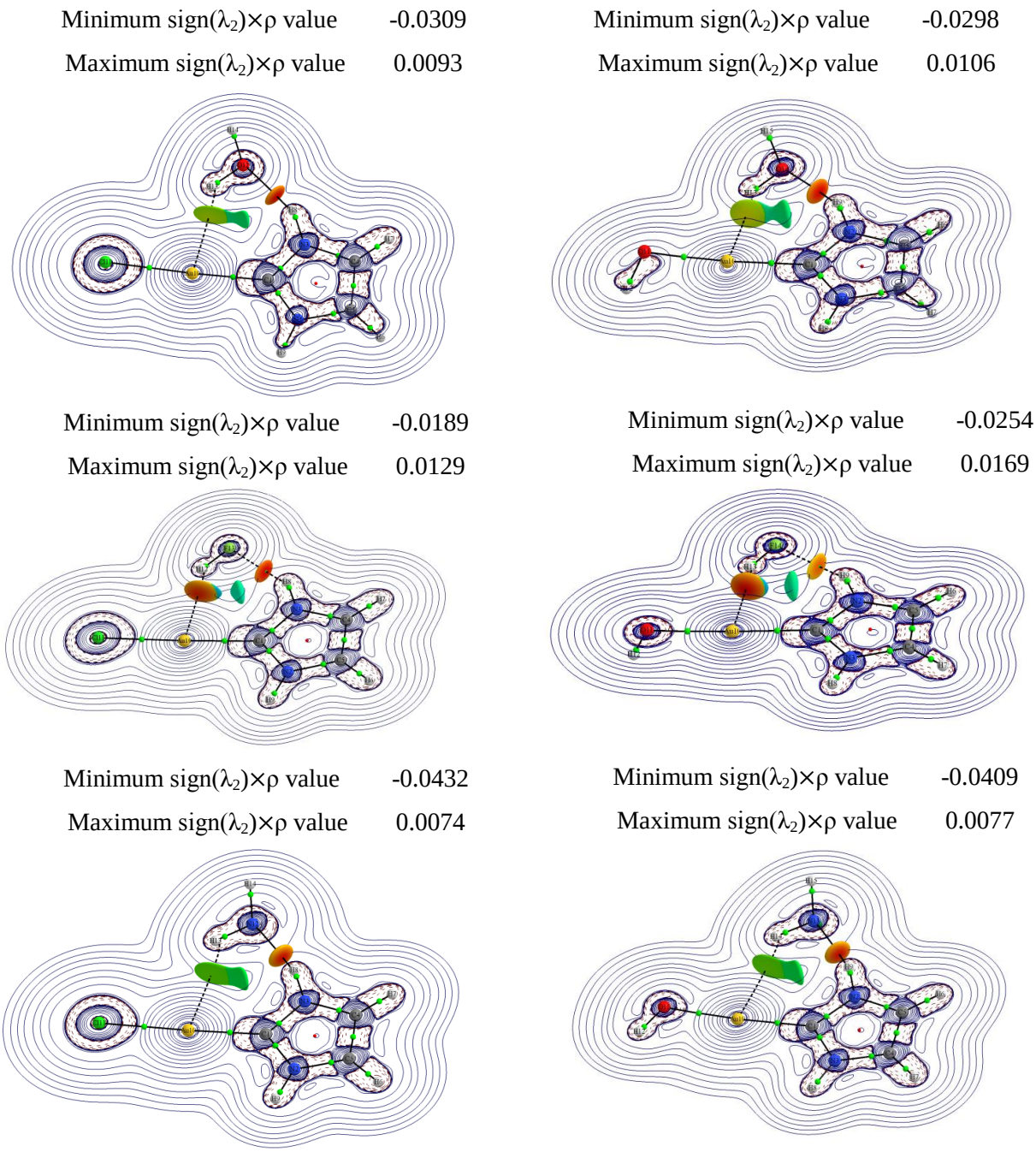

Figure 5 – Molecular graphs with two dimensional contour plots of $\nabla^2\rho$ (ea_0^{-5}) with the NCI plots displayed as coloured regions ranging from red (minimum) to blue (maximum) of **3** (left) and **4** (right) H-bonded to H_2O, HF and NH_3. The red regions correspond to the stabilising interactions and the blue regions to non-bonding/repulsive interactions. All values are in Atomic units.

The most important features of the molecular graphs in Figure 5 are the AILs confirming the existence of both H-bonds, in particular the $Au^I\cdots H$ interaction. Furthermore, the NCI plots correlate with the trends observed for the geometrical parameters of the $Au^I\cdots H$ and $NH\cdots XH$ interactions, where the secondary H-bond of **3** and **4** H-bonded to H_2O and NH_3 are dominant. The NCI plots for all these adducts of **3** and **4**, suggest that the $Au^I\cdots H$ interactions

for the HF adducts are stronger than dispersion-type interactions and thus more electrostatic, as indicated by their large |minimum sign(λ_2)×ρ| values, with the H_2O and NH_3 adducts yielding an interaction that is a weaker, possibly dispersion type interaction. The NCI plots for **3.HF** and **4.HF** suggest that these are the only adducts where the $Au^I\cdots H$ interactions rival, or supercede, the NH···XH interactions in strength, judged by the intensity of the red colouring.

If we assume that the minimum sign(λ_2)×ρ values of **3.H_2O** and **4.H_2O** correspond to the NH···XH interactions, we can conclude that this interaction is more stabilising for **3.H_2O** since this adduct exhibits a greater negative sign(λ_2)×ρ value. This is also true for **3.NH_3**, since it yields a greater negative sign(λ_2)×ρ value than **4.NH_3**. This trend in the NCI plots correlates with the increase in stability reflected in E_{INT}.

The AIM parameters at the H-bond BCPs of the optimised geometries at the MP2/aug-cc-pVTZ-pp level of theory summarised in Table 5 typify the characteristics of the two H-bonds observed for **3** and **4**.

Table 5 –Selected AIM parameters for the optimised adducts of complexes **3** and **4** H-bonded to H_2O, HF and NH_3 at the MP2/aug-cc-pVTZ-pp level of theory.

Complex **3**	**H-Bond**	$\boldsymbol{\rho_b}$ $(\boldsymbol{e a_0^{-3}})$	$\boldsymbol{\nabla^2(\rho_b)}$ $(\boldsymbol{e a_0^{-5}})$	$\mathbf{H_b}$ **(au)**
H_2O	Au···H-X	0.012	0.037	0.00087
	R-NH···X-H	0.029	0.105	-0.00012
HF	Au···H-X	0.017	0.047	-0.00006
	R-NH···X-H	0.019	0.090	0.00307
NH_3	Au···H-X	0.008	0.027	0.001
	R-NH···X-H	0.038	0.084	-0.006
Complex **4**				
H_2O	Au···H-X	0.014	0.041	0.0006
	R-NH···X-H	0.028	0.103	0.0003
HF	Au···H-X	0.023	0.051	-0.0023
	R-NH···X-H	0.020	0.094	0.0032
NH_3	Au···H-X	0.009	0.029	0.0009
	R-NH···X-H	0.036	0.084	-0.0053

Most of the ρ_b values for the Au···H interactions and the NH···XH interactions in Table 5 fall within the expected range for H-bonding, with only the ρ_b values of the $Au^I\cdots H$ interactions for **3.NH_3** and **4.NH_3** indicative of vdW-type interactions. The largest ρ_b values for both **3** and **4** occur when these complexes form adducts with HF, yielding values of 0.023 $e a_0^{-3}$ and 0.017 $e a_0^{-3}$, respectively.

On the other hand, only the $\nabla^2(\rho_b)$ values of the Au$^{I}\cdots$H interaction of **3.HF**, **4.H$_2$O** and **4.HF** fall within the range expected for H-bonding. It is surprising that the $\nabla^2(\rho_b)$ value for the Au$^{I}\cdots$H interaction of the **3.H$_2$O** adduct is outside the range expected for H-bonds, since the ρ_b value within the H-bond range. However, it is only 0.003 $e a_0^{-5}$ less than what is expected for H-bonds, we thus describe this as a borderline case, i.e. a very weak H-bond with a substantial vdW contribution. The $\nabla^2(\rho_b)$ values for **3.NH$_3$** and **3.NH$_3$** are within the range expected for weak vdW-type interactions, thus correlating to the trends seen for ρ_b.

Another important feature is that the ρ_b values for the NH$\cdots$XH interactions are on average twice those of the Au$^{I}\cdots$H interactions, allowing us to conclude that the NH$\cdots$XH interaction contributes most to the stabilisation seen in E_{INT}, which agrees with the geometrical parameters and NCI plots given earlier in Table 4 and Figure 5, respectively.

All of the H_b values for the Au$^{I}\cdots$H interactions of **3** and **4** are within the expected range for H-bonds, although complexes **3** and **4** H-bonded to H_2O and NH_3 fall within the expected range for vdW interactions, suggesting that these are weak H-bonds.

The Au$^{I}\cdots$H interactions for the NH_3 H-bond donor are therefore significantly weaker and characteristic of vdW-type interactions. This may be due to the H atom being less acidic than H_2O and HF, or more likely that, since the NH$\cdots$XH interaction is stronger for NH_3 that this forces a larger separation between the Au and H atom, thus resulting in a weaker interaction.

To gain further insight into the Au$^{I}\cdots$H interaction, we look at the charges of the Au(I) atom before adduct formation obtained from the AIM calculations, as well as the change in the charge on the Au(I) centre upon adduct formation, see Table 6.

Table 6 – Atomic charges (AIM) obtained by integration across the atomic basin at the MP2/aug-cc-pVTZ-pp level of theory.

		Δq(A) of the Au(I) centre in (*e*)		
[R – Au(I) – NHC]^0	**q(A) of Au(I)**	**H-bond donor**		
R Group	**monomer**	**NH$_3$**	**H$_2$O**	**HF**
H^-	-0.0793	0.1287	0.1315	0.1348
CH_3^-	-0.0013	0.1318	0.1328	0.1336
Cl^-	0.1726	0.1310	0.1328	0.1325
OH^-	0.2470	0.1305	0.1329	0.1385

As expected, we observe that the electron-donating groups yield partially negative charges on the gold for **1** and **2**, and the electron-withdrawing groups induce partially positive charges on the Au(I) centre for **3** and **4**. An important trend to note is that the charge of Au(I) is less negative after adduct formation than before. Furthermore, the most important trend is that even though the Au(I) centre is positively charged to complexes **3** and **4**, it still loses a comparable amount of electrons when compared in complexes **1** and **2**. These results also suggest that even if gold has a partial positive charge, it can still act as H-bond acceptor. Similar behaviour was exhibited by gold, in Chapter 3, wthin the $[(CF_3)_2Au]^-$ complex. Another general trend is that of the change in charge $\Delta q_{HF} > \Delta q_{H2O} > \Delta q_{NH3}$ for all complexes.

4.5. Conclusions

The results for the H-bonded neutral Au(I) adducts shown here suggest that for the $Au^I\cdots H$ interaction to occur in a complex containing an NHC ligand, a secondary H-bond, i.e. the NH···XH interaction needs to be present serving as an "anchor" (a term coined by Kryachko [39]), since the geometries shown here are the only stable conformations we could obtain. No stable conformation was obtained where only the $Au^I\cdots H$ interaction is present. We postulate that this might also be true for other neutral Au(I) complexes, due to the relative lower basicity of the Au(I) atom compared to anionic complex such as the $[(Me)_2Au]^-$ complex studied previously in Chapter 2 and 3, and also since our results agree with what was previously found by Kryachko [39]. This prerequisite of an anchoring H-bond due to the decrease in gold's basicity could also explain why the $Au^I\cdots H$ interaction has not been frequently observed in the solid state and in solution. There are, however, two crystal structures with this novel Au···H contacts present [3], but even in these cases, the $Au^I\cdots H$ interaction is accompanied by other additional interactions (as can be seen in their AIM molecular graphs found in the SI of ref [4]).

High quality wave functions analysed using AIM and NCI show that HF and H_2O form $Au^I\cdots H$ hydrogen bonds to **1**, **2**, **3** and **4**, with the NH_3 hydrogen bond donor generally yielding a weak, dispersion-like $Au^I\cdots H$ interaction, except **2.NH$_3$**. The highest accumulation of electron density between the Au and H atoms occur when R = H_3C^- and the lowest is when R = Cl^- for all the H-bond donors. This trend follows the Lewis basicity and agrees with the calculated atomic charges where it was found that the hydride and methanide analogues produced the largest partially negative charges on the Au(I) atom.

The analyses suggest that the NH···XH interactions add the most stabilisation to the total E_{INT} values and are generally independent of the R groups. On the other hand, electron-donating R groups increase the strength of the Au^{I}···H interactions, as we have shown previously in Chapter 3.

Nevertheless, the overall stability of the adduct results from a compromise between satisfying the geometrical requests of the two H-bonds. For instance, **3**.**NH_3** has the highest E_{INT} despite having the weakest Au^{I}···H interaction, based on the AIM parameters. We postulate that the weak Au^{I}···H interaction allows the NH_3 to move into a position that decreases repulsion between the NH_3 hydrogen and the NHC ring [compare Figure 5 (c) and (g)].

The most stable H-bonded adduct is **3.NH_3** with an E_{INT} of -13.6 kcal/mol with the weakest H-bonded adduct being **3.HF** with an E_{INT} of -9.03 kcal/mol at the MP2* level of theory. The geometrical data obtained for the Au^{I}···H interaction suggest that the shortest Au···H distance was obtained for **2.HF** and is 2.29 Å, and the largest Au···H distance is 2.90 Å for **3.NH_3** at the MP2/cc-pVTZ-pp level of theory. The Au···H-X angles are below 160º, but have been shown [36] to be characteristic of weak to moderately strong H-bonds. Deviations from the expected trends occur due to the influence of the secondary H-bond.

References

1. Kazarian, S.G., Hamley, P.A., Poliakoff, M., *J. Am. Chem. Soc.*, 1993. **115**(20): p. 9069-9079.
2. Schmidbaur, H., Raubenheimer, H.G., Dobrzanska, L., *Chem. Soc. Rev.*, 2014. **43**(1): p. 345-380.
3. Koskinen, L., Jääskeläinen, S., Kalenius, E., Hirva, P., Haukka, M., *Cryst. Growth & Des.*, 2014. **14**(4): p. 1989-1997.
4. Groenewald, F., Esterhuysen, C., Dillen, J., Raubenheimer, H., *To be published.*
5. Collado, A., Gomez-Suarez, A., Martin, A.R., Slawin, A.M.Z., Nolan, S.P., *Chem. Commun.*, 2013. **49**(49): p. 5541-5543.
6. Phillips, N., Dodson, T., Tirfoin, R., Bates, J.I., Aldridge, S., *Chem. Eur. J.*, 2014. **20**(50): p. 16721-16731.
7. Nahra, F., Patrick, S.R., Collado, A., Nolan, S.P., *Polyhedron*, 2014. **84**(0): p. 59-62.
8. Grabowski, S.J., *J. Phys. Org. Chem.*, 2004. **17**(1): p. 18-31.
9. Groenewald, F., Esterhuysen, C., Dillen, J., *Theo. Chem. Acc.*, 2012. **131**(10): p. 1-12.
10. Riley, K.E., Hobza, P., *J. Phys. Chem. A*, 2007. **111**(33): p. 8257-8263.
11. Grabowski, S.J., *J. Phys. Chem. A*, 2001. **105**(47): p. 10739-10746.
12. González, L., Mó, O., Yáñez, M., Elguero, J., *J. Chem. Phys.*, 1998. **109**(7): p. 2685-2693.
13. Koch, W., Frenking, G., Gauss, J., Cremer, D., Collins, J.R., *J. Am. Chem. Soc.*, 1987. **109**(20): p. 5917-5934.
14. Rozas, I., Alkorta, I., Elguero, J., *J. Am. Chem. Soc*, 2000. **122**(45): p. 11154-11161.
15. Nakanishi, W., Hayashi, S., Narahara, K., *J. Phys. Chem. A*, 2008. **112**(51): p. 13593-13599.
16. Margaret C. Etter, J.C.M., Joel Bernstein, *Acta Crystallog. B.*, 1990. **46**(2): p. 256-262.
17. Boys, S.F., Bernardi, F., *Mol. Phys.*, 1970. **19**(4): p. 553-566.
18. Simon, S., Duran, M., Dannenberg, J.J., *J. Chem. Phys.*, 1996. **105**(24): p. 11024-11031.
19. Frisch, M.J., Trucks, G.W., Schlegel, H.B., Scuseria, G.E., Robb, M.A., Cheeseman, J.R., Scalmani, G., Barone, V., Mennucci, B., Petersson, G.A., Nakatsuji, H., Caricato, M., Li, X., Hratchian, H.P., Izmaylov, A.F., Bloino, J., Zheng, G., Sonnenberg, J.L., Hada, M., Ehara, M., Toyota, K., Fukuda, R., Hasegawa, J., Ishida, M., Nakajima, T., Honda, Y., Kitao, O., Nakai, H., Vreven, T., Montgomery, J.A.,

Peralta, J.E., Ogliaro, F., Bearpark, M., Heyd, J.J., Brothers, E., Kudin, K.N., Staroverov, V.N., Kobayashi, R., Normand, J., Raghavachari, K., Rendell, A., Burant, J.C., Iyengar, S.S., Tomasi, J., Cossi, M., Rega, N., Millam, J.M., Klene, M., Knox, J.E., Cross, J.B., Bakken, V., Adamo, C., Jaramillo, J., Gomperts, R., Stratmann, R.E., Yazyev, O., Austin, A.J., Cammi, R., Pomelli, C., Ochterski, J.W., Martin, R.L., Morokuma, K., Zakrzewski, V.G., Voth, G.A., Salvador, P., Dannenberg, J.J., Dapprich, S., Daniels, A.D., Farkas, Foresman, J.B., Ortiz, J.V., Cioslowski, J., Fox, D.J., *Gaussian 09, Revision B.01*. 2009.

20. Becke, A.D., *J. Chem. Phys.*, 1993. **98**(7): p. 5648-5652.
21. Lee, C., Yang, W., Parr, R.G., *Phys. Rev. B*, 1988. **37**(2): p. 785-789.
22. Miehlich, B., Savin, A., Stoll, H., Preuss, H., *Chem. Phys. Lett.*, 1989. **157**(3): p. 200-206.
23. Tao, J., Perdew, J.P., Staroverov, V.N., Scuseria, G.E., *Phys. Rev. Lett.*, 2003. **91**(14): p. 146401.
24. Peterson, K.A., Puzzarini, C., *Theo. Chem. Acc.*, 2005. **114**(4-5): p. 283-296.
25. Figgen, D., Rauhut, G., Dolg, M., Stoll, H., *Chem. Phys.*, 2005. **311**(1–2): p. 227-244.
26. Kendall, R.A., Dunning, T.H., Harrison, R.J., *J. Chem. Phys.*, 1992. **96**(9): p. 6796-6806.
27. Dunning, T.H., *J. Chem. Phys.*, 1989. **90**(2): p. 1007-1023.
28. Møller, C. Plesset, M.S., *Phys. Rev.*, 1934. **46**(7): p. 618-622.
29. Binkley, J.S. Pople, J.A., *Int. J. Quant. Chem.*, 1975. **9**(2): p. 229-236.
30. Feller, D., *J. Comp. Chem.*, 1996. **17**(13): p. 1571-1586.
31. Schuchardt, K.L., Didier, B.T., Elsethagen, T., Sun, L., Gurumoorthi, V., Chase, J., Li, J., Windus, T.L., *J. Chem. Inf. Model.*, 2007. **47**(3): p. 1045-1052.
32. Zhurko G.A, Zhurko, .D.A., *ChemCraft*, 2012.
33. Bondi, A., *J. Phys. Chem.*, 1964. **68**(3): p. 441-451.
34. Keith, T.A., *AIMAll* 2012 TK Gristmill Software.
35. Johnson, E.R., Keinan, S., Mori-Sánchez, P., Contreras-García, J., Cohen, A.J., Yang, W., *J. Am. Chem. Soc.*, 2010. **132**(18): p. 6498-6506.
36. Jeffrey, G.A., *An Introduction to Hydrogen Bonding*, ed. D.G. Truhlar1997, University Of Pittsburgh: Oxford University Press.
37. Keith, T.A., Frisch, M.J., *J. Phys. Chem. A*, 2011. **115**(45): p. 12879-12894.
38. Tiana, D., Francisco, E., Blanco, M.A., Pendás, A.M., *J. Phys. Chem. A*, 2009. **113**(27): p. 7963-7971.

39. Kryachko, E.S., *J. Mol. Struct.*, 2008. **880**(1–3): p. 23-30.

5. Gold acting as a Lewis base in the formation of halogen bonds; A theoretical investigation

5.1. Abstract

A theoretical investigation has been performed to determine the abilities of the auride anion (Au^-) and the dimethyl aurate $[(Me)_2Au]^-$ anionic complex to act as Lewis bases and as a result, act as halogen bond (X-bond) acceptors. We present here novel results obtained by calculating the adducts of Au^- and $[(Me)_2Au]^-$ with a variety of X-bond donors at the B3LYP/aug-cc-pVTZ-pp, TPSS/aug-cc-pVTZ-pp, MP2/cc-pVTZ-pp and MP2/aug-cc-pVTZ-pp levels of theory. It was found that Au^- can form halogen bonds with interaction energies ranging from -3.7 kcal/mol to -33.4 kcal/mol, while the $[(Me)_2Au]^-$ complex also forms halogen bonds with interaction energies ranging from -1.3 kcal/mol to -19.1 kcal/mol. Atoms in Molecules (AIM) analysis was performed at the MP2/aug-cc-pVTZ-pp level of theory and revealed accumulation of electron density between the Au and X atoms, with values of 0.009 to 0.0415 ea_0^{-3}.

5.2. Introduction

Halogen bonds (X-bonds) have been gaining attention lately due to their widespread presence [1] and versatility, since it is widely accepted that there are parallels between halogen bonding and hydrogen bonding [1].

The IUPAC definition [2] of a halogen bond reads as follows: "A halogen bond R-X···Y-Z occurs when there is evidence of a net attractive interaction between an electrophilic region on a halogen atom X belonging to a molecule or molecular fragment R-X (where R can be another atom, including X, or a group of atoms) and a nucleophilic region of a molecule, or molecular fragment, Y-Z". The features of these interactions in a halogen-bonded complex R-X···Y-Z, are, amongst others [2]:

- The distance between X and Y is less than the sum of van der Waals radii of X and Y;
- The R-X···Y angle tends to be close to 180º;
- The R-X bond length increases upon adduct formation;
- The X···Y interaction becomes less stabilising when the electronegativity of X increases or the electron-withdrawing capability of R decreases;

- The formation of a halogen bond is dependent on effects such as electrostatic interactions (polarisation included) and dispersion, with other forces also contributing, although their roles vary from case to case;
- Analysis of the electron density topology reveals a bond path connecting atoms X and Y accompanied by a bond critical point between the two atoms;
- The halogen atom (X) may be involved with more than one halogen bond;
- The halogen bond may be involved with halogen transfer reactions.

Although most studies focus on halogen bonds to organic compounds there have been a variety of investigations of halogen bonds involving organometallic systems. For instance, in 2008, Brammer and co-workers [3] wrote an overview paper entitled "Combining metals with halogen bonds", where they studied C-X···X'-M halogen bonds that form networks in crystal structures. The strength of these interactions could be altered by changing the organic halogen bond donor or inorganic halogen bond acceptor. The authors stated that "Preferences for interaction geometries at the acceptor (Lewis base) are also generally consistent with those observed for hydrogen bonds…" Libri *et al.* [4] studied halogen bonds similar in nature to those studied by Brammer, but showed that similar complexes could form both strong hydrogen and halogen bonds, further illustrating the parallels between hydrogen and halogen bonding. We have recently [5] shown that Au···H hydrogen bonds exist between the Au^- and $[(Me)_2Au]^-$ anions and a variety of hydrogen bond (H-bond) donors. Based on the similarities between H-bonding and X-bonding [6-8] we postulate that Au could also act as a halogen-bond acceptor.

To the best of our knowledge, we believe that this is the first proposal of the possibility that any metal centre, in particular Au, can act as a halogen bond acceptor where the halogen bond is formed between the metal centre and halogen-bond donor (e.g. Au···ICH_3). Au···X contacts have been noted before, for instance an Au···Cl contact was described for $[Ph_3PPNPPh_3]^+.[Au(CN)]^-.0.5CHCl_2$ between the anionic aurate complex and the solvent molecule. It was pointed out that this contact is preferred over anion-anion interactions but the authors [9] did not mention whether that this was a stabilising interaction or could be described as a halogen bond. In another investigation by Schneider *et al*. [10] a crystal structure containing an Au···I contact was obtained, however, this was again not labelled as a halogen bond.

The concept of the "σ-hole" was introduced in 2007 [8], as an explanation for the origin of halogen bonding. Since then the understanding of halogen bonding has increased

significantly; for instance, it is known that halogen bonding is highly directional, even more so than hydrogen bonding [11, 12]. The directionality of hydrogen and halogen bonding may be explained by the electrostatic surface potential of the donor atoms, as shown by Shields *et al*. [12], where the σ-hole on the hydrogen-bond donor involves a larger positive region at the tip of the H atom than the halogen atom σ-hole.

As in our previous theoretical investigation, and to be systematic and consistent, we will first study the ability of the Au^- ion to yield halogen bonds, since the auride anion is the strongest possible Lewis base gold could form.

The Au^- ion exists in the gas phase, and occasionally in solution, and from our previous work [5] and work by others [13, 14], it is known to form hydrogen bonds, illustrating the Au^- ion's ability to act as H-bond acceptor and Lewis base. Furthermore, we expect the Au^- ion to interact with the σ-hole on the halogen atom and, since it is known that the auride anion behaves similarly to the iodide ion with regards to hydrogen bonding [15], we expect similar trends for halogen bonding.

We have shown that the $[(Me)_2Au]^-$ ion forms weaker H-bonds than Au^-, hence we will test to see whether it will also form halogen bonds. Furthermore, if the Au(I) metal centre possesses electrostatic properties such that a halogen bond can form, we suspect there might be other examples of other metals that could possibly do the same. To this extent we expanded the study to briefly investigate the ability of anionic Cu(I) and Ag(I) complexes to form halogen bonds.

We start our theoretical investigation by considering the interaction energy, E_{INT}, and geometrical parameters as a function of the halogen bonded adducts of Au^- and $[(Me)_2Au]^-$ with XCH_3 (X=I, Br, Cl). We will investigate the effect of an electron-withdrawing group on the halogen bond donors and the effect the polarisibility of the X-R bond has on the X-bond strength. This will be probed by utilising chloroform and I_2 as X-bond donors.

5.3. Methodology

All geometry optimisations were performed with the Gaussian 09 rev B.01 [16] package in the gas phase. Symmetry constraints were omitted with the keyword "NoSymm" along with counterpoise corrections [17, 18] to correct for the basis-set superposition error. The IR frequencies of the optimised adducts were calculated to confirm that they correspond to energy minima.

The interaction energy was calculated by

$$E_{INT} = E_{AB}^{BSSE} - (E_A + E_B)$$

where the geometries of fragment A and B were extracted from the AB adduct and the energies of fragments E_A and E_B were calculated. The elongation in the X-R bond of the X-bond donor was calculated by subtracting the distance in the X-bonded donor $[(XR)_{AB}]$ from the optimised bond length of the X-bond donor monomer (XR_B):

$\Delta R = (XR)_{AB} - (XR)_B$.

The subscripts AB and B indicate the X-R bond length in the adduct and isolated X-bond donor, respectively.

The B3LYP [19-21] and TPSSTPSS (TPSS) [22] Density Functionals (DFs) were utilised in combination with the aug-cc-pVTZ-pp [23] basis set to describe the Au, Cu, Ag, I atoms with the effective core potential (ECP) designed by Friggen *et al.*[24], while the the H, C, F, Br, Cl atoms were represented by the all electron aug-cc-pVTZ [25-28] basis set. Furthermore, the Wave Function Theory (WFT) method MP2 [29, 30] was utilised in combination with the cc-pVTZ-pp and the aug-cc-pVTZ-pp [23] basis set incorporating ECPs [24], in order to describe the Au, Ag, Cu and I atoms. As before, the cc-pVTZ and aug-cc-pVTZ basis sets were used to describe the H, C, F, Br and Cl atoms. All basis sets utilised in this study were downloaded from the EMSL basis set exchange website [31, 32]. The ChemCraft [33] suite was utilised to visualise the optimised geometries. We need to mention that we consider the MP2* level of theory (MP2/cc-pVTZ-pp) as the benchmark for geometrical and energetic values, as we have in our previous studies [34], since it is known to give the best balance between electrostatics and correlation. We selected the van der Waals (vdW) radii of Au, Cl, Br and I as 1.66 Å, 1.75 Å, 1.85 Å and 1.98 Å, respectively, as defined by Bondi [35].

Atoms in Molecules (AIM) analysis was performed utilising AIMAll [36] version 14.06.21. The electron density $[\rho_b\ (e a_0^{-3})]$ and Laplacian of the electron density $\nabla^2(\rho_b)\ (e a_0^{-5})$ were obtained as is from AIMAll and the total electronic energy density was calculated as $[H_b\ (au)] = -1 * K\ (au)$. The b subscript indicates that it is a property of the intermolecular bond critical point (BCP) of interest, which in this case is between the Au and X atom. The wave functions of the optimised geometries at the MP2/aug-cc-pVTZ-pp level of theory were written as wfx files, using Gaussian09. Electrostatic Surface Potentials were calculated at the B3LYP/aug-cc-pVTZ-pp level of theory for the $[(Me)_2Cu]^-$, $[(Me)_2Ag]^-$ and $[(Me)_2Au]^-$ complexes utilising AIMAll, with the isosurface defined at 0.001 au. The

ESPs were visualised by selecting the "minimum to maximum" colour scale in order to accentuate fine structure.

Noncovalent Interaction (NCI) plots, as proposed by Johnson *et al.*[37], were calculated from the same wave function and were graphically displayed utilising AIMAll. The Reduced Electron Density Gradient (RDG) isosurfaces were calculated with a resolution of 0.04 au. The visualisation of the RDG isosurfaces were calculated at a value of 0.5 au and with minimum and maximum electron densities of 0.0001 and 0.05 $e a_0^{-3}$, respectively. The maximum density was changed to 0.05 $e a_0^{-3}$ and 0.07 $e a_0^{-3}$ for $[(Me)_2Cu]^-$ X-bonded to ICF_3 and ICH_3, respectively, and to 0.045 $e a_0^{-3}$ for $[(Me)_2Ag]^-$ X-bonded complexes when performing the NCI plot analyses. This was done to eliminate artefacts that arise at higher electron-density values and occur around the BCP of the M-C bond. Also, the maximum density of the NCI plots for the $Cu^{I}\cdots ICF_3$ interaction was increased due to the large density accumulation between the Cu(I) and I atoms. The maximum density was also changed to 0.058 $e a_0^{-3}$ for the $[(Me)_2Au]^-$ halogen bonded to ICF_3. The RDG surfaces were colour coded by mapping the "Sign(HessRho_EigVal_2)*Rho" [$\text{sign}(\lambda_2)\times\rho$] onto them. The colour scale ("Range Method") was the "-Maximum Magnitude to +Minimum Magnitude". Red indicates a negative or greater negative $\text{sign}(\lambda_2)\times\rho$ value and blue the positive value of $\text{sign}(\lambda_2)\times\rho$ and are scaled to the largest absolute value. Therefore, each colour scheme has been scaled in proportion to itself, however, we have included the value of $\text{sign}(\lambda_2)\times\rho$ for each example, for reference.

5.4. Results and Discussion

We start our systematic investigation by considering the Au^- ion and its ability to act as X-bond acceptor to the X-bond donors XCH_3 and XCF_3 (X=I, Br, Cl), in order to determine trends and bonding characteristics. Figure 1 shows the optimised geometries of the auride anion X-bonded to the iodomethane, bromomethane and chloromethane.

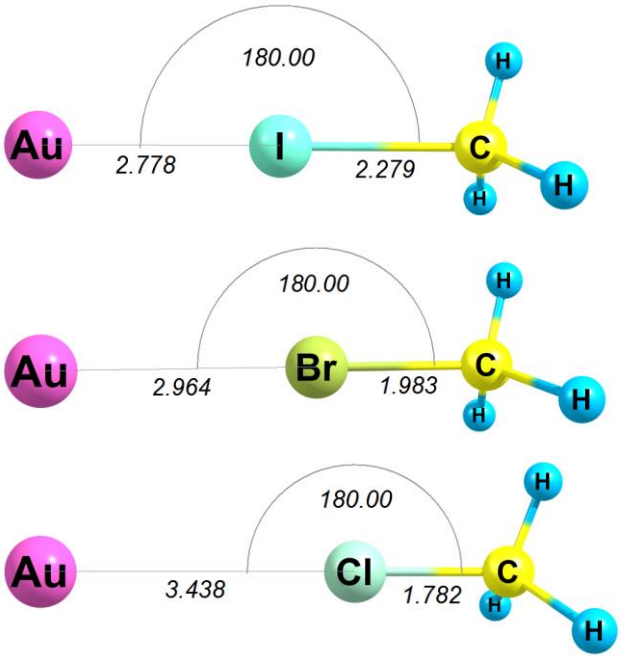

Figure 1 – Optimised geometries of the auride anion X-bonded to X-CH_3 X-bond donors calculated at the MP2/aug-cc-pVTZ-pp level of theory.

The interaction energies (E_{INT}) and various important geometrical parameters of the optimised geometries of the adducts, shown in Figure 1, calculated at the DFT level (B3LYP and TPSS) with the aug-cc-pVTZ-pp basis set and also at the MP2 level with the aug-cc-pVTZ-pp (MP2 ≡ MP2/aug-cc-pVTZ-pp) and cc-pVTZ-pp (MP2* ≡ MP2/aug-cc-pVTZ-pp) basis sets are given in Table 1. In our previous work [34] we have shown that MP2/aug-cc-pVTZ-pp can overestimate interaction energies when iodines (highly polarisable atoms with large dispersion contributions) are present. We therefore expect MP2 to yield larger interactions for the cases where dispersion has a substantial contribution to the total interaction energy, thus we consider the MP2* level of theory to be our benchmark.

Table 1 – The E_{INT} values in kcal/mol, the Au···X-CH_3 distances (Å), the Au···X-CH_3 angles (º), the X-CH_3 bond elongation (Å) indicated as $\Delta R(X\text{-}CH_3)$ for the optimised X-bonded adducts to the Au^- ion at the B3LYP, TPSS, MP2* and MP2 levels of theory. The ratio of the Au···X distances with respect to the sum of the vdW radii is included as $(Au\cdots X)/\Sigma_{vdW}$.

Method	**X-bond donor**	**E_{INT} (kcal/mol)**	**Au···XCH_3 (Å)**	**$(Au\cdots X)/\Sigma_{vdW}$**	**Au···X-CH_3 (deg)**	**$\Delta R(X\text{-}CH_3)$ (Å)**
B3LYP	ICH_3	-12.38	2.963	0.814	180.0	0.140
TPSS		-19.75	2.829	0.777	179.8	0.184
MP2*		-16.13	2.829	0.777	180.0	0.135
MP2		-20.06	2.778	0.763	180.0	0.156
B3LYP	$BrCH_3$	-2.67	3.092	0.881	180.0	0.074
TPSS		-9.52	2.786	0.794	179.9	0.154
MP2*		-3.70	3.044	0.867	180.0	0.047
MP2		-5.64	2.964	0.845	180.0	0.058
B3LYP	$ClCH_3$	2.29	3.990	1.170	179.9	-0.001
TPSS		0.49	3.071	0.901	180.0	0.052
MP2*		1.19	3.588	1.052	180.0	-0.001
MP2		0.10	3.438	1.008	180.0	0.002

If the E_{INT} values of MP2* in Table 1 are considered, we see that ICH_3 yields the most stable adduct, followed by the bromine and chlorine derivatives. This agrees with the IUPAC definition [2] with regards to the E_{INT} dependence on the electronegativity of the halogen. The E_{INT} values of the $Au^-\cdots ClCH_3$ interaction suggest the interaction is repulsive and not favourable. We see that B3LYP and MP2* yield the least favourable energy values for this adduct and therefore Cl-C bonds that are shorter than in the isolated X-bond donor. The overestimation of the correlation contribution at the MP2 level can be seen if the E_{INT} values are compared to those obtained with MP2*.

The ratios of the Au···X distance to the sum of the vdW radii are also included, with the iodine and bromine analogues yielding comparable values, and the chloromethane yielding Au···Cl distances longer than the sum of the vdW radii. This long Au···Cl distance is not unexpected, since the E_{INT} values are destabilising. There is a concomitant lengthening of the X-C distance, with ΔR values upon adduct formation all being positive for the iodomethane (0.154±0.022 Å) and bromomethane (0.083±0.049 Å). The ΔR values for chloromethane fluctuate since it yields an unstable adduct. This meets one of the requirements for halogen bonding according to the IUPAC definition where X-R bond elongation is expected for halogen bond donors upon adduct formation.

Also, the Au···X-C angles are all almost perfectly linear, consistent with the directionality of halogen bonding and also H-bonding. This linearity correlates with the IUPAC definition that states the angle should be approximately 180º.

The geometrical parameters of the $Au^{-}\cdots ICH_3$ and $Au^{-}\cdots BrCH_3$ adducts exhibit similar behaviour to what we have seen previously [5] for H-bonds to Au^{-}: as the E_{INT} values increase, the $Au^{-}\cdots X$ distances decrease and the X-R bond length increases. However, these halogen bond interactions somewhat resemble weaker version of the $X^{-}\cdots X$ interaction found in trihalides, in particular the triiodides [40], since gold is known to behave like iodide as an H-bond acceptor [15]. The $Au^{-}\cdots X$ interaction is therefore fundamentally different to $Au^{-}\cdots H$, since there is a higher degree of charge-transfer (dative bond characteristics) and as a result, covalency.

Next, we investigate the effects of an electron-withdrawing group bonded to the halogen donor atoms. The optimised geometries are shown in Figure 2. It is well known that the X-bonding ability of a compound can be improved by substituting H atoms with F atoms [1], hence we repeated the calculations above with ICF_3, $BrCF_3$ and $ClCF_3$, see Figure 2 and Table 2.

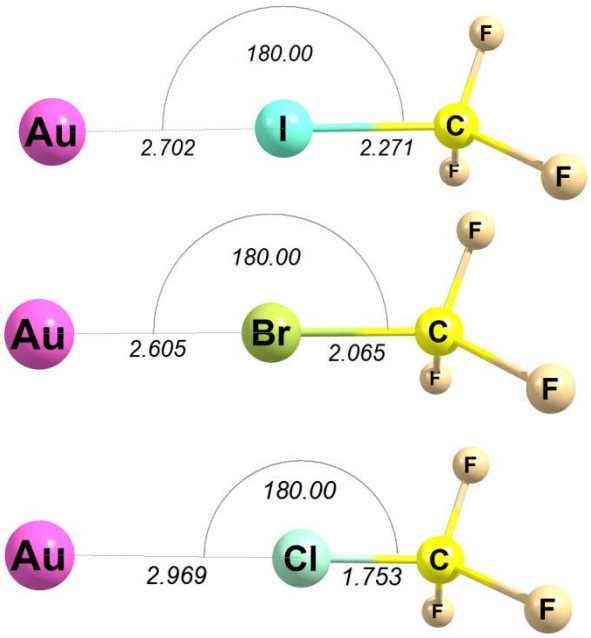

Figure 2 – Optimised geometries of the auride anion X-bonded to X-CF_3 X-bond donors calculated at the MP2/aug-cc-pVTZ-pp level of theory.

The E_{INT} and geometrical parameters of the X-bonded adducts of the Au^{-} ion are summarised in Table 2.

Table 2 - The E_{INT} (kcal/mol), Au···X-CF_3 distances (Å), Au···X-CF_3 bonding angle (º), (Au···X)/Σ_{vdW} ratios, X-CF_3 bond lengths (Å) and X-CF_3 bond-length elongations [ΔR(X-CF_3) (Å)] of the optimised geometries of Au^-.ICF_3, Au^-.$BrCF_3$ and Au^-.$ClCF_3$.

Method	X-bond donor	E_{INT} (kcal/mol)	Au···X-CF_3 (Å)	(Au···X)/Σ_{vdW}	Au···X-CF_3 (deg)	ΔR(X-CF_3) (Å)
B3LYP	ICF_3	-36.76	2.788	0.766	179.9	0.212
TPSS		-46.15	2.710	0.745	180.0	0.240
MP2*		-33.27	2.739	0.753	180.0	0.121
MP2		-39.73	2.702	0.742	180.0	0.141
B3LYP	$BrCF_3$	-22.65	2.754	0.785	180.0	0.152
TPSS		-36.09	2.601	0.741	179.9	0.255
MP2*		-20.70	2.694	0.767	180.0	0.104
MP2		-28.32	2.605	0.742	180.0	0.153
B3LYP	$ClCF_3$	-8.59	3.05	0.895	180.0	0.022
TPSS		-18.63	2.64	0.775	180.0	0.153
MP2*		-9.00	3.10	0.910	180.0	-0.010
MP2		-12.00	2.97	0.871	180.0	0.002

The E_{INT} values exhibit the trend Au^-.ICF_3 > Au^-.Br CF_3 > Au^-.$ClCF_3$, with E_{INT} values of -33.27, -20.70 and -9.00 kcal/mol at the MP2* level of theory, respectively.

This trend corresponds with the Au···XCF_3 distances, where the ICF_3 and $BrCF_3$ distances are considerably shorter than the sum of the vdW radii, and less than those with the ICH_3 and $BrCH_3$ analogues, as can be seen from the Au···X/Σ_{vdW} ratios given in Tables 1 and 3. Again, the $ClCF_3$ analogue yields the largest Au···X/Σ_{vdW} values, although these values are below 1.0 indicating that there is shortening.

Furthermore, we see that the Au···X-CF_3 angles are all almost perfectly linear, with consistently positive ΔR values characteristic of halogen bonds, according to the IUPAC definition [2]. However, we still see that the $ClCF_3$ adduct at the MP2* level of theory yields a Cl-C bond length shorter than the isolated X-bond donor, similarly to that found for the Au^-···$ClCH_3$ adduct, while the MP2 level of theory shows a very small ΔR value and the DFs result in longer Cl-C lengths. We are unsure as to why the Cl-C lengths are shorter for this adduct than the isolated monomer. The chlorinated X-bond donor seems to be an outlier when compared to its iodine and bromine analogues.

The effect of fluorine substitution is, however, most profound for the Au^-···$ClCF_3$ adduct, since the Au^-···Cl interaction has now become stabilising. The Au···Cl distances are correspondingly shorter than the sum of the vdW radii. The variation in E_{INT} values suggest that these are dependent on the potential of the σ-hole, which in turn is influenced by the R

group (R = CH_3 and CF_3) that is bonded to the halogen. Consider the molecular graphs in Figure 3, obtained at the MP2/aug-cc-pVTZ-pp level of theory, where the atomic interaction line between the Au^- ion and the donors provides evidence for X-bonding.

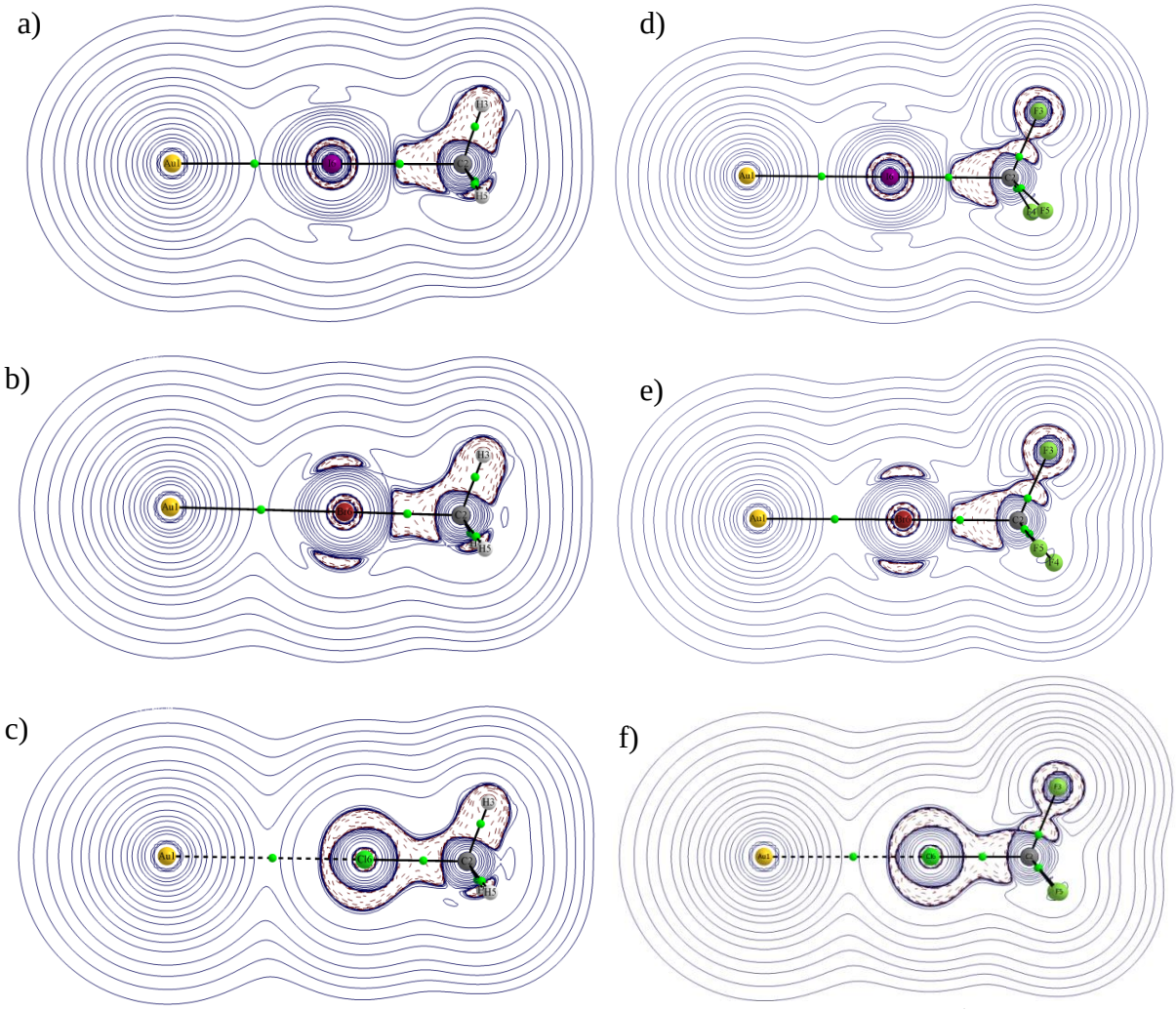

Figure 3 – Molecular graphs with the two-dimensional contour plot of $\nabla^2\rho$ (ea_0^{-5}) for the optimised geometries of the Au^- ion X-bonded to XCH_3 [X = a) I, b) Br, c) Cl] on the left and XCF_3 [X = d) I, e) Br, f) Cl] on the right at the MP2/aug-cc-pVTZ-pp level of theory. Atomic interaction lines are indicated by solid and dotted black lines, using the default cutoffs as defined by AIMAll, with the BCPs represented by green spheres.

The molecular graphs with the two-dimensional contour plots of $\nabla^2(\rho_b)$ for the Au^- ion X-bonded to iodomethane, bromomethane, chloromethane are and their fluorinated analogues are shown in Figure 3. If we consider and compare the topological changes from Figure 3, especially around the region of the carbon atom, the effect of the fluorine atoms is noticeable in the two-dimensional contour plots of the Laplacian: the fluorine atoms withdraw electron density, thus decreasing the electron density in the X-C bonds. However, our focus is on the

properties of the BCP separating the Au and the neighbouring X atom, i.e. the $Au^{-}\cdots X$ interaction. The AIM parameters at this BCP for all six X-bonded adducts are shown in Table 3. Ranges for these AIM parameters expected for various types of interactions are summarised in Table 4 from the work of Nakanishi *et al.* [39]. It is important to note that some of the ranges overlap and it would therefore be normal if the AIM parameters for an interaction's correspond to more than one interaction type.

Table 3 – The electron density at the intermolecular BCP [ρ_b (ea_0^{-3})], the Laplacian of the electron density [$\nabla^2(\rho_b)$ (ea_0^{-5})] and the total electronic energy density H_b in au of the auride anion X-bonded to the selected X-bond donors.

X-bond donor	$\boldsymbol{\rho_b}$ $\boldsymbol{(ea_0^{-3})}$	$\boldsymbol{\nabla^2(\rho_b)}$ $\boldsymbol{(ea_0^{-5})}$	$\boldsymbol{H_b}$ **(au)**
ICH_3	0.0503	0.0810	-0.0117
$BrCH_3$	0.0273	0.0696	-0.0018
$ClCH_3$	0.0090	0.0283	0.0011
ICF_3	0.0604	0.0715	-0.0179
$BrCF_3$	0.0597	0.0997	-0.0149
$ClCF_3$	0.0228	0.0670	-0.0003

Firstly, let us consider the ρ_b and $\nabla^2(\rho_b)$ values for the XCH_3 halogen bond donor series. As we can see, the ρ_b and $\nabla^2(\rho_b)$ values increase as the E_{INT} values increase, with the iodine analogue having the highest ρ_b and $\nabla^2(\rho_b)$ values and $ClCH_3$ having the lowest. The ρ_b and $\nabla^2(\rho_b)$ values of the $Au^{-}\cdots ICH_3$ adduct are within the CT-TBP range, which are also typical for trihalide anions such as triiodide [39]. The weaker $Au^{-}\cdots BrCH_3$ interaction does not fall within these ranges and correlates better with a H-bond type interaction. The ρ_b and $\nabla^2(\rho_b)$ values for the $Au^{-}\cdots ClCH_3$ adduct suggest that it involves a dispersion-type interaction, which is not surprising since we obtained a repulsive E_{INT} value for this adduct. Furthermore, the ρ_b values of $BrCH_3$ and $ClCH_3$ X-bonded to Au^{-} are 54 % and 18 % of that of the ICH_3 adduct, respectively. Interestingly, we see that the H_b values for the ICH_3 and $BrCH_3$ are negative and positive for $ClCH_3$, where the H_b values for the iodine and bromine adducts are within the CT-TBP interaction range, with the $ClCH_3$ adduct yielding an H_b value characteristic of vdW interactions.

When the fluorinated analogues are compared to the halogen methane analogues, we see that there is a 20 % increase in the ρ_b value of the $Au^{-}\cdots ICF_3$ adduct compared to its $Au^{-}\cdots ICH_3$ analogue, which, in combination with the extremely high E_{INT} value suggests that the $Au^{-}\cdots ICF_3$ interaction has a high degree of covalency. Nevertheless, the influence of the

fluorine atoms is substantially more noticeable for the bromine and chlorine derivatives than for the iodine analogues, with ρ_b values 119 % and 153 % higher for the $Au^{-}\cdots BrCF_3$ and $Au^{-}\cdots ClCF_3$ adducts over their non-fluorinated counterparts. This is compelling evidence for the effect electron-donating or -withdrawing groups have on the halogen's ability to act as an X-bond donor.

As before, the ρ_b and $\nabla^2(\rho_b)$ values of $Au^{-}\cdots ICF_3$ and $Au^{-}\cdots BrCF_3$ adducts indicate CT-TBP type interactions, while the $Au^{-}\cdots ClCF_3$ interaction is similar to those for H-bonding. As mentioned before, Kryachko compared the behaviour of the Au^{-} to that of halogens (see ref. [13] and references therein) and this similarity is reflected in the AIM parameters of the BCP separating Au and I/Br due to yielding values in the same range expected for trihalides ($X^{-}\cdots X_2$ interaction noted as CT-TBP in Table 4). Furthermore, values of ρ_b and $\nabla^2(\rho_b)$ are comparable to the calculated values of other types of halogen bonds [40, 41].

Table 4 – Expected ranges of AIM parameters for van der Waals (vdW), hydrogen bonding (H-bond), Charge-Transfer – Molecular Complex (CT-MC) and Charge Transfer – Trigonal Bipyramidal adducts (CT-TBP) as defined by Nakanishi *et al.* [39].

Interaction type	$\boldsymbol{\rho_b}$ $(\boldsymbol{ea_0^{-3}})$	$\boldsymbol{\nabla^2(\rho_b)}$ $(\boldsymbol{ea_0^{-5}})$	$\mathbf{H_b}$ **(au)**
vdW	$0.00 < \rho_b < 0.01$	$0.00 < \nabla^2(\rho_b) < 0.04$	$0.000 < H_b < 0.002$
H-bond	$0.01 < \rho_b < 0.04$	$0.04 < \nabla^2(\rho_b) < 0.12$	$-0.004 < H_b < 0.002$
CT-MC	$0.01 < \rho_b < 0.03$	$0.02 < \nabla^2(\rho_b) < 0.06$	$-0.001 < H_b < 0.002$
CT-TBP	$0.03 < \rho_b < 0.12$	$-0.01 < \nabla^2(\rho_b) < 0.1$	$-0.06 < H_b < -0.003$

Since our calculations contain ECPs, the H_b values are expected to fluctuate [44], however, the author of AIMAll has only described the influence of the ECPs on the electron density, but has not made any statements regarding the influence of ECPs on energetic terms [43]. Hence, since the H_b values may be inaccurate they were included for completeness, but will not be discussed further.

Our results suggest that halogen bonding has much in common with hydrogen bonding, as has been previously noted [12]. Nevertheless, the AIM parameters suggest that there is a degree of charge transfer occurring, with the amount depending on the X-bond donor involved. Also, we see that in some cases the Au^{-} ion does behave comparably to a halogen, since the AIM parameters fall within the CT-TBP ranges found for trihalide ions [39]; the

$X^{-}\cdots X_2$ bonding mechanism in trihalide ions is known to involve charge transfer and a dative-type interaction yielding an extremely strong interaction.

On the other hand, it is to be expected that the Au(I) centre in a complex with its formal positive charge would not be as good a Lewis base as the auride anion, and thus a weaker X-bond acceptor. Hence, in the following section we investigate X-bonds formed between the $[(Me)_2Au]^{-}$ complex (DMA) and various X-bond donors.

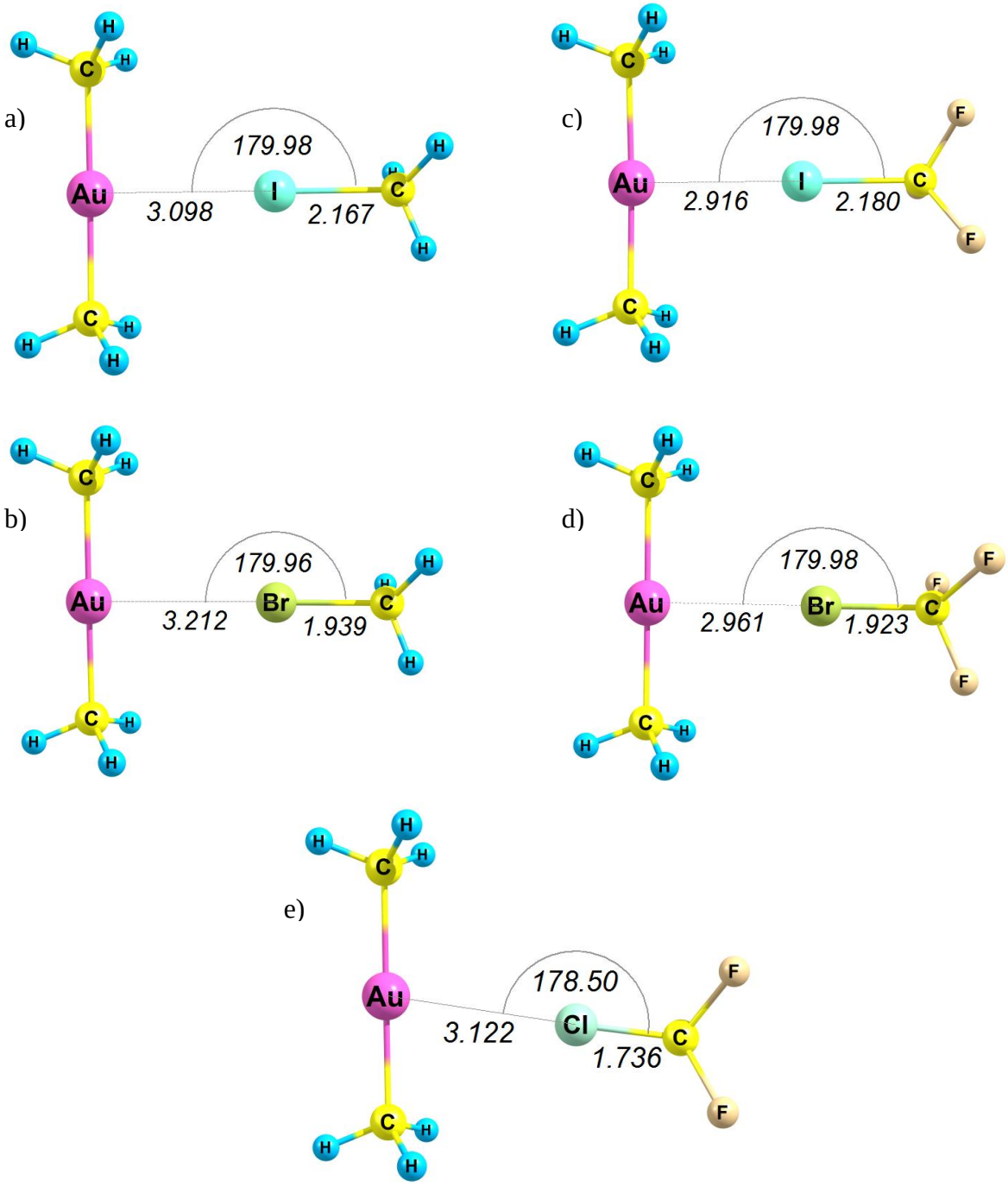

Figure 4 – Optimised geometries of DMA X-bonded to a) ICH_3, b) $BrCH_3$, c) ICF_3, d) $BrCF_3$ and e) $ClCF_3$ at the MP2/aug-cc-pVTZ-pp level of theory.

All the stable adducts obtained at the MP2/aug-cc-pVTZ-pp level of theory are shown in Figure 4 with various interaction energies and important geometrical parameters summarised in Table 5. No stationary point was found for the DMA complex X-bonded to the chloromethane halogen-bond donor, however, a stationary point was obtained for the fluorinated analogue. This is not surprising, since $ClCH_3$ yielded a destabilising E_{INT} values even with Au^-, which is a strong Lewis base.

Table 5 - The E_{INT} values (kcal/mol), Au···X distances (Å), the Au···X-C angles (º), the X-C bond lengths (Å) and the X-C bond length elongation shown as ΔR(X-C) (Å), at four different levels of theory for the optimised geometries of DMA.ICH_3, DMA.$BrCH_3$, DMA.ICF_3, DMA.$BrCF_3$ and the DMA.$ClCF_3$.

Method	**X-bond donor**	**E_{INT} (kcal/mol)**	**Au···X (Å)**	**Au···X-C (deg)**	**X-C (Å)**	**ΔR(X-C) (Å)**
B3LYP	ICH_3	-3.71	3.283	179.7	2.206	0.041
TPSS		-7.81	3.065	179.8	2.242	0.076
MP2*		-6.74	3.150	180.0	2.164	0.039
MP2		-8.44	3.098	180.0	2.167	0.044
B3LYP	$BrCH_3$	0.79	3.507	179.7	1.970	0.010
TPSS		-1.17	3.128	179.7	1.970	0.008
MP2*		-1.24	3.304	180.0	1.935	0.010
MP2		-2.49	3.212	180.0	1.939	0.014
B3LYP	ICF_3	-18.05	3.016	179.6	2.24	0.063
TPSS		-24.80	2.889	179.6	2.28	0.102
MP2*		-19.11	2.963	180.0	2.18	0.040
MP2		-22.12	2.916	180.0	2.18	0.050
B3LYP	$BrCF_3$	-9.92	3.061	179.9	1.97	0.022
TPSS		-15.01	2.856	179.9	2.02	0.069
MP2*		-10.83	3.034	180.0	1.92	0.003
MP2		-13.13	2.961	180.0	1.92	0.012
B3LYP	$ClCF_3$	-5.42	3.260	179.9	1.76	-0.014
TPSS		-7.32	3.000	179.9	1.79	0.009
MP2*		-6.75	3.237	178.3	1.73	-0.019
MP2		-8.48	3.122	178.5	1.74	-0.015

As we can see by analysing the E_{INT} values of the DMA.ICH_3 and DMA.$BrCH_3$ adducts, the $Au^{I}\cdots ICH_3$ interaction is more stabilising than the $Au^{I}\cdots BrCH_3$ interaction, as expected, due to the difference in the electrostatic properties of the σ-holes on bromine and iodine.

The Au···X distances of the DMA.ICH_3 and DMA.$BrCH_3$ adducts are 87 % and 94 % of the sum of the vdW radii, characteristic of weakly attractive interactions, in particular DMA.$BrCH_3$. Furthermore, the Au···X angles are almost perfectly linear, with the ΔR values

indicating bond elongation upon adduct formation, with the iodomethane yielding larger ΔR values than bromomethane, due to relatively shorter Au···X distances and more stabilising E_{INT} values. The trends seen in the E_{INT} and geometrical parameters for the DMA anion bonded to iodomethane and bromomethane are consistent with what was found earlier for the auride anion.

The E_{INT} values for DMA.ICF_3 and DMA.$BrCF_3$ again reflect the influence of the electron-withdrawing groups bonded to the halogen donor atom, with these adducts becoming approximately 10 kcal/mol more stabilising than the iodomethane and bromomethane X-bond adducts. Furthermore, we see that the electron-withdrawing CF_3 group results in the Au^{I}···Cl interaction becoming stabilising, although it only constitutes 35 % of the stabilisation found for the DMA.ICF_3 adduct.

Furthermore, we note that all the Au^{I}···X distances are shorter than the sums of the vdW radii, the DMA.ICF_3 adduct yields an Au···I distance that is approximately 20 % shorter than its sum of vdW radii, while DMA.$BrCF_3$ yields a comparable Au···Br distance indicative of the significant weaker Au^{I}···Br interaction. Similarly, the ΔR values for the DMA.ICF_3 and DMA.$BrCF_3$ adducts are approximately 0.04 Å and 0.01 Å, respectively. All the Au···X-C angles of the fluorinated analogues are almost perfectly linear, characteristic of halogen bonding. These two adducts thus satisfy the expected geometrical changes upon adduct formation, as defined by IUPAC [2].

Even though the DMA.$ClCF_3$ yields stabilising, albeit weak, E_{INT} values and an Au···Cl distance approximately 5 % shorter than the sum of the vdW radii, it behaves differently in that it yields a shorter Cl-C distance upon adduct formation than the isolated $ClCF_3$. This is similar to what we observed for the Au^- ion, but we are unsure why the chlorinated adducts behave in such a way.

In order to confirm that the Au^{I}···X interactions exist AIM analysis was performed for all the DMA adducts, with results shown in Figure 5 and listed in Table 6.

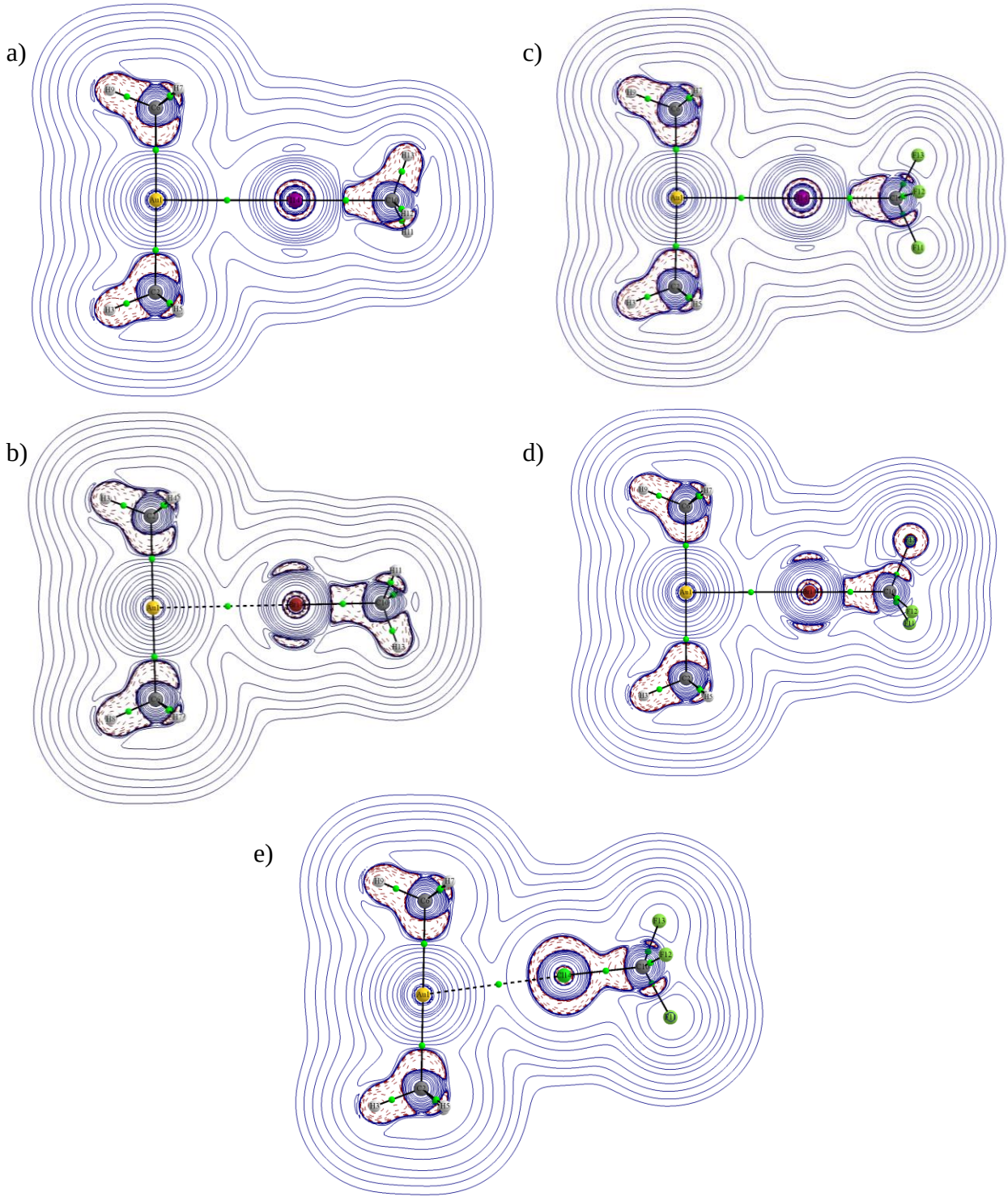

Figure 5 – Molecular graphs and two-dimensional contour plots of $\nabla^2\rho$ ($e a_0^{-5}$) for the optimised geometry of $[(Me)_2Au]^-$ complex X-bonded to a) ICH_3, b) $BrCH_3$ (left) and c) ICF_3, d) $BrCF_3$ and e) $ClCF_3$ (right) at the MP2/aug-cc-pVTZ-pp level of theory. Atomic interaction lines are indicated by solid and dotted black lines, with the BCPs represented by green spheres.

The most important feature of the molecular graphs in Figure 5 is that all of them exhibit an AIL connecting the X atom to the Au^{I} atom with a BCP separating the two atoms. The

presence of the BCP is one of the requirements for halogen bonding, as proposed by IUPAC [2].

Table 6 – The ρ_b, $\nabla^2(\rho_b)$ and the total electronic energy density (H_b) values of the $[(Me)_2Au]^-$ complex interacting with the ICH_3, $BrCH_3$, ICF_3, $BrCF_3$ and $ClCF_3$ X-bond donors at the MP2/aug-cc-pVTZ-pp level of theory.

X-bond donor	$\boldsymbol{\rho_b}$ $(\boldsymbol{ea_0^{-3}})$	$\boldsymbol{\nabla^2(\rho_b)}$ $(\boldsymbol{ea_0^{-5}})$	$\mathbf{H_b}$ **(au)**
ICH_3	0.0291	0.0573	-0.0032
$BrCH_3$	0.0163	0.0483	0.0005
ICF_3	0.0415	0.0674	-0.0080
$BrCF_3$	0.0305	0.0671	-0.0032
$ClCF_3$	0.0184	0.0525	0.0002

If the ρ_b values are considered, we can conclude that the more stabilising the E_{INT} value, the higher the accumulation of electron density between Au and X, with the DMA.ICF_3 adduct yielding the largest value of 0.0415 ea_0^{-3} and the DMA.$ClCF_3$ adduct the lowest value of 0.0184 ea_0^{-3}. Also, the fluorinated analogues yield ρ_b values that are up to twice as large as those for the methyl analogues. We see that the calculated ρ_b values for the DMA.ICF_3 and DMA.$BrCF_3$ adducts are within the expected range for CT-TBP type bonds, similar to what was found for the halogen-bonded adducts of the auride anion. The remainder of the adducts, including DMA.$BrCF_3$, fall within the expected range for H-bonding, according to the parameters in Table 6.

The differences between the $\nabla^2(\rho_b)$ and H_b values for the fluorinated and non-fluorinated donors are less pronounced than with the ρ_b values, but follow similar trends.

NCI analysis is a useful tool for investigating noncovalent interactions, such as the intramolecular X-bonding [46] within CX_3-CX_3 groups. The NCI plots showed that the interactions are stabilising in some cases and suggested that they are dispersion-type interactions. One advantage of the NCI method is that no atomic interaction line is needed to observe a noncovalent interaction. The NCI plots approach was also utilised by Herrebout *et al*. [45] in their study of halogen bonds published in 2013.

In the work of Kozuch and Martin (see ref. [46] and references therein) entitled "Halogen Bonds: Benchmarks and Theoretical Analysis", the authors performed an "extensive survey of wave function and DFT methods to test their accuracy for geometries and dissociation energies of halogen bonds." Additional topics include NCI plots as a theoretical tool that can be utilised in order to analyse X-bonds. In the article they mention disputes within the

scientific community that exist when bonding mechanisms of the different X-bonds are proposed. The authors state that these disputes occur due to the meaning assigned to various complex energetic components calculated by different "bonding models", which vary between adducts and sometimes lead to different conclusions. The authors argue that these components are not experimentally observable and great care should be taken when interpreting these values, but they do help to rationalise and understand why interactions occur. They propose NCI plots as an alternative and describes it as "an elegant way to assess the characteristics of the X-bond". Here they mention that when $\text{sign}(\lambda_2)\times\rho$ is negative, implying λ_2 is negative, the interaction is stabilising and when $\text{sign}(\lambda_2)\times\rho$ is positive, the interaction is destabilising. Furthermore, they also point out that vdW type interactions have $\text{sign}(\lambda_2)\times\rho$ values of small negative values that are close to zero, due to the instability of $\text{sign}(\lambda_2)$ at low electron densities [37].

In Figure 6 we have included the NCI plots of the $[(Me)_2Au]^-$ complex X-bonded to ICH_3, $BrCH_3$, ICF_3, $BrCF_3$ and $ClCF_3$.

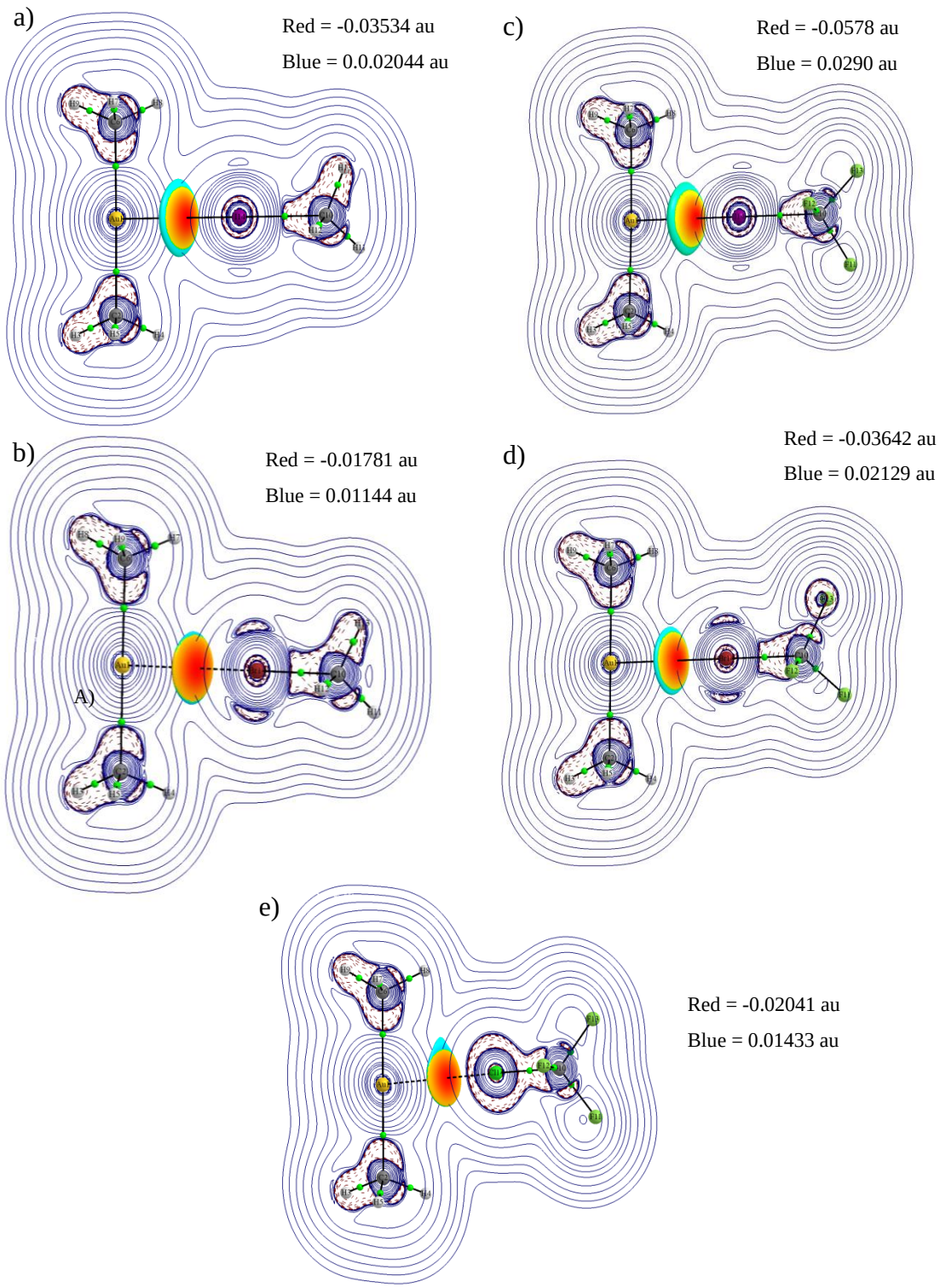

Figure 6 – Molecular graphs and two-dimensional contour plots of $\nabla^2\rho$ (ea_0^{-5}) with the NCI plots included of the $[(Me)_2Au]^-$ complex X-bonded to a) ICH_3 b) $BrCH_3$ and c) ICF_3, d) $BrCF_3$ and e) $ClCF_3$ at the MP2/aug-cc-pVTZ-pp level of theory. The red (minimum) regions indicate a stabilising interaction with blue (maximum) regions indicating repulsion.

The most important features of the NCI plots in Figure 6 are attractive intermolecular interactions between the halogen atom and the gold atom. The stabilising interactions are displayed in red, which corresponds to the interaction between the gold atom and the σ-hole

found at the tip of the halogen. These are surrounded by blue regions indicating repulsion, due to the regions on the halogen atom that act as a Lewis base. Also, we see that as the Au···X distances decrease, the blue regions become larger, suggesting that the negatively charged regions on the halogen atom repel the gold to a larger extent. There is an inverse relation between the E_{INT} values and the sign(λ_2)×ρ values, where the minimum values become more negative as E_{INT} becomes more stabilising. These calculated minimum sign(λ_2)×ρ values are comparable to values calculated for $H_2CO\cdots BrF$ in ref. [46].

We have previously shown [5] that only the $[(Me)_2Au]^-$ complex forms a hydrogen bond to HF, whereas the Cu(I) and Ag(I) analogues do not, due to differences in the electrostatic surface potential. We are, therefore, interested to see if the same is true for halogen bonding.

The ICH_3 and ICF_3 X-bond donors were selected as model halogen bond donors, since the results shown here suggest that they are the most likely to form halogen bonds. The conformations of the X-bond donors with Au^-, Ag^- and Cu^- are shown in Figure 7, with E_{INT} values and important geometrical parameters summarised in Table 7.

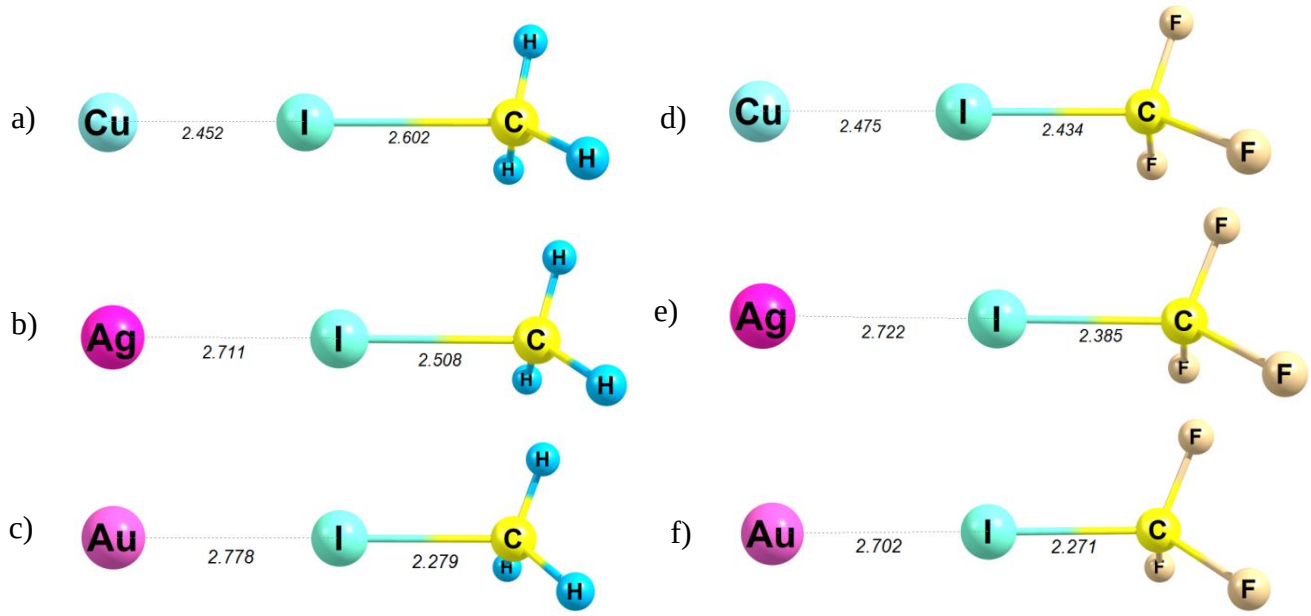

Figure 7 – Optimised geometries of the Cu^-, Ag^- and Au^- ions X-bonded to ICH_3 [a), b), and c), respectively] and ICF_3 [d), e) and f), respectively] at the MP2/aug-cc-pVTZ-pp level of theory.

Table 7 – E_{INT} and M···I distances of the M^- (M = Cu, Ag and Au) anions halogen bonded to ICH_3 and ICF_3 obtained with the B3LYP and MP2 methods in combination with the aug-cc-pVTZ-pp basis set.

M	Method	X-bond donor	E_{INT} (kcal/mol)	M···I (Å)	ΔR (Å)
Cu	B3LYP	ICH_3	-22.63	2.660	0.495
Ag			-14.38	2.990	0.203
Au			-12.38	2.963	0.140
Cu	MP2		-43.25	2.452	0.480
Ag			-30.15	2.711	0.378
Au			-20.06	2.778	0.156
Cu	B3LYP	ICF_3	-65.56	2.506	0.488
Ag			-49.36	2.776	0.374
Au			-36.76	2.788	0.212
Cu	MP2		-56.50	2.434	0.304
Ag			-45.66	2.722	0.256
Au			-39.73	2.702	0.141

The large E_{INT} values for Cu^- X-bonded to both X-bond donors suggest that there is a significant covalency to the interaction, while the large ΔR values suggest that the adduct is better described as Cu-I···R^-. In order to explain this, we turn to the electron affinities (EA) of each of the metals, with Cu^-, Ag^- and Au^- having EAs of 1.24 eV, 1.3 eV and 2.31 eV, respectively [15, 47]. A trend emerges: the lower the electron affinity, the higher the E_{INT} values. We postulate that this relationship is a result of the metal's ability to donate electron density into empty anti-bonding orbitals of the X-C bond. Another way of viewing this relationship is the lower the EA of the metal centre, the less likely it is to hold onto its negative charge. As a result, more charge is transferred from the metal centre to the halogen bond donor molecule. To deduce the degree of charge transfer we consider the AIM charges in Table 8.

Table 8 – AIM charges of the metal centres X-bonded to ICH_3 and ICF_3 at the MP2/aug-cc-pVTZ-pp level of theory.

	X-bond donor (*e*)	
Anion	**ICH_3**	**ICF3**
Cu	-0.34	-0.24
Ag	-0.53	-0.40
Au	-0.77	-0.65

The most import trend to notice is that the magnitude of the negative charge on the metal is inversely proportional to the E_{INT} value, i.e. the more stabilising E_{INT} is, the more charge is transferred to the X-bond donor.

To further illustrate that the interactions are due to charge-transfer, we will compare the BCP situated between the metal anion and halogen to the BCP between the halogen and carbon atom.

Table 9 – Electron densities of the M···I and I-C BCPs at the MP2/aug-cc-pVTZ-pp level of theory.

	ρ_b ($e a_0^{-3}$) of BCP	
M^-	**M···I**	**I-C**
X-bond donor	**ICH_3**	
Cu	0.0656	0.0565
Ag	0.0506	0.0677
Au	0.0503	0.0999
X-bond donor	**ICF_3**	
Cu	0.0652	0.0763
Ag	0.0519	0.0843
Au	0.0604	0.1028

There is a general trend where the E_{INT} values tend to increase for both BCPs upon an increase of the ρ_b values. Furthermore, we see that ρ_b(M···I) > ρ_b(I-C), for the Cu adduct when ICH_3 is the donor and can be written as $Cu - I \cdots CH_3^-$. All the other five adducts yield ρ_b(M···I) < ρ_b(I-C).

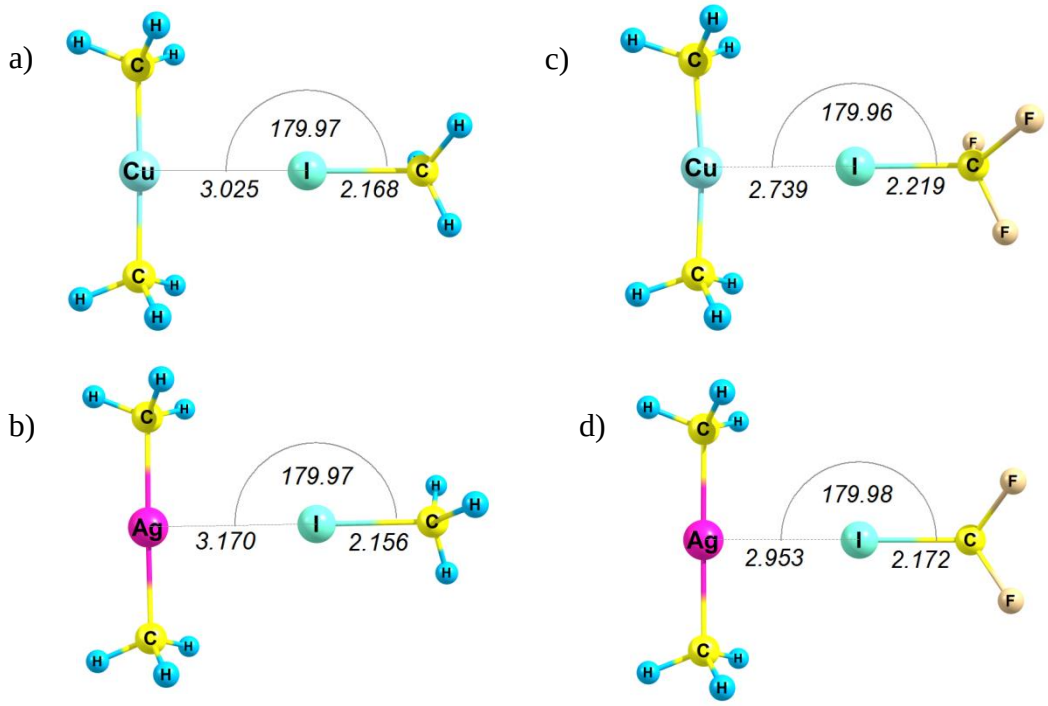

Figure 8 – Optimised geometries of $[(Me)_2Cu]^-$ and $[(Me)_2Ag]^-$ X-bonded to ICH_3 (a and b, respectively) and ICF_3 (c and d, respectively) at the MP2/aug-cc-pVTZ-pp level of theory.

The Cu(I) and Ag(I) analogues of DMA also form halogen bonded adducts with ICH_3 and ICF_3 (see Figure 8). Important interaction energies and geometrical parameters for these adducts at the B3LYP and MP2 level of theory are summarised in Table 10.

Table 10 – E_{INT} values and M···I distances of the optimised geometries of $[(Me)_2M]^-$(M = Cu(I), Ag(I) and Au(I)) X-bonded to ICH_3 and ICF_3 at the B3LYP and MP2 levels of theory.

$[(Me)_2M]^-$	Method	X-bond donor	E_{INT} (kcal/mol)	M···I (Å)	ΔR (Å)
Cu^I	B3LYP	ICH_3	-4.55	3.128	0.059
Ag^I			-3.05	2.855	0.042
Au^I			-3.71	3.283	0.041
Cu^I	MP2		-6.41	3.025	0.045
Ag^I			-5.93	3.308	0.033
Au^I			-8.44	3.283	0.044
Cu^I	B3LYP	ICF_3	-20.74	2.855	0.096
Ag^I			-16.93	3.028	0.070
Au^I			-18.05	3.016	0.063
Cu^I	MP2		-22.91	2.739	0.089
Ag^I			-18.36	2.953	0.043
Au^I			-22.12	2.916	0.050

All the M···X distances are within the sum of the vdW radii, while the M···X-C angles are almost perfectly linear. Also, the ΔR values are all positive implying that there is a bond elongation upon X-bond formation, however this is much less than the M^- ions. The E_{INT} values are also correspondingly lower. As before with the M^- ions, the copper analogue, $[(Me)_2Cu]^-$, yields the most stable X-bonded adducts. However, $[(Me)_2Au]^-$ yields the second most stable X-bonded adducts, with $[(Me)_2Ag]^-$ yielding the least stable adducts. This is a different trend when compared to the metal anions, where gold yielded the least stable adduct. Surprisingly, the $Au^{I}\cdots ICH_3$ interaction is even more stabilising than the $Cu^{I}\cdots ICH_3$ interaction at the MP2 level of theory. We suspect that the latter to be an artefact that may be ascribed to the MP2 method's tendency to overestimate dispersion-type interactions. In order to gain further insight into these surprising results we performed AIM analysis of the $Cu^{I}\cdots I$ and $Ag^{I}\cdots I$ interactions, with the molecular graphs shown in Figure 9.

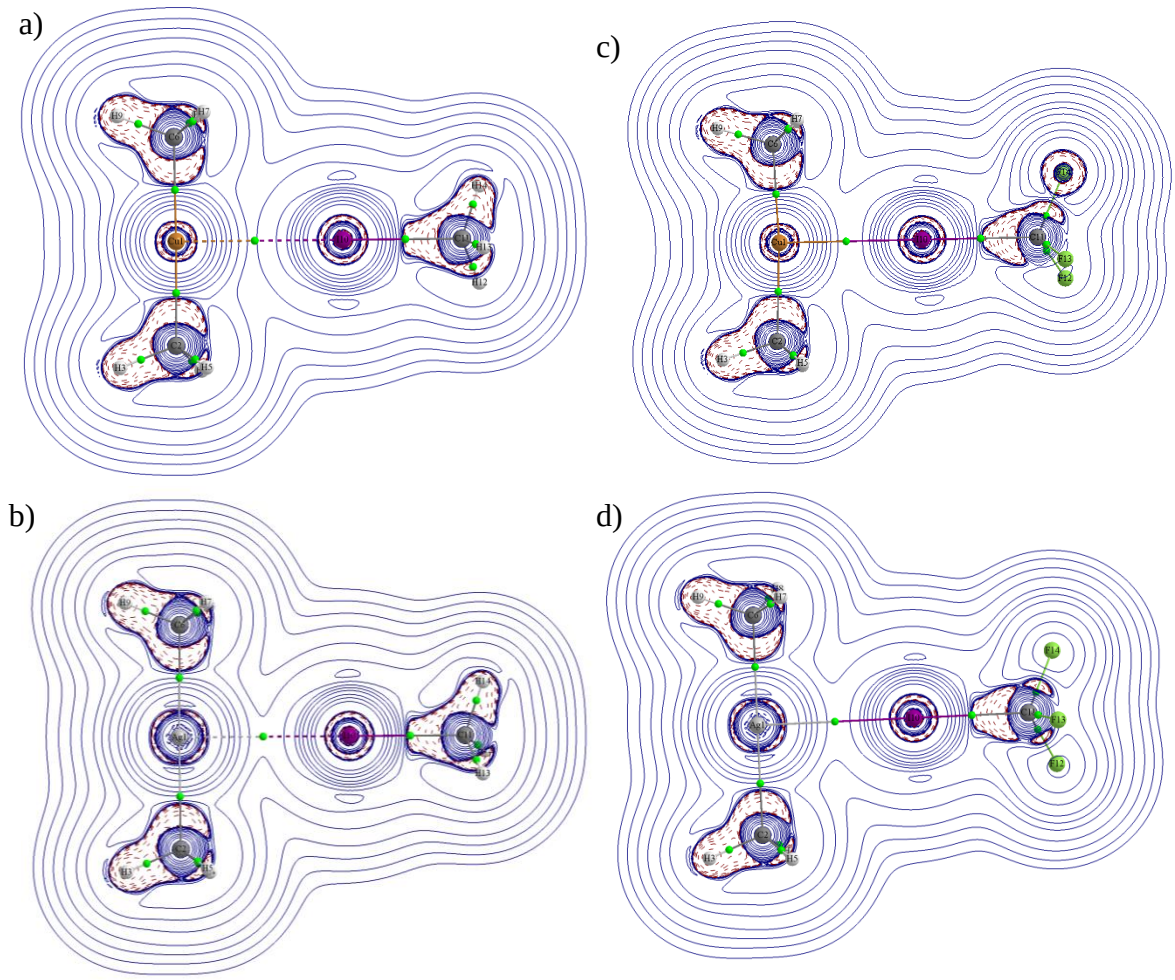

Figure 9 – Molecular graphs with two-dimensional plots of $\nabla^2\rho$ (ea_0^{-5}) of the optimised geometries of $[(Me)_2Cu]^-$ (top) and $[(Me)_2Ag]^-$ (bottom) X-bonded to ICH_3 [a and b] and ICF_3 [c and d] at the MP2/aug-cc-pVTZ-pp level of theory.

As we can see from the molecular graphs in Figure 9, there are indeed AILs connecting the iodine atoms to the Cu(I) and Ag(I) metal centres. The properties of the BCPs are summarised in Table 11.

Table 11 – The ρ_b, $\nabla^2(\rho_b)$ and the total electronic energy density (H_b) values of the $[(Me)_2M]^-$ [M = Cu(I), Ag(I) and Au(I)] complexes halogen bonded to the ICH_3, and ICF_3 X-bond donors at the MP2/aug-cc-pVTZ-pp level of theory.

	$M^{I}\cdots ICH_3$			I-CH_3
$[(Me)_2M]^-$	ρ_b (ea_0^{-3})	$\nabla^2(\rho_b)$ (ea_0^{-5})	H_b (au)	ρ_b (ea_0^{-3})
Cu(I)	0.0240	0.0379	-0.0030	0.113
Ag(I)	0.0214	0.0451	-0.0014	0.116
Au(I)	0.0291	0.0573	-0.0032	0.114
	$M\cdots ICF_3$			
Cu(I)	0.0428	0.0440	-0.0107	0.108
Ag(I)	0.0330	0.0593	-0.0047	0.119
Au(I)	0.0415	0.0674	-0.0080	0.117

All the electron densities at the intermolecular BCP are within the expected range for H-bonds, except the $Cu^{I}\cdots ICF_3$ and $Au^{I}\cdots ICF_3$ halogen bonds, with electron densities that are larger than those for H-bonding, but are within the CT-TBP range. The ρ_b values correlate with the E_{INT} values, where an increase in stability corresponds to an increase in the electron density.

The $\nabla^2(\rho_b)$ and the values are generally within the excepted ranges for H-bonding or CT-TBP. Again, the AIM parameters confirm that the $Au^{I}\cdots I$ interactions are stronger than those for Ag(I).

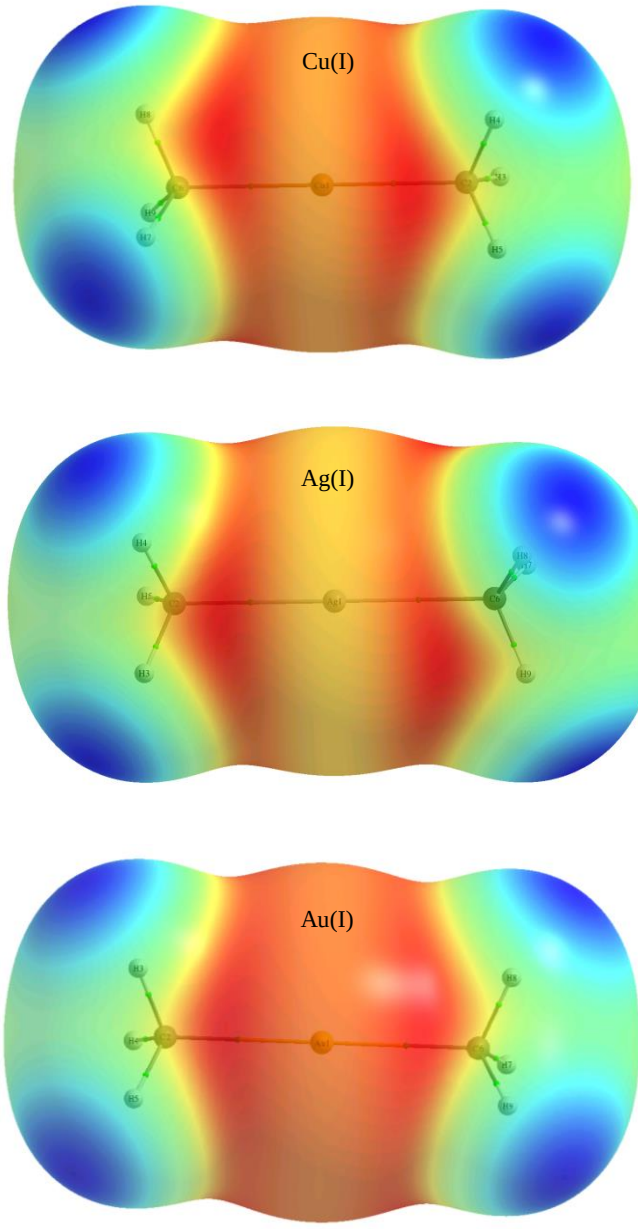

$[(Me)_2Cu]^-$ ESP potential (au)	
Red (min)	Blue (max)
-0.182898	-0.13909

$[(Me)_2Ag]^-$ ESP potential (au)	
Red (min)	Blue (max)
-0.17925	-0.13539

$[(Me)_2Au]^-$ ESP potential (au)	
Red (min)	Blue (max)
-0.18237	-0.13428

Figure 10 – ESP isosurfaces of the $[(Me)_2M]^-$ [M = Cu(I), Ag(I) and Au(I)] complexes calculated at the B3LYP/aug-cc-pVTZ-pp level of theory. *d*(Cu-C) = 1.964 Å, *d*(Ag-C) = 2.153 Å, *d*(Au-C) = 2.119 Å).

If the minimum values for each complex are compared, we observe that the $[(Me)_2Cu]^-$ complex yields the greatest negative ESP value with $[(Me)_2Au]^-$ closely second and $[(Me)_2Ag]^-$ least negative. This confirms the electrostatic nature of the $M^{I}\cdots X$ halogen bond, since it follows the trend of the E_{INT} values. The ESP isosurfaces shown in Figure 10 suggest that the origin of this trend is the electron density distribution, due to a combination of the size of the metal centre and the polarisibility of the M-C bond. The small size of the Cu atom results in an overall greater negative ESP near the Cu. The Ag^{I}-C bond lengths are longer than those of the Cu^{I}-C and Au^{I}-C leading to greater polarisation and a reduction in the

value of the ESP at the Ag(I) centre. The shorter Au^{I}-C distance, combined with the higher electron density on the gold (AIM charge of -0.14 *e*) leads to an ESP numerically increases at the Au(I) atom. In addition, it is clear from Figure 11, which shows the NCI analysis, that there is greater repulsion between the Cu(I) complex and the halogen bond donors than for the Ag(I) complex and Au(I) complex [see Figure 6 (a) and (c)]. This suggests that the E_{INT} values obtained are due to a balance between the $M^{I}\cdots I$ attraction and ligand$\cdots$X-bond donor repulsion.

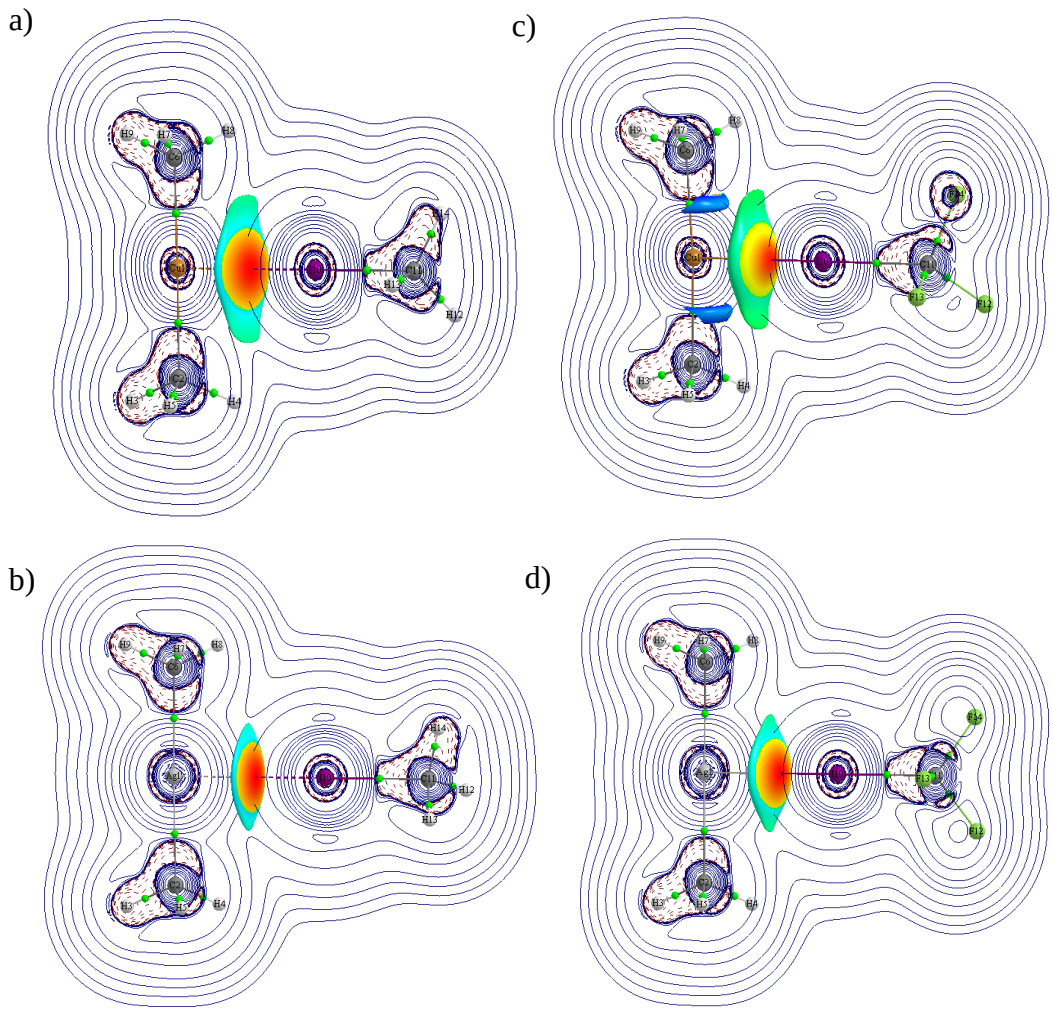

Figure 11 – Molecular graphs and two-dimensional contour plot of $\nabla^2\rho$ (ea_0^{-5}) with the NCI plots included of the $[(Me)_2Cu]^-$ (top) and the $[(Me)_2Ag]^-$ (bottom) complex X-bonded to ICH_3 (a and b) and ICF_3 (c and d) at the MP2/aug-cc-pVTZ-pp level of theory. The red (minimum) regions indicate a stabilising interaction with blue (maximum) regions indicating repulsion.

A further aspect of interest is the role of the polarisibility of the X-D bond on the X-bond interaction energy. We selected chloroform and iodine as model X-bond donors with more

polarisible bonds than already discussed, since these species are commonly used in synthetic chemistry, resulting in them being often included in crystal structures. In addition, since Au^- is known to mimic halides, we were interested to see whether $Au^-\cdots I_2$ would be comparable to the triiodide ion ($I^-\cdots I_2$)

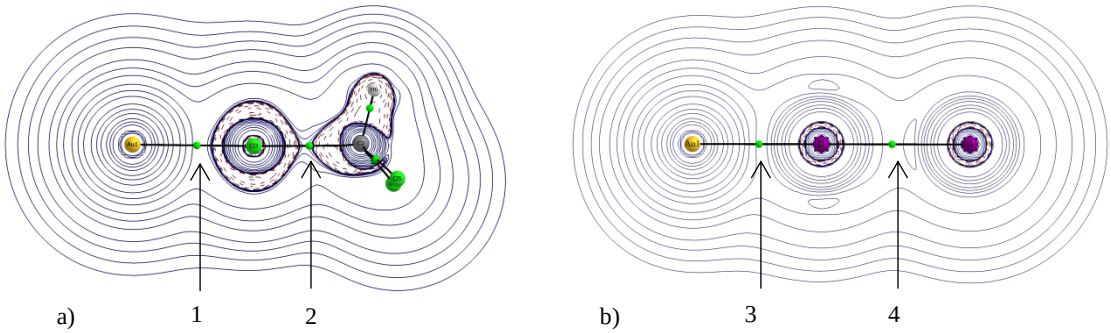

Figure 12 – Two-dimensional contour plot of the $\nabla^2\rho$ (ea_0^{-5}) showing the Au^- halogen bonded to a) chloroform and b) iodine at the MP2/aug-cc-pVTZ-pp level of theory. The BCPs that will be compared are denoted by 1, 2, 3 and 4

The molecular graphs of Au^- interacting with $CHCl_3$ and I_2 are given in Figure 12 show that atomic interaction lines connect gold to the chlorine and iodine atoms, thus confirming the X-bond interactions. The interaction energies and geometrical parameters are listed in Table 12.

Table 12 – E_{INT} in kcal/mol, Au···X distances (Å), Au···X-D angles (°) and ΔR (Å) of the X-D bond upon X-bond formation of the optimised geometries of the auride anion X-bonded to chloroform and iodine at the B3LYP, TPSS, MP2* and MP2 level of theory.

Method	**X-bond donor**	**E_{INT} (kcal/mol)**	**Au···X (Å)**	**Au···X-D (deg)**	**ΔR (X-D) (Å)**
B3LYP	$CHCl_3$	-8.53	2.897	174.2	0.062
TPSS		-24.36	2.517	175.2	0.972
MP2*		-22.90	2.418	177.5	0.298
MP2		-29.76	2.381	177.8	0.338
B3LYP	I_2	-69.42	2.628	180.0	0.509
TPSS		-74.09	2.601	179.9	0.476
MP2*		-59.35	2.581	180.0	0.284
MP2		-64.41	2.563	180.0	0.292

The most noticeable difference between the $Au^-\cdots Cl$ interaction involving $CHCl_3$ and those with $ClCH_3$ and $ClCF_3$ is that it is significantly more stabilising. Furthermore, the $Au^-\cdots Cl$

interaction in the chloroform adduct yields a more stabilising interaction than with $BrCH_3$, ICH_3 and $BrCF_3$. This added stabilisation may be due to the polarisability of the Cl-C bond as opposed to the Cl-CH_3 and Cl-CF_3 bonds. The $Au^{-}\cdots Cl$ distance is correspondingly shorter (2.42 Å as compared to 3.10 Å for the $ClCF_3$ adduct), while remaining properties are characteristic of halogen bonding.

If the E_{INT} values of the $Au^{-}\cdots I_2$ adduct are considered, we note an extremely stabilising value that is in the range of covalent bonds. This is the strongest halogen bond we have studied. This is not surprising since the mechanism of formation of this adduct is comparable to that of triiodides and also $[I\text{-}Au(I)\text{-}I]^{-}$. Interestingly, we see that both the DFT methods overestimate the E_{INT} values. When we compare the Au···I distances to those found in Table 2, we see that the Au···I distance of 2.581 Å given in Table 12 is much shorter than the value of 2.739 Å obtained for the $Au^{-}\cdots ICF_3$ adduct at the MP2* level of theory. Furthermore, we note that the Au···I-I angle is again perfectly linear, as found for examples of gold X-bonding to a halogen above.

From these examples we can construct a hypothesis: 1) the polarisibility of the X-R bond has a substantial influence on E_{INT}; and 2) gold polarises the Cl-C bond in $CHCl_3$ more easily than the Cl-C bond in $ClCF_3$.

Table 13 – Interaction energy (E_{INT}) in kcal/mol, the intermolecular distance (Au···X) in Å, the electron density at the intermolecular and intramolecular BCP [ρ_b $(e a_0^{-3})$], the Laplacian of the electron density [$\nabla^2(\rho_b)$ $(e a_0^{-5})$] and the total electronic energy density H_b in au of the auride anion X-bonded to the $CHCl_3$ and I_2 X-bond donors at the MP2/aug-cc-pVTZ-pp level of theory.

BCP	X-bond donor	$\boldsymbol{\rho_b}$ $\boldsymbol{(e a_0^{-3})}$	$\boldsymbol{\nabla^2(\rho_b)}$ $\boldsymbol{(e a_0^{-5})}$	$\boldsymbol{H_b}$ **(au)**
1)	Au···$ClCHCl_2$	0.0854	0.1455	-0.0280
2)	Cl-C	0.1083	0.0173	-0.0393
3)	Au···I_2	0.0829	0.0552	-0.0333
4)	I-I	0.044	0.0559	-0.008

If we consider the ρ_b values at the intermolecular BCPs 1 and 3 given in Table 13, we see they are comparable, with a difference of 0.0025 $e a_0^{-3}$. However, the corresponding E_{INT} values do not display this similarity, with the Au···I_2 interaction energy being 2.2 times more stabilising than the E_{INT} value found for Au···$CHCl_3$. This is significant, since it shows that the ρ_b values cannot always be linearly linked to the interaction energy. Interestingly, we note that the ρ_b at BCP 3, situated between the Au and I atom, is higher than the ρ_b value at

BCP 4 situated between the two iodine atoms, thus indicating that the I_2 bond has broken in order to form an Au-I bond. The adduct can therefore be viewed as Au-I···I^-.

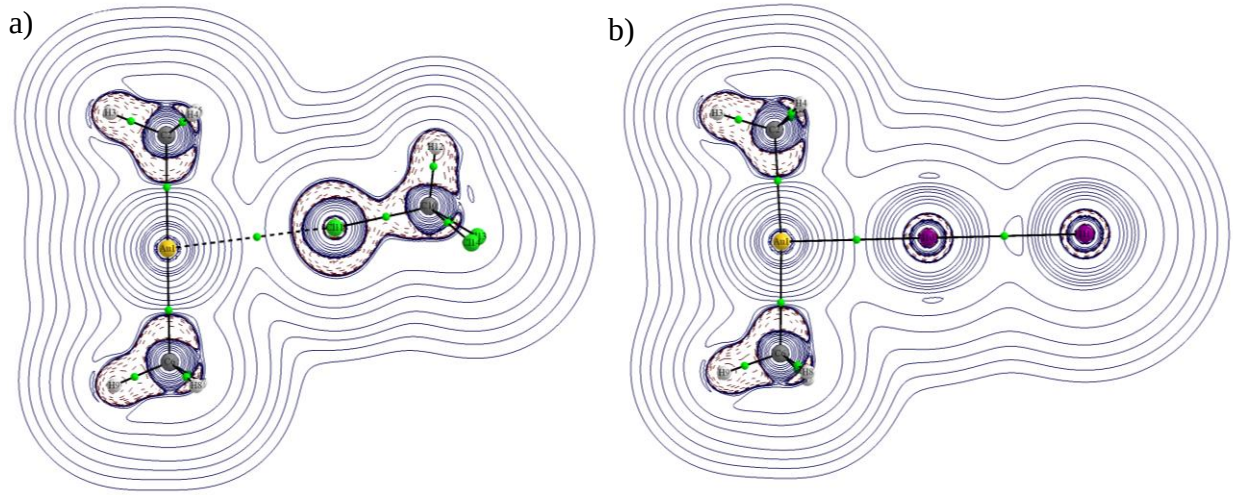

Figure 13 – Two-dimensional contour plot of the Laplacian of the electron density, $\nabla^2\rho$ (ea_0^{-5}), showing the $[(Me)_2Au]^-$ X-bonded to a) $CHCl_3$ and b) I_2 at the MP2/aug-cc-pVTZ-pp level of theory.

The interactions between DMA and chloroform and iodine are shown in Figure 13, where the atomic interaction lines shown in Figure 13 (a) and (b) confirms the formation of Au^{I}···X halogen bonds.

Table 14 – E_{INT} in kcal/mol, Au···X distances (Å), Au···X-R angles (°) and X-R bond lengths of the optimised geometries of the auride anion X-bonded to $ClCHCl_2$ and I_2 at the B3LYP, TPSS, MP2* and MP2 level of theory.

Method	X-bond donor	E_{INT} (kcal/mol)	Au···X (Å)	Au···X-R (deg)	ΔR (Å)
B3LYP	$CHCl_3$	-3.86	3.25	171.1	-0.01
TPSS		-6.62	2.93	172.2	0.72
MP2*		-5.38	3.17	173.0	0.67
MP2		-6.86	3.06	174.1	0.67
B3LYP	I_2	-35.22	2.78	180.0	0.27
TPSS		-42.75	2.74	179.8	0.28
MP2*		-38.49	2.72	180.0	0.22
MP2		-41.21	2.70	180.0	0.23

When the E_{INT} values of chloroform are considered, we see that they indicate weak X-bonds in comparison to those with ICF_3 and $BrCF_3$. However, chloroform yields comparable results to ICH_3 X-bonded to the $[(Me)_2Au]^-$ complex and yields a more stabilising interaction than

$BrCH_3$. Furthermore, chloroform X-bonded to the $[(Me)_2Au(I)]^-$ complex yields an E_{INT} value comparable to $ClCF_3$. This is further evidence of the importance of the polarisibility of the X-R bond in forming the X-bond.

The E_{INT} values of DMA with I_2 (-38.49 kcal/mol) show that this is the most stabilising X-bond of all those studied here. We therefore postulate that this is the strongest X-bond that Au(I) can form with a neutral X-bond donor, since it is in the range of the I-I bond in triiodide. AIM results for chloroform and iodine X-bonded to the DMA anionic complex are given in Table 15, where there are no longer similarities in Table 5 with regards to the ρ_b values at the intermolecular BCPs of $Au^{I}\cdots CHCl_3$ and $Au^{I}\cdots$I-I. It is interesting to note that the ρ_b accumulation between the Au and I is larger than between the two iodine atoms, indicative of bond breaking. This could also explain the initiation of the mechanism of oxidative addition of I_2 to anionic gold complexes: The Au(I) atom has to exhibit slight basicity, in order to first form an X-bond to I_2, whereafter strengthening of the Au-I interaction would lead to concomitant weakening of the I_2 bond as shown by the BCPs given in Table 15.

Table 15 – Interaction energies, the intermolecular distances, the electron density [ρ_b ($e a_0^{-3}$)], the Laplacian of the electron density [$\nabla^2(\rho_b)$ ($e a_0^{-5}$)] and the total electronic energy density H_b in au of the DMA anionic complex X-bonded to the $ClCHCl_2$ and I_2 X-bond donors at the MP2/aug-cc-pVTZ-pp level of theory.

X-bond donor	$\boldsymbol{\rho_b}$ $(\boldsymbol{e a_0^{-3}})$	$\boldsymbol{\nabla^2(\rho_b)}$ $(\boldsymbol{e a_0^{-5}})$	$\boldsymbol{H_b}$ **(au)**
$Au\cdots CHCl_3$	0.021	0.058	-0.0002
Cl-C	0.203	-0.254	-0.1451
$Au\cdots I_2$	0.063	0.071	-0.0194
I-I	0.052	0.039	-0.0121

5.5. Conclusions

We have shown that the auride anion can indeed act as an X-bond acceptor with E_{INT} values of approximately -20 kcal/mol. These are comparable in strength to the hydrogen bond between the auride anion and HF and HCN [5]. Our results also highlight gold's affinity for iodine, in that both the auride anion and the DMA anionic complex yield favourable E_{INT} values for the ICH_3 and ICF_3 X-bond donors. The optimised geometries confirm the directionality of these halogen bonds: whether the X-bond acceptor is the auride anion or the DMA anionic complex, the Au···X-C angles are almost always perfectly linear, typically with less than 5º deviation from 180º. Furthermore, our results show that there is elongation

of the X-R bond upon X-bond formation, except with cases involving chlorine as the donor atom.

We have shown that DFTs can be employed to calculate the strength of halogen bonds to gold, with B3LYP being the most consistent and TPSS consistently overestimating the E_{INT} values. As expected, iodine is the best X-bond donor when compared to bromine and chlorine, with the latter halogen not forming X-bonds unless there is an electron-withdrawing group attached to it. It is thus most likely that the iodine and bromine derivatives would provide favourable $Au^{I}\cdots X$ interactions in the solid state, while $Au^{I}\cdots Cl$ contacts found in the CSD should be treated with caution. We have also shown that Cu^{-} and Ag^{-} yield stronger X-bonds than the auride ion, but we ascribe the stability of these adducts to the electron affinity of the metal centre. Furthermore, we also showed that the $[(Me)_2Cu]^{-}$complex yields stronger X-bonds than the Au and Ag analogues, due to its electrostatic surface potential when the ICH_3 X-bond donor is considered. However, the DMA anionic complex yielded comparable results to the $[(Me)_2Cu]^{-}$ complex when an electron-withdrawing group was attached to the halogen donor atom, i.e. the ICF_3 X-bond donor.

This paper has shown that it is possible for gold to act as a halogen-bond acceptor, at least for anionic complexes where the ligand bonds to gold through an electron-rich carbon atom. Our AIM results verify that the X-bond donor binds to the gold centre with a considerable amount of electron density accumulating at the intermolecular BCP of the Au···X-R contact.

Our results with regards to chloroform and I_2 as X-bond donors illustrate that the polarisibility of the X-R bond is important for X-bonding to the auride anion and can influence the intermolecular distances and also increase the electron density accumulation at the intermolecular BCP. We also see that I_2 forms the strongest X-bonds to gold, to the extent of weakening the I-I bond. By considering all the results shown here, we conclude that the $M^{I}\cdots X$ interactions arise due to the δ- region situated on the metal centre, as shown by the ESP of the isosurface, which interacts with the δ+ region (positive or least negative region) on the halogen atom, i.e. σ-hole. The strong E_{INT} values suggest the presence of substantial charge-transfer, which is the subject of future investigations.

References

1. Metrangolo, P., Neukirch, H., Pilati, T., Resnati, G., *Acc. Chem. Res.*, 2005. **38**(5): p. 386-395.
2. Desiraju, G.R., Ho, P.S., Kloo, L., Legon, A.C., Marquardt, R., Metrangolo, P., Politzer, P., Resnati, G., Rissanen, K., *Pure Appl. Chem*., 2013. **85**(8): p. 1711-1713.
3. Brammer, L., Minguez Espallargas, G., Libri, S., *CrystEngComm*, 2008. **10**(12): p. 1712-1727.
4. Libri, S., Jasim, N.A., Perutz, R.N., Brammer, L., *J. Am. Chem. Soc.*, 2008. **130**(25): p. 7842-7844.
5. Groenewald, F., Esterhuysen, C., Dillen, J., Raubenheimer, H., *To be published*.
6. Politzer, P., Lane, P., Concha, M., Ma, Y., Murray, J., *J. Mol. Model*., 2007. **13**(2): p. 305-311.
7. Grabowski, S.J., *J. Phys. Chem. A*, 2011. **115**(44): p. 12340-12347.
8. Clark, T., Hennemann, M., Murray, J., Politzer, P., *J. Mol. Model*., 2007. **13**(2): p. 291-296.
9. Ruei-Yang, L., Ehlich, H., Schier, A., Schmidbaur, H., *Z. Naturforsch.*, 2002. **57b**: p. 1085-1089.
10. Schneider, D., Schier, A., Schmidbaur, H., *Dalt Trans.*, 2004(13): p. 1995-2005.
11. Politzer, P., Murray, J.S., Clark, T., *Phys. Chem. Chem. Phys.*, 2010. **12**(28): p. 7748-7757.
12. Shields, Z.P., Murray, J.S., Politzer, P., *Int. J. Quant. Chem.*, 2010. **110**(15): p. 2823-2832.
13. Kryachko, E.S., *J. Mol. Struct*., 2008. **880**(1–3): p. 23-30.
14. Jansen, M., *Chem. Soc. Rev.*, 2008. **37**(9): p. 1826-1835.
15. Schmidbaur, H., Raubenheimer, H.G., Dobrzanska, L., *Chem. Soc. Rev.*, 2014. **43**(1): p. 345-380.
16. Frisch, M.J., Trucks, G.W., Schlegel, H.B., Scuseria, G.E., Robb, M.A., Cheeseman, J.R., Scalmani, G., Barone, V., Mennucci, B., Petersson, G.A., Nakatsuji, H., Caricato, M., Li, X., Hratchian, H.P., Izmaylov, A.F., Bloino, J., Zheng, G., Sonnenberg, J.L., Hada, M., Ehara, M., Toyota, K., Fukuda, R., Hasegawa, J., Ishida, M., Nakajima, T., Honda, Y., Kitao, O., Nakai, H., Vreven, T., Montgomery, J.A., Peralta, J.E., Ogliaro, F., Bearpark, M., Heyd, J.J., Brothers, E., Kudin, K.N., Staroverov, V.N., Kobayashi, R., Normand, J., Raghavachari, K., Rendell, A., Burant, J.C., Iyengar, S.S., Tomasi, J., Cossi, M., Rega, N., Millam, J.M., Klene, M., Knox,

J.E., Cross, J.B., Bakken, V., Adamo, C., Jaramillo, J., Gomperts, R., Stratmann, R.E., Yazyev, O., Austin, A.J., Cammi, R., Pomelli, C., Ochterski, J.W., Martin, R.L., Morokuma, K., Zakrzewski, V.G., Voth, G.A., Salvador, P., Dannenberg, J.J., Dapprich, S., Daniels, A.D., Farkas, Foresman, J.B., Ortiz, J.V., Cioslowski, J., Fox, D.J., *Gaussian 09, Revision B.01*. 2009.

17. Boys, S.F., Bernardi, F., *Mol. Phys.*, 1970. **19**(4): p. 553-566.
18. Simon, S., Duran, M., Dannenberg, J.J., *J. Chem. Phys.*, 1996. **105**(24): p. 11024-11031.
19. Becke, A.D., *J. Chem. Phys.*, 1993. **98**(7): p. 5648-5652.
20. Lee, C., Yang, W., Parr, R.G., *Phys. Rev. B*, 1988. **37**(2): p. 785-789.
21. Miehlich, B., Savin, A., Stoll, H., Preuss, H., *Chem. Phys. Lett.*, 1989. **157**(3): p. 200-206.
22. Tao, J., Perdew, J.P., Staroverov, V.N., Scuseria, G.E., *Phys. Rev. Lett.*, 2003. **91**(14): p. 146401.
23. Peterson, K.A. Puzzarini, C., *Theo. Chem. Acc.*, 2005. **114**(4-5): p. 283-296.
24. Figgen, D., Rauhut, G., Dolg, M., Stoll, H., *Chem. Phys.*, 2005. **311**(1–2): p. 227-244.
25. Kendall, R.A., Dunning, T.H., Harrison, R.J., *J. Chem. Phys.*, 1992. **96**(9): p. 6796-6806.
26. Dunning, T.H., *J. Chem. Phys.*, 1989. **90**(2): p. 1007-1023.
27. Wilson, A.K., Woon, D.E., Peterson, K.A., Dunning, T.H., *J. Chem. Phys.*, 1999. **110**(16): p. 7667-7676.
28. Woon, D.E., Dunning, T.H., *J. Chem. Phys.*, 1993. **98**(2): p. 1358-1371.
29. Møller, C. Plesset, M.S., *Phys. Rev.*, 1934. **46**(7): p. 618-622.
30. Binkley, J.S. Pople, J.A., *Int. J. Quant. Chem.*, 1975. **9**(2): p. 229-236.
31. Feller, D., *J. Comp. Chem.*, 1996. **17**(13): p. 1571-1586.
32. Schuchardt, K.L., Didier, B.T., Elsethagen, T., Sun, L., Gurumoorthi, V., Chase, J., Li, J., Windus, T.L., *J. Chem. Inf. Model.*, 2007. **47**(3): p. 1045-1052.
33. Zhurko, G.A, Zhurko, .D.A., *ChemCraft*, 2012.
34. Groenewald, F., Esterhuysen, C., Dillen, J., *Theo. Chem. Acc.*, 2012. **131**(10): p. 1-12.
35. Bondi, A., *J. Phys. Chem.*, 1964. **68**(3): p. 441-451.
36. Keith, T.A., *AIMAll* 2012 TK Gristmill Software.
37. Johnson, E.R., Keinan, S., Mori-Sánchez, P., Contreras-García, J., Cohen, A.J., Yang, W., *J. Am. Chem. Soc.*, 2010. **132**(18): p. 6498-6506.
38. Svensson, P.H. Kloo, L., *Chem. Rev.*, 2003. **103**(5): p. 1649-1684.

39. Nakanishi, W., Hayashi, S., Narahara, K., *J. Phys. Chem. A*, 2008. **112**(51): p. 13593-13599.
40. Zou, J.-W., Lu, Y.-X., Yu, Q.-S., Zhang, H.-X., Jiang, Y.-J., *Chinese J. Chem.*, 2006. **24**(12): p. 1709-1715.
41. Kaur, D., Kaur, R., *J. Chem. Sci.*, 2014. **126**(6): p. 1763-1779.
42. Tiana, D., Francisco, E., Blanco, M.A., Pendás, A.M., *J. Phys. Chem. A*, 2009. **113**(27): p. 7963-7971.
43. Keith, T.A. Frisch, M.J., *J. Phys. Chem. A*, 2011. **115**(45): p. 12879-12894.
44. Johansson, M.P. Swart, M., *Phys. Chem. Chem. Phys.*, 2013. **15**(27): p. 11543-11553.
45. Pinter, B., Nagels, N., Herrebout, W.A., De Proft, F., *Chem. Eur. J.*, 2013. **19**(2): p. 519-530.
46. Kozuch, S. Martin, J.M.L., *J. Chem. Theo. Comp.*, 2013. **9**(4): p. 1918-1931.
47. René, C.B., Michael, S., Harold, K.H., *J. Phys. B-At. Mol. Opt.*, 1998. **31**(17): p. 3885.

6. Conclusions

We started this dissertation by considering the IUPAC definition of hydrogen bonding, along with additional views on H-bonding that suggest that it can be seen as an incipient proton-transfer reaction. We then examined H-bonding in transition metal complexes; listing geometrical characteristics and AIM parameters for these types of interactions, thus familiarising ourselves with unconventional H-bonding interactions within transition metal compounds. The discussion was then expanded to halogen bonding and how it represents a world similar to H-bonding with regards to directionality, interaction energies and geometrical changes upon adduct formation. Halogen bonding was also briefly discussed in the context of transition metal complexes, where these interactions generally appear in the solid state. In both hydrogen and halogen bonding, the common denominator is that the negative site of the Lewis base forms an adduct with the positive or acidic site of the donor atom, be it a hydrogen or halogen atom. In this context we have investigated the ability of Au(I) to act as a Lewis base.

In order to exclude the possibility that the adducts calculated were artefacts, but were instead based on sound theoretical evidence, four different levels of theory were used: two types of DFs, B3LYP and TPSS, along with MP2/cc-pVTZ-pp and MP2/aug-cc-pVTZ-pp calculations for comparison. The MP2/cc-pVTZ-pp level of theory was chosen as the benchmark since it provides a balance between electrostatic and dispersion contributions to the interaction energy and is also computationally less expensive than its augmented counterpart. On the other hand, MP2/aug-cc-pVTZ-pp calculations were our preferred level of theory for AIM analysis since this method yields a high quality wave function. In conjunction with the AIM results, we also calculated the NCI regions for each adduct to provide additional insight into the interactions that are not represented by an AIL.

Initially, as a reference, the best known example of gold acting as a Lewis base, i.e. the Au^- ion, was used to obtain energetic, geometrical and AIM parameters for the known $Au^-\cdots H$ interaction. The AIM results led us to conclude that these are indeed H-bonds.

A similar analysis was then performed with the $[(Me)_2Au(I)]^-$ ion where the calculated geometrical and AIM parameters followed the same trends identified for the Au^- ion and also proved that DMA satisfies the requirements for H-bonding according to the IUPAC definition. The interaction energies for $[(Me)_2Au]^-$ were found to be less than those for the Au^- ion, while the geometrical parameters were characteristic of weaker H-bonds. Molecular

graphs obtained from the wave function displayed AILs connecting the Au and H atoms, with NCI plots providing three-dimensional visual representations of the interaction regions. In order to determine whether the ability of the $[(Me)_2Au]^-$ ion to form H-bonds is unique to gold only, we deemed it logical to determine whether the Cu(I) and Ag(I) analogues can also act as H-bond acceptors. HF was selected as model H-bond donor, since it consistently yields the strongest $Au^I\cdots H$ interaction and would be most likely to form an H-bond. We found that the $[(Me)_2Cu]^-$ and $(Me)_2Ag]^-$ do not form M···H interactions with HF, based on the fact that no AILs connecting the metal centre to the HF could be identified. Instead, AILs were found connecting HF to the carbon atom of the methanide ligand. The ESP at the isosurfaces defined at an electron density of 0.001 au revealed that Cu(I) and Ag(I) have different topologies, such that the negative (red) regions are concentrated around the BCP between the metal centre and the coordinating carbon atom, leading to the AIL connecting HF to the C atom, as observed. In the case of Au(I), the negative regions of the ESP were more delocalised across the isosurface corresponding to metal centre. This difference could be a result of the differences in the electronegativities of Cu and Ag compared to Au. Relativistic effects seem responsible for the H-bond formation to Au(I), since no AIL connecting the Au and the H atoms was observed for the $[(Me)_2Au]^-$ if relativistic effects were omitted. We showed one cannot only consider interaction energies and geometrical parameters for determining the existence of the M···H interaction and that AIM analysis is a crucial step. This was seen for $[(Me)_2Cu]^-$ and $[(Me)_2Ag]^-$ H-bonded to HF where the M···H distances and E_{INT} values are comparable to HF bonded to $[(Me)_2Au]^-$. The ESP of the $[(Me)_2Au]^-$ complex with the relativistic effects of gold omitted revealed that, as with the Cu(I) and Ag(I) analogues, the negative regions of the ESP are localised around the BCP connected Au and C, thus agreeing with the AIM results. This chapter served as a proof of concept that Au(I) can H-bond to a variety of H-bond donors.

The next logical progression in our study was to determine how inductive effects could influence the $Au^I\cdots H$ interaction. Therefore the $[C(Me)_3Au]^-$ and $[CF_3Au]^-$complexes were selected as model complexes, where the ligands change from electron-donating to electron-withdrawing. We concluded that the electron-donating effects are observed in the Au···H distances as well as the AIM parameters, but are not reflected in the calculated interaction energies due to repulsion between the heteroatoms of the H-bond donor and the ligands coordinated to gold. This was shown qualitatively by NCI plots. However, when electron-withdrawing groups coordinate to Au(I), changes characteristic of a weakening of the

$Au^{I}\cdots H$ interaction were observed for all the geometrical and AIM parameters calculated, thus illustrating the reduction in basicity of the Au(I) atom.

We were further interested to see if the H-bond ability of Au(I) is restricted to anionic complexes and thus also undertook an investigation into the H-bond ability of neutral Au(I) complexes where one of the ligands is an *N*-heterocyclic carbene. It was expected that the gold in the neutral Au(I) complexes would be a still-weaker Lewis base than in the $[(CF_3)_2Au]^-$ complex. Essentially, we were probing to see what the limit for Lewis basicity was in order to still obtain an H-bond. The investigation of the neutral Au(NHC)X complexes yielded a common denominator: when the basicity of the Au(I) atom is decreased an "anchor" in the form of a second H-bond between the H-bond donor and the NHC ligand is needed so that the H-bond donor is in close proximity to the Au(I) centre. The $Au^{I}\cdots H$ interaction manifests itself as a weak, dispersion-type interaction. This result suggests that even when Au(I) exhibits a partial positive charge it could still form a weak hydrogen bond arising from dispersion-type interactions. On the other hand, NHC complexes containing an electron-donating ligand such as CH_3^- yield adducts with strong H-bond donors like H_2O and HF that are characteristic for H-bonds. The prerequisite for an anchor could possibly explain why these $Au^{I}\cdots H$ interactions have not been more frequently observed in the solid state and in solution.

The same *modus operandi*, as used for investigating $Au^{I}\cdots H$ interactions was then employed in studying halogen-bond formation to gold. We began by analysing the ability of the Au^- ion to act as halogen bond acceptor and concluded that it behaves like the Br^- and I^- anions, with interaction energies comparable to the dative bonds found in trihalides. Thereafter the halogen-bonding capabilities of the $[(Me)_2Au]^-$ ion were investigated and we consider this as additional evidence towards the Lewis basicity that the Au(I) centre can exhibit with the correct ligands. It is interesting to note that the halogen bonds formed yield a higher stability than their H-bonded counterparts. From an interaction-energy point of view, it seems that formation of the halogen-bonded adducts is favourable, particularly when the correct ligands are selected. We stress that these halogen bonds are of the $Au^{\delta-}\cdots X^{\delta+}$ type, where the gold has the electrostatic properties needed to interact with the least negative portion of the σ-hole on the halogen donor atom.

We have thus provided theoretical evidence that, by means of the $[(Me)_2Au]^-$ ion's ability to noncovalently bond to both a number of hydrogen and halogen bond donors that, first and foremost, the Au(I) centre can act as a Lewis base.

This study is only the first step towards fully understanding when and how these $Au^{I}\cdots H$ and $Au^{I}\cdots X$ interactions occur, even though we have provided valuable initial insight as to why they occur. The main drawback to further study of this phenomenon is the lack of experimental evidence available for us to analyse and compare our results to. We hope that the theoretical results shown here will initiate more interest in these novel $Au^{I}\cdots H$ and $Au^{I}\cdots X$ interactions, thus yielding more experimental examples for us to investigate.

We would like to end our conclusions by providing the reader with criteria and characteristics that need consideration in the design of compounds where the $Au^{I}\cdots H$ interaction could be utilised as supramolecular synthons:

- The ligands should preferably be anionic;
- The Au(I) complex should exhibit a partial negative charge on the Au(I) atom;
- The negative regions of electrostatic surface potential on the Au(I) should not be localised on the coordinating atoms, but across the gold atom;
- The ligand should not be a better H-bond acceptor than Au(I);
- If the Au(I) atom has a partial positive charge it can yield weak H-bonds, but then an anchor site on one of the ligands for the H-bond donor is required;
- Halogen bond formation seems more favourable than H-bonding, and we postulate that extremely stable X-bonded adducts are intermediates for oxidative addition, for instance with halogen bond donors such as I_2 and ICF_3.

This research has also raised a number of questions that need answering. We pose the following questions to the community that we believe need answering in the future to aid in fully characterising and understanding these phenomena:

- Can other anionic Au(I) complexes form hydrogen and halogen bonds?
- Can other neutral Au(I) complexes yield this interaction with, or without, the anchoring H-bond present?
- Can other transition metals form hydrogen and halogen bonds that we are unaware of?
- How stable will these adducts be in general, and compared to gold?
- Can these interactions be observed using NMR or IR in selected solvents or the solid state?
- Can these interactions be utilised by experimentalists to design crystals?
- What customisable and interesting structure-related properties will these structures yield?